

Traffic Volume Estimation using Dynamic Response Data acquired in a Cable-stayed Bridge

Kaiwan Wattana

2016

Traffic Volume Estimation using Dynamic Response Data acquired in a Cable-stayed Bridge

A DISSERTATION

SUBMITTED TO THE GRADUATE SCHOOL OF
URBAN INNOVATION IN PARTIAL FULFILLMENT OF THE
REQUIREMENTS

for the degree

DOCTOR OF PHILOSOPHY (IN ENGINEERING)

By

Kaiwan Wattana



Department of Civil Engineering
YOKOHAMA NATIONAL UNIVERSITY
March, 2016

Abstract

In most structural health monitoring (SHM) projects, the structural conditions are tried to be assessed only from their static and/or dynamic responses, i.e., outputs. However, those structural responses are actually caused by the inputs, which include both operational and environmental ones. Therefore, the behaviors of those inputs themselves must effect on the structural conditions. The effective condition assessments of existing structures will be realized if not only the structural responses but also the information about input loads can be understood from the SHM data. This thesis presents analyses of the response data acquired by a structural health monitoring SHM system installed on an in-service cable-stayed bridge in Thailand (or Bangkok), and shows applications of the acquired data in the bridge planning. The SHM system consists of various sensors including accelerometers, tilt sensors, temperature sensors, and the vehicle counting system. In this study, the correlations between the response features from dynamic data; peak frequencies and amplitudes of responses, and the temperature and the traffic volume were firstly investigated. The results revealed that the traffic volume was a dominant factor that influenced on variances of the extracted features while the temperature showed low effects on them in the target bridge. In addition, the traffic effects were more investigated by using finite element (FE) models. The FE analysis results agreed with those of the data analysis and showed more that not only the traffic volumes, but also vehicle speeds had effects on the dynamic responses. In the case of the same traffic volumes, the response amplitudes decreased when the speeds of vehicles decreased. Furthermore, some of the response features that showed high correlations were then selected for constructing a linear regression model to estimate the total traffic volume per five minutes. The constructed model then showed the accurate fitting performance to the data, and it was also capable of predicting the traffic volume on the bridge. The predicted traffic volume could be used for identifying traffic conditions and estimating vehicular live loads in determining the safe load capacities of the bridge.

To my family

Acknowledgments

First of all I would like to express my heartfelt and sincere gratitude to my supervisor, Associate professor Dr. Mayuko Nishio for her deliberate guidance, time and continuous encouragement during the study period at the Yokohama National University. It was my pleasure and privilege to work with her during my Ph.D. course.

I would also like to thank my other advisors, Professor Dr. Hitoshi Yamada and Professor Dr. Hiroshi Katsuchi for their constructive advices and suggestions they gave me during the research period. I am also grateful to my other committee members, Professor Dr. Yozo Fujino, Associate Professor Dr. Dionysius M. Siringoringo and Associate Professor Dr. ShinjiTnaka for their important comments and recommendations.

I would like to thank Dr. Haeyoung Kim and all of my laboratory members for their kind cooperation, support and assistance.

I am highly obliged and grateful to Department of Rural Roads for their incessant financial assistance and Japanese people for their friendly attitude during my study period in Japan.

Kaiwan Wattana

March, 2016

Contents

Abstract	ii
Dedication	iii
Acknowledgement	iv
Contents	v
List of Figures	viii
List of Tables	xii
Nomenclatures	xiv
1. INTRODUCTION.....	1
1.1 MOTIVATION	2
1.2 INTRODUCTION OF SHM	3
1.2.1 Objectives and Benefits of SHM	4
1.2.2 SHM organization.....	4
1.2.3 Structural Condition Assessment from SHM Data.....	7
1.3 TRAFFIC MONITORING	8
1.3.1 WIM Technologies	9
1.3.2 Non-intrusive technologies	12
1.3.3 Novelty Traffic Monitoring	12
1.3.4 Traffic load information in Bridge Reliability.....	12
1.4 AIMS AND SCOPE.....	13

1.5	OUTLINES OF THE THESIS	14
2.	ACQUIRED SHM DATA AND FEATURE EXTRACTION.....	19
2.1	TARGET BRIDGE AND SHM SYSTEM	19
2.1.1	Target Bridge Descriptions	20
2.1.2	Installed SHM System	22
2.2	ACQUIRED SHM DATA.....	23
2.2.1	Bridge Responses and Environmental Data.....	23
2.2.2	Traffic Data.....	24
2.3	MODAL PARAMETERS	27
2.3.1	Resonant Frequencies	27
2.3.2	Mode Shapes.....	31
2.4	RMS OF BRIDGE RESPONSES	32
2.5	CONCLUSIONS	35
3.	BRIDGE RESPONSES IN CHANGING ENVIRONMENTAL AND OPERATIONAL CONDITIONS.....	36
3.1	INTRODUCTION.....	37
3.2	RESPONSE DATA.....	38
3.3	THEORETICAL DESCRIPTION OF REGRESSION MODELS	44
3.4	MATHEMATICAL MODELS OF RESONANT FREQUENCIES.....	46
3.5	CONCLUSIONS	51
4.	FINITE ELEMENT MODELING FOR DYNAMIC RESPONSES	54
4.1	FINITE ELEMENT MODELING AND MODEL VALIDATION.....	55
4.2	TRAFFIC LOAD MODELING AND ASSIGNMENT.....	59
4.3	MODEL OUTPUT VALIDATION	65
4.4	EFFECTS OF TRAFFIC VOLUME AND SPEED ON DYNAMIC RESPONSES.....	71

4.4.1 Traffic Volume Effects	71
4.4.2 Traffic-flow speed Effects	71
4.5 CONCLUSIONS	76
5. TRAFFIC VOLUME ESTIMATION	77
5.1 CORRELATIONS WITH THE TRAFFIC VOLUME AND TEMPERATURE	78
5.2 SELECTION OF FEATURES FOR ESTIMATION.....	80
5.3 CONSTRUCTED MODEL FOR TRAFFIC VOLUME ESTIMATION.....	83
5.4 CONCLUSIONS	90
6. SAFE LOAD CAPACITY AND RELIABLY EVALUATION.....	92
6.1 LOAD AND RESISTANCE FACTOR RATING	92
6.1.1 Load Rating Procedure	93
6.1.2 Determination of force effect.....	97
6.1.3 Load Rating Factor and Rating Factor Determination	100
6.2 RELIABILITY ANALYSIS	102
6.2.1 Background Theory	102
6.2.2 Reliability Index Determination	104
6.3 CONCLUSIONS.....	106
7. CONCLUSIONS	109

List of Figures

Fig. 1.1 Flow chart of SHM organization.....	6
Fig. 1.2 B-WIM installation.....	10
Fig. 2.1 A picture of Bhumibol-Bridge-I	20
Fig. 2.2 Bridge descriptions	21
Fig. 2.3 Sensor configuration of the SHM system.....	23
Fig. 2.4 Acquired dynamic responses and temperature for three days; Saturday, May 17, 2014, Sunday, May 18, 2014 and Monday, May 19, 2014.....	25
Fig. 2.5 Restricted axle and gross weights of a single truck and trailer.....	26
Fig. 2.6. Monitored traffic volume for three days; Saturday, May 17, 2014, Sunday, May 18, 2014 and Monday, May 19, 2014	26
Fig. 2.7. Traffic congestion on the bridge.....	27
Fig. 2.8 PSD and its first ten peaks of vertical acceleration of the deck.....	28
Fig. 2.9 First four peak frequencies	29

Fig. 2.10 First four peaks of the three PSD determined from the interval of 3:00 – 3:05 am, interval of 7:00 – 7:05 am and interval of 11:00 – 11:05 am ,of May, 17th, 18th and 19th.....	30
Fig. 2.11 Identified mode shapes	31
Fig. 2.12 RMS of responses	33
Fig. 2.13 RMSs of filterd responses.....	34
Fig. 3.1 Acquired dynamic responses for three days; 2nd - 4th August, 2014	40
Fig. 3.2 Monitored traffic volume for three days; 2nd - 4th August, 2014.....	40
Fig. 3.3 Monitored temperature for three days; 2nd - 4th August, 2014	41
Fig. 3.4 PSD and its first ten peaks of vertical acceleration of the deck.....	41
Fig. 3.5 Fluctuations of resonant frequencies (a) 1st mode, (b) 2nd mode, (c) 3rd mode, (d) 4th mode, (e) 5th mode, (f) 6th mode, (g) 7th mode, (h) 8th mode and (i) 9th mode.....	42
Fig. 3.6 Correlation coefficients between eight resonant frequencies and traffic loading, temperature and RMS of the deck and cable accelerations plotted against mode of resonant frequencies.	43
Fig. 3.7 Measured and predicted resonant frequencies of the (a) 1st and (b) 2nd modes.....	49
Fig. 3.8 Model prediction errors and theirs 99.5% confidence limits of the (a) 1st and (b) 2nd modes	50
Fig. 3.9 Autocorrelation function of the 2nd modes frequency	50
Fig. 4.1 FE model of the Bhumibol I Bridge.	56
Fig. 4.2 FE model of main span deck (a) 3D model and (b) Wire frame model	56
Fig. 4.3 FE model of side span deck (a) 3D model and (b) Wire frame model.....	57

Fig. 4.4 FE model of towers (a) 3D model and (b) Wire frame model.....	57
Fig. 4.5 Calculated mode shapes.....	58
Fig. 4.6 Vehicular load models	60
Fig. 4.7 Lane occupancies on the Bhumibol I bridge.	60
Fig. 4.8 Traffic lane arrangement in the FE model.....	61
Fig. 4.9 Spacing between the axles of the trailers in load models	61
Fig. 4.10 Vehicular load time history during 11.00 – 11.01 am in the southbound direction on 19th May.	62
Fig. 4.11 Load assignment on the deck.....	63
Fig. 4.12 Traffic data on Monday, May 19th for model inputs	64
Fig. 4.13 Samples of input time history for two consecutive nodes	64
Fig. 4.14 Calculated and measured accelerations on 19th May.....	66
Fig. 4.15 RMSs of the calculated and measured accelerations on 19th May.....	67
Fig. 4.16 RMSs of the calculated and measured accelerations during traffic congestion on 19th May	68
Fig. 4.17 RMSs of the filtered accelerations of the deck and cable	70
Fig. 4.18 PSDs obtained from the measurement in different traffic volumes.....	73
Fig. 4.19 PSDs obtained from FE models assigned different traffic volumes and constant speed of traffic flow.....	74

Fig. 4.20 PSDs obtained from FE models assigned constant traffic volume and different speed of traffic flow.....	75
Fig. 4.21 RMSs of deck accelerations.....	75
Fig. 5.1 Correlation coefficients between peak frequencies and temperature, and traffic volume plotted against order of peak frequencies.....	79
Fig. 5.2 Correlation coefficients between the RMSs of responses, and the temperature and the traffic volume data	79
Fig. 5.3 Flow chart for parameter selection	81
Fig. 5.4 Estimated and predicted traffic volumes from the constructed model and their residuals.....	87
Fig. 5.5 Autocorrelation function of the residuals of estimated traffic volumes	87
Fig. 5.6 Measured, fitted and predicted traffic volumes.....	87
Fig. 5.7 Measured, fitted and predicted traffic volumes on May, 17th, 18th, 19th and 21st, 2014.....	89
Fig. 6.1 AASHTO LRFD flow chart (AASHTO, 2013) for the Bhumibol I Bridge.....	94
Fig. 6.2 HL-93 design live load (AASHTO, 2013) for the Bhumibol I Bridge.....	95
Fig. 6.3 AASHTO legal load (AASHTO, 2013) for the Bhumibol I Bridge.....	95
Fig. 6.4 State legal load and AASHTO lane load for the Bhumibol I Bridge	95
Fig. 6.5 Live load combinations.....	98
Fig. 6.6 Stress contour of the bridge tower due to dead load and AASHTO HL-93 lane load applied only on the main span.....	99

List of Tables

Table 3.1 Correlation coefficient matrix of traffic loading, temperature, RMS of the deck accelerations and RMS of cable accelerations.	43
Table 3.2 Estimated coefficients of regression models for the nine resonant frequencies.	47
Table 4.1 Calaulated and Identified resonant frequencies.	59
Table 5.1 Correlation coefficients between traffic volme variable and peak frequency variables	82
Table 5.2. Correlation coefficients between traffic volme variable and accepted RMS of bridge responses variables.....	83
Table 5.3 Candidate models for traffic volume estimation and the root mean squared error....	85
Table 5.4 Estimated parameter coefficients, significant levels in OLS, variance inflation factors, coefficient standard errors (SE) obtained by OLS and HAC estimates, and adjusted significant levels in HAC	85
Table 5.5. Actual and predicted average traffic volume per day (Number of equivalent trucks per day).....	88
Table 5.6. Estimated parameters and the root mean square error of the models constructed from a half-day, a day and two-day trained data.....	88
Table 6.1 Table 6.1 Calculated tower compression stress at the critical section and parameters for rating.....	99

Table 6.2 factors used in determining rating factors in each level of evaluation.....	101
Table 6.3 Nominal values and the statistical parameters of the variables.....	106

Nomenclatures

Roman Symbols

C	Capacity
CA	Normalized RMS of cable acceleration
DC	Dead load effect due to structural components and attachments
DW	Dead load effect due to wearing surface and utilities
F	Peak frequency
f_n	Measured normalized resonant frequencies
\hat{f}_n	Predicted normalized resonant frequencies
f_X	Joint probability density function of X
IM	Dynamic load allowance
k	Number of predictor variable
LL	Live load effect
N_{TR}	Traffic volume
P	Permanent loads other than dead loads
p	Number of observations
P_f	Probability of failure
Q	Load effect
Q_{DL}	Dead load effect

Q_{LL}	Live load effect
R	Resistance
R_n	Nominal member resistance
R^2	R-square
RF	Rating factor
RMS	Root mean square
$RMSE$	Root mean square error
RMS_{CA}	RMS of the accelerations of the cable
RMS_{DE}	RMS of the vertical acelerations of the mid-span deck
RMS_{TLY}	RMS of the longitudinal tilts of the mid-span deck
RMS_{TLY}	RMS of the transversal tilts of the mid-span deck
RMS_{CAi}	Filtered RMS of the accelerations of the cable
RMS_{DEi}	Filtered RMS of the vertical acelerations of the mid-span deck
RMS_{TLYi}	Filtered RMS of the longitudinal tilts of the mid-span deck
RMS_{TLYi}	Filtered RMS of the transversal tilts of the mid-span deck
se	Standard error
TR	Normalized traffic loading
TE	Normalized temperature
VIF	Variance inflation factor
X	Predictor variable
X_i	Input parameter
y	Predicted variable
y_i	Observed values
\hat{y}_i	Predicted values

z Score of standard normal distribution

Greek Symbols

β reliability index

β_i Regression coefficient

$\hat{\beta}$ Estimated regression coefficient

γ_{DC} LRFD load factor for structural components and attachments

γ_{DW} LRFD load factor for wearing surface and utilities

γ_P LRFD load factor for permanent loads other than dead loads

γ_{LL} Evaluation live load factor

ε Error

$\bar{\varepsilon}$ Mean of errors

μ_Q Mean value of the load effect

μ_R Mean value of the resistance

σ_ε Standard deviation of the errors

σ_Q^2 Variance of the load effect

σ_R^2 Variance of the resistance

Φ Standard normal distribution function

ϕ LRFD resistance factor

ϕ_C Condition factor

ϕ_S System factor

Chapter 1

1. INTRODUCTION

There are several sensing technologies to measure the environmental inputs on the structures, such as temperature sensors, wind sensors, and so on. On the other hand, the understanding of the operational inputs, i.e., the traffic live loads on the bridge, is complex to measure directly. There is actually some approaches to capture the traffic loads on the bridges, which is the weight-in-motion (WIM), for the applications of rating fatigue loads, capturing overloads, and so on. However, most WIM systems require the strict strain measurements to estimate accurate axial loads of each vehicle. Meanwhile, the load rating, which is another application of the live load information, are expected to realize stochastic discussions of the structural reliability and also the maintenance planning. For instance, the bridge load rating is recommended by the American Association of State Highway and Transportation Officials (AASHTO) in the *Manual for Bridge Evaluation* (AASHTO, 2013). It can provide a basis for determining the safe load capacities. It requires the traffic load information to define the live load factors that are used in the load rating determination. Furthermore, the traffic volume information is considered to be useful also for the effective bridge planning; e.g. the capacity

and congestion analysis, forecasting the future traffic demand, estimating the economic benefits.

This chapter aims to provide overviews of the thesis. Firstly, the motivation for this research and review of traffic load estimation are presented. Then the chapter gives aims and scope of present thesis. Finally, the layouts of this thesis are summarized.

1.1 MOTIVATION

The effective condition assessments of existing structures will be realized if not only the structural responses but also the information about input loads can be understood from the structural health monitoring (SHM) data. A number of passing vehicles associate with the degradation of bridges especially a number of trucks. The daily truck traffic volume associates with fatigue damage and is used in estimating the fatigue life of steel bridges recommended by *AASHTO Guide Specifications for Fatigue Evaluation of Existing Steel Bridges* (AASHTO, 1990). For concrete bridges, the National Cooperative Highway Research Program (NCHRP) stated in the *Effect of Truck Weight on Bridge Network Costs report* (Fu et. al, 2003) that environmental factors such as, water presence, exposure to salt might not necessarily play a driving role in concrete deck deterioration, the number of passing trucks could be the major factor for concrete deck deterioration. In addition, truck load induces fatigue cracks in reinforced concrete bridge decks and a moving load is much more damaging than a stationary pulsating load (Matsui and Muti, 1992; Perdikaris et al., 1993).

In most SHM projects, the structural conditions are tried to be assessed only from their static and/or dynamic responses, i.e., outputs. However, those structural responses are actually caused by the inputs, which include both operational and environmental ones. Therefore, the behaviors of those inputs themselves must affect on the structural conditions. For bridge structures, the traffic loads are the dominant inputs. Therefore, their information can be estimated by using the corresponding response data acquired in the SHM system.

The study contributes to the bridge evaluation and planning that are summarized in below:

- The bridge load rating that requires the traffic volume information to define the live load factors used in the load rating determination.
- The bridge reliability evaluation that requires the traffic load effects on the bridge components.
- The effective bridge planning; e.g. enhancing the bridge inspection scheduling by taking account of the traffic volume, the capacity and congestion analysis, forecasting the future traffic demand, estimating the economic benefits.

1.2 INTRODUCTION OF SHM

SHM is any automated monitoring system which aims to assess the condition of a structure in order to ensure the safety and enhance the maintenance management of the structure. The SHM process began in oil rig structures and then have been applied in aircrafts (Doebeling et al., 1996). Now, the SHM is a prefer system for structures and mechanical systems that are expensive or difficult to replace, or associate with safety of users such as bridges, power plants, rotating machines and large scale buildings. The SHM system can be operated on-line and on in-service systems. While, the conventional approaches for assessing structural conditions such as the nondestructive testing (NDT), are usually off-line operation or time-based inspections. In addition, the SHM is technology that can develop the traditional time-based maintenance approaches to the condition-based maintenance approaches (Farrar and Worden, 2013).

1.2.1 Objectives and Benefits of SHM

There have been several researches on SHM applications including damage identification, structural service-life estimates, and load capacity evaluations. There were a large number of studies that devote to damage detection using SHM data processing. In contrast, a relatively small number of studies were associated with the evaluation of structural capacity or estimation of service-life of structures (Seo et al., 2015). The damage detection have been interested because it is expected to detect damages, or faults in the structural system at the earliest possible time to prevent severe consequences. For the ideal SHM implemented to damage identification, it is expected to determine all of damage states classified by Rytter (1993) into four levels as follows:

1. Damage detection: detecting damages in the system.
2. Damage localization: determining where damages take place in the system.
3. Damage extent: evaluating type and severity of the damages.
4. Prognosis: predicting the remaining life of the system.

The difficulty of damage state determination increases by these levels and no method can solve all problems. There have been many initiatives that have contributed to detection strategies while the damage extent and prognosis are the most difficult issues (Montalvao et ai., 2006). However, only the first level, damage detection could create a great benefit in human life safety if the SHM can early alarm that the system might be unsafe. Moreover, the SHM could detect damages in any areas of the system that are difficult to access or cannot be detected by visual inspections.

1.2.2 SHM organization

In order to achieve the aims of SHM, there are many ways to organize the SHM process (Farrar and Worden, 2007). The well known way defined by Farrar et al. (2001) is a four-step statistical pattern recognition paradigm. This process begins to set the limitations on what and how will be monitored and accomplished, as call *operational and evaluation*. It answers two

questions in the implementation of SHM as following; (i) what are the operational and environmental conditions under which the system to be monitored functions and (ii) what are the limitations on acquiring data in the operational environment. It also starts to set the damage detection process to define the features associating with damages that are to be detected.

The next process is *data acquisition and cleansing*, the data acquisition process involves selecting types of sensors used in the SHM and locations where the sensors should be installed, and defining the data acquisition hardware. In this process, it should be considered how often and how long the data have to be collected, and economic factors play a dominant role in decision making. In the data collection, the data should be measured adequately to cover environmental and operational variability in order to normalize the measured data. The data normalization is important to the damage detection process. It allows one to understand changes in measured data caused by the environmental and operational conditions leading to detection the changes caused by other factors. For data cleansing, it is the process that chose the measured data to be accepted or rejected in the next process. Usually, the data cleansing method is individual and depends on data acquisition aspects (Sohn, 2007).

Typically, the SHM system produces a large amount of data therefore it is necessary and advantageous to consider the acquired data for using in analysis, this procedure is call *feature selection*. The feature selection process aims to identify the data features that can be used to distinguish between the undamaged and damaged conditions. In general, the damage can be defined as changes of the system that adversely effect on its performance (Farrar and Worden, 2007). For structural systems, such changes include the changes in material properties and the boundary conditions. Therefore, the features that are sensitive to the system changes caused by damages are desirable. However, the damage-sensitive features usually are sensitive to the structural changes caused by environmental and operational variability as well. The multivariate features have been adopted for effective features used in damage detection.

For the last step, *statistical model* is developed to enhance the damage identification process by using the algorithms that analyze the selected features to assess the damage states of the structure. There is advantage in using the statistical technique that only measured data of undamaged structure can be used for detection damage. If any output of the statistical model

constructed from undamaged data by using the measured data as inputs, deviates from the outputs obtained from undamaged data, it could be suggested that there is damage or anomaly in the structure. Based on statistical technique, it provides the probability of the structure being undamaged or damaged conditions. The accuracy of the condition assessment of the model involves with the trained data and the algorithms.

Figure 1.1 shows a flow chart that summarize the SHM organization. The process involves measurement of responses, excitation and environment of the structure, extraction the features from the acquired data, and analysis the selected features to assess the conditions of the structure.

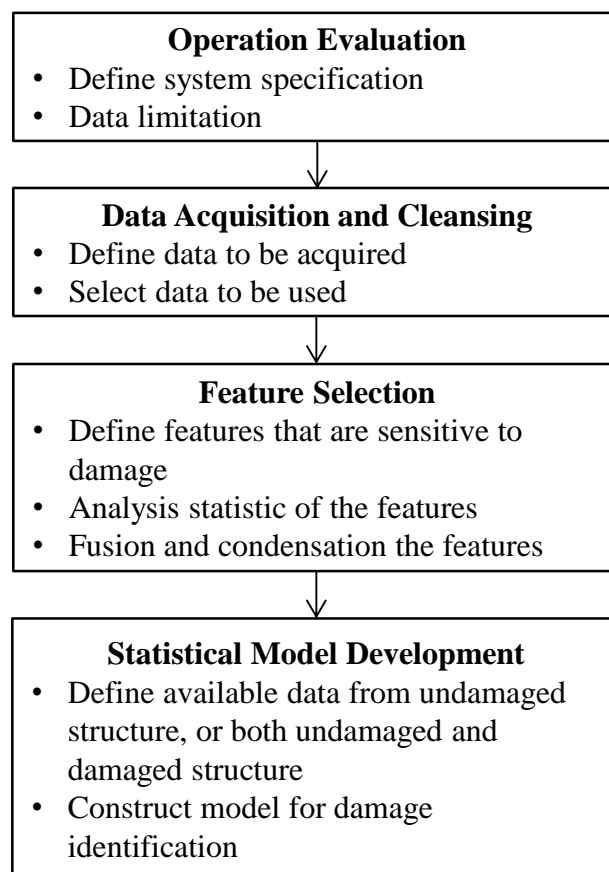


Fig. 1.1 Flow chart of SHM organization (Farrar et al., 2001)

1.2.3 Structural Condition Assessment from SHM Data

The most common measured data in the SHM system are dynamic responses that can be measured by installed sensors. Usually, no sensor can detect damage in the structure directly (Worden et al., 2007). However, the dynamic responses can be associate with the physical properties of the structure. For this reason, there have been several researches in vibration-based damage identification. The background of this method is that the modal parameters (resonant frequencies, mode shapes and modal damping) that are extracted from the measured dynamic responses, are functions of the mass, stiffness and damping of the structure. Therefore, detectable changes in extracted modal parameters will be caused by changes in the physical properties (mass, stiffness and damping) (Doebbling et al., 1998) that might be caused by damage. For measured strain data, the measurements of strain are very common and most generally applied for small scale structures (Cross, 2013). Especially in the SHM of aerospace structures, the strain data are applicable for monitoring (Staszewski et al., 2004, Hunt et al., 2001)

When the dynamic responses or modal properties of a structure are used in the SHM, the excitation properties are also important for modal analysis. The artificial excitation that can be known the properties has been applied, such as a hammer and a shaker (Peerter et al., 2001). The artificial excitation is usually applied on small to moderate structures. In the case of large structures such as long-span bridges, it is difficult and costly to obtain significant levels of response by using the artificial excitation. Therefore, ambient vibration becomes the practical ways of exciting the structure (Siringoringo and Fujino, 2007). The ambient excitation of bridge structures is excitation from environmental loads such as wind and temperature, and operational loads such as traffic load which, in practice, is complex to be measured. It could be said that in the SHM system, most acquired data are usually only the responses of the bridge. Whereas, the information of operational excitation or traffic load can be obtained from traffic monitoring systems.

1.3 TRAFFIC MONITORING

Information about the dynamic loading that is traffic live loads on bridges can contribute to rating and maintenance of bridges and transportation infrastructures. The bridge load rating is the process of evaluation the safe load capacity of the bridge or the maximum load that a particular bridge can carry for a one time loading (Wall et al., 2009). Typically, live load effects from trucks have a more significant effect on the safe-life of the bridge than passenger cars. Therefore, truck data are important for many applications of bridge maintaining and planning.

There are varieties of systems for monitoring traffic data. Different techniques can measure different traffic data such as traffic volume, classification, speed and weight data. Traffic monitoring technologies are divided into two categories as followed: (1) intrusive detectors which require installing sensors in or on the roadway surface, and (2) non-intrusive detectors of which sensors are installed above, beside or below the roadway. So the installed sensor do not disturb the traffic flow (AASHTO, 2009).

The intrusive sensor technologies can be categorized into two groups that are the technologies measuring only number of axles or vehicles, and those that can provide axle weight information in addition to axle counting. The axle counting technologies include *road tubes*, *contact closure and other switches*, *inductive loops*, and *magnetic detectors*. The road tubes and contact closure switches are vulnerable to be dislodged from the roadway because they are placed on top of the road surface. Therefore, they can be used as temporary counting equipment. The inductive loops are commonly used for permanent vehicle detector. The loop wires are placed into the surface pavement. When the installation are poor, the loop wires can be easily broken. Moreover, water infiltration can adversely effect on the loop performance. Like inductive loops, magnetic detectors are used for permanent vehicle counting by installing sensors underneath the roadway. For the technologies that can be used to estimate axle weight information, they include piezoelectric sensors, fiber optic cable, capacitance sensors, bending plate, hydraulic load cell, and bridge strain sensors. These sensor technologies are applied in the WIM systems that are prominent traffic monitoring technologies and have been developed in recent years.

1.3.1 WIM Technologies

Information on traffic data especially, trucks is important for maintaining and planning the infrastructures in transportation networks as aforementioned. WIM is the process of estimating a moving vehicle's gross weight and the portion of that weight that is carried by each wheel, axle or axle group or combination thereof, by measurement and analysis of dynamic vehicle tire forces (ASTM, 2009). Before development of WIM, gross vehicle weights were only obtained by using static weigh stations. The static stations can get data of a very small portion of a total of vehicle population and illegally overloaded drivers avoid the stations when weighing operations are processing. It can lead to biasness of statistical data (O'Brien and Leahy, 2011). While the WIM systems can weigh vehicle they are moving. The WIM systems usually use sensors installed in road pavements for determining characteristics of the passing vehicles, that are vehicle speed, gross weight, axle weights, and spacing of the axles. The WIM systems adopt different technologies of sensors, depending on various factors that are target applications, environment, budget, and desired accuracies. The basic sensor technologies are piezoelectric systems, capacitive mats, bending plates, load cells and optical fibers (Yannis and Antoniou, 2005). As the measured vehicles are moving, the WIM measures dynamic loads, but actually, the statistic load or actual loads are need measuring. Subsequently, the actual loads are estimated based on the measured dynamic loads and appropriate calibration parameters (Bushman and Pratt, 1998). There are efforts associated with use of the WIM technologies to overcome challenges in installing the WIM sensors in the road surface. The sensors need to be embedded in or adhered in road pavements. Both techniques require working in the traffic pavements. Therefore, it makes the WIM systems dangerous and costly for installing and maintenance. Additional, WIM approach roughness critically effects on the accuracy of the WIM systems because of influences of the vehicle dynamics and it is difficult to install and maintain the smooth WIM approaches (Wall, 2009).

Bridge weigh-in-motion (B-WIM) is an alternative WIM. The B-WIM involves sensor instrumentation of a bridge and uses the bridge responses to determine WIM data. B-WIM systems utilize strain sensors or transducers, installed underneath the bridge decks as

shown in **Fig. 1.2** and use algorithms to estimate vehicle gross weights and axle weights when the vehicles are passing the bridge. B-WIM was first proposed in the USA by Moses (1979) but the advanced B-WIM systems were developed by the European research project *Weigh-in-motion of Axles and Vehicles for Europe* (WAVE) (Jacob, 1999 and 2002). The commercial marketed system is the SiWIM (Ieng et al., 2011). The earlier B-WIM systems required both strain sensors installed underneath the bridge decks and axle detectors installed on the pavements. While the SiWIM system uses only removable strain sensors placed under the decks. This technique is called “Free of Axle Detectors” (Znidaric et al., 1999). Therefore, the B-WIM systems have advantages over the road WIM systems, that: civil engineering works on the traffic pavements are not needed for installing the systems, the installation does not interrupt the traffic flow, the systems are not visible for the drivers, and the systems should be more durable because they are not directly exposed to the traffic loads and adverse environmental (Ieng et al., 2011).

Developments and Limitations of WIM Systems

There have been several initiatives that contributing to the enhancement of WIM systems in recent years. In Europe, the WAVE is a significant advancement (WAVE, 2001) as aforementioned and there have been considerable researches conducted under the *European Cooperation in Science and Technology* (COST) project 323 resulted in a WIM standard with a standardized accuracy classification method (Jacob et al., 2002).



(a) Installation of B-WIM



(b) Installed strain sensor

Fig. 1.2 B-WIM installation (Ieng et al., 2011).

In the United States, the *Standard Specification for Highway Weigh-In-Motion (WIM) Systems with User Requirements and Test Methods* by the American Society for Testing and Materials (ASTM) (ASTM, 2009) is the primary specification including specific installation, calibration procedure and data validation procedure. For international society, there is the *International Society for Weigh-In-Motion (ISWIM)* which comprises of researcher, manufacturers and end users of the WIM (ISWIM, 2007). The ISWIM was founded for supporting uses of WIM technologies, such as, development in WIM technologies, standardization of WIM system, promoting on use of WIM, and WIM data applications.

The accuracy of road WIM systems depend on site characteristics which have influences on the in-motion behaviors of vehicles. The effects of vehicle behaviors can lead to large discrepancies between the axle impact forces and the corresponding static loads. There are specified criterion about road geometry and pavement characteristics, proposed by the COST323 to reduce the discrepancies. For the B-WIM systems, their accuracy highly depends on the type of the bridge superstructure and the roughness of the approach (Jacob et al., 2002). The current B-WIM systems are efficient for appropriate kinds of bridges, such as integral slab bridges (Ieng et al., 2011). In the WAVE projects, the B-WIM techniques were investigated and found that the presence of multi heavy vehicles on the bridge at the time of weighing induced higher errors than when only one vehicle was present individually. If short bridges were used, the probability of multi presence vehicles was very low (WAVE, 2001).

It can be concluded that the WIM systems have some limitations of applications that have not been solved yet and strictly require measured strain data. Especially the sites that have a large number of heavy vehicles or multiple traffic lanes, it is very difficult and dangerous to install and maintain the WIM systems on the large traffic volume roads and the discrepancies between the axle impact forces and the corresponding static loads tend to be large or unacceptable. For the long span or complex structure bridges, it is also not suitable to use for instrumenting B-WIM systems as the presence of more than one vehicle at the weighing time, and recent WIM algorithms have not been developed for the complex bridges.

1.3.2 Non-intrusive technologies

Although, the intrusive traffic monitoring technologies are most usually used, there are significant drawbacks that these technologies require installing sensors in or on the roadway. As a result, staffs must work in hazardous conditions and the traffic flow must be disrupted for sensor installation and maintenance (excluding the B-WIM that can solve these drawbacks). Therefore, the non-intrusive technologies for traffic monitoring have been developed in order not to install sensors in or on the roadway. These sensor technologies observe the traffic flow from beside or above the roadway. However, the non-intrusive technologies can provide only number of vehicles without weight information. The currently available non-intrusive technologies are *video image detection systems (VIDS)*, *doppler and microwave radar*, *Infrared*, *Laser detectors*, *acoustic arrays*, *ultrasonic*, and *automatic vehicle identification (AVI) systems*. These technologies also have some drawbacks. The common drawback is that the equipment detecting vehicles from beside or above the roadway, sometimes cannot detect the hidden vehicles from the view of the equipment by other vehicles. Each technology has individual drawbacks, for example, the video image detection system cannot work well under poor visibility conditions such as heavy rain, snow, lack of light and changing light conditions. The acoustic technologies also cannot work properly under high level of noise. Therefore, no traffic monitoring is suitable for all sites.

1.3.3 Novelty Traffic Monitoring

This study proposes the new approach for estimating the bridge traffic volume by constructing a statistical model using only the dynamic response data acquired in the SHM system, and proposes the methodology of modeling based on the correlation coefficients.

1.3.4 Traffic load information in Bridge Reliability

For bridge evaluation, it is generally based on reliability analysis. The reliability-based evaluation refers to procedures in which reliability determination considers the statistical

distributions of loads and resistances. In the reliability-based evaluation of bridges circumstances, there is bridge load rating that providing a basis for determining the safe load capacity at the target reliability (AASHTO, 2013). In the evaluation of bridges, the evaluators will determine various rating depended on the considered loads (Moses, 2001). For example, in the Load and Resistance Factor Rating (LRFR) method (AASHTO, 2013), there is rating for the design loads, legal loads, and permit loads. Likewise, if information of the operating loads or traffic loads is acquired, the reliability of the bridge under operation can be determined. The operating reliability is useful and practical for bridge maintenance and planning more than those based on the standard loads. In the reliability analysis, the traffic loads are considered as random quantities that can be described by statistical parameters reflecting the uncertainties of their values.

1.4 AIMS AND SCOPE

The aims of this study are to estimate the traffic live loads by using available dynamic response data obtained from the SHM system installed on an in-service cable-stayed bridge in Bangkok, Thailand, and to evaluate the safe load capacity and reliability of the bridge based on the estimated traffic loads. In order to accomplish the aims, the first task is to investigate effects of varying environment and operation on the measured responses of the bridge especially, the effects of traffic loads. With a sound understanding of this gained, response features associating with the traffic loads can be selected and ways to construct relationships between the selected responses and the traffic loads by using statistical models can be attempted. The second half of this study is devoted to applications of estimated traffic loads obtained from the statistical models for evaluating safety of the bridge and bridge planning.

1.5 OUTLINES OF THE THESIS

The thesis is consists of seven chapters. The first chapter is introductory chapter. In second chapter, the details of a target bridge, its SHM system and data for analysis are described. Chapter 3, 4, 5 and 6 presents the methodology and results of the study. Last chapter gives conclusions and provides some recommendations. Tables and figures are embedded in the text and all the references cited in the text are listed at the end of thesis. The nomenclatures are consistent throughout the thesis. The detailed organization of the thesis is summarized as follows:

Chapter 1 mentions the motivation, aims and scope of the present thesis. At the end, the outline of the thesis is presented.

Chapter 2 introduces the target bridge and SHM campaign. Details of the acquired data available for analysis in this study and extracted features are given.

Chapter 3 investigates and discusses the effects of environmental and operational variability on the dynamic responses and extracted features.

Chapter 4 presents Finite Element (FE) modeling of the target bridge and analytical dynamic responses, and compares the analytical responses with those from the measurement.

Chapter 5 presents developing a estimation model of the traffic volume. The procedure based on the detail correlation analysis for selecting features using in the model is proposed, and after constructing a statistical model, the estimation and prediction qualities are discussed by the comparison with the actual traffic data.

Chapter 6 demonstrates the applications of the estimated traffic loads for the safe load capacity evaluation and reliability analysis and results are discussed.

Finally, the conclusions and discussions of this study are provides in Chapter 7.

REFERENCES

American Association of State Highway and Transportation Officials (AASHTO). *Guide Specifications for Fatigue Evaluation of Existing Steel Bridges*. Washington, DC: American Association of State Highway and Transportation Officials; 1990.

American Association of State Highway and Transportation Officials (AASHTO). *Guidelines for traffic data programs*. Washington, DC: American Association of State Highway and Transportation Officials; 2009.

American Association of State Highway and Transportation Officials (AASHTO). *The Manual for Bridge Evaluation second edition*. Washington, DC: American Association of State Highway and Transportation Officials; 2013.

ASTM International. *Standard Specification for Highway Weigh-In-Motion (WIM) Systems with User Requirements and Test Methods*. Designation: E 1318-09, West Conshohocken, PA, 1-16; 2009.

Bushman R. and Pratt J. A. Weigh In motion Technology - Economics and Performance. *Proc. NATMEC 98 : North American Travel Monitoring Exhibition and Conference*, May 11-15, Charlotte, NC, US; 1998.

Jacob, B., OBrien, E.J., & Jehaes, S. *Weigh-In-Motion of Road Vehicles*. Final Report of the COST 323 Action. LCPC Publications, Paris; 2002.

Cross E. J., Brownjohn J.M.W. & Worden K. Long-term monitoring and data analysis of the Tamar bridge. *Mechanical systems and signal processing*, pp. 16-34; 2013

Doebbling S.W., Farrar C.R., Prime M.B., and Shevitz D.W. A summary review of vibration-based damage identification methods. Technical report, Los Alamos National Laboratories; 1998.

Farrar, C. R., Doebbling, S. W. & Nix, D. A. Vibration-based structural damage identification. *Phil. Trans. R. Soc. A* 359, 131–149; 2001.

Farrar C. R. and Worden K. An introduction to structural health monitoring: *Phil. Trans. R. Soc. A*(365): 303-315; 2007.

Farrar C.R. and Worden K. *Structural Health Monitoring: A Machine Learning Perspective*, New York, NY John Wiley; 2013.

Fu et al. *Effect of Truck Weight on Bridge Network Costs report*. National Cooperative Highway Research Program (NCHRP) Washington, D.C. : Transportation Research Board; 2003.

Hunt S.R. and Hebden I.G.. Validation of the Eurofighter Typhoon structural health and usage monitoring system. *Smart materials and structures*, 10:497; 2001.

Ieng S. S., Schmidt F., Romboni F., and Jacob B. Assessment of a Bridge WIM System on Integral Concrete Bridges and on Steel Orthotropic Decks *Proc. 1st International Seminar of Weigh in Motion* Florianópolis, Santa Catarina, Brazil, April 3 rd to 7 th; 2011.

ISWIM. “International Society for Weigh-In-Motion.” LCPC, Website <<http://iswim.free.fr/>>; 2007.

Jacob, B. *Proceedings of the Final Symposium of the project WAVE (1996-99)*, Paris, May 6-7, Hermes Science Publications, Paris, 352 pp; 1999.

Jacob, B. *Weigh-in-motion of Axles and Vehicles for Europe*, Final Report of the Project WAVE, LCPC, Paris, 103 pp; 2002.

Matsui, S. and Muti, K. "Rating of Lifetime of A Damaged RC Slab and Replacement by Steel Plate-Concrete Composite Deck", Technology Reports of the Osaka University, Vol.42, No.2115, p.329, October, 1992.

Montalvao, D., N. M. M. Maia, et al. A review of vibration-based structural health monitoring with special emphasis on composite materials. *Shock and Vibration Digest* 38(4): 295-324; 2006.

Moses, F. Weigh-in-Motion System Using Instrumented Bridges. *Transportation Engineering Journal of ASCE*, 105 (TE3), 233-249; 1979.

O'Brien J. E., and Leahy C. Review of weigh-in-motion systems. *Proc. 1st international Seminar of Weigh in Motion* Florianópolis, Santa Catarina, Brazil, April 3 rd to 7 th; 2011.

Peeters B., Maeck J., and De Roeck G. Vibration-based damage detection in civil engineering: Excitation sources and temperature effects. *Smart Materials and Structures*, 10(3):518–527, 2001.

Perdikaris, Philip C., and Petrou, Michael, "Code Predictions Versus Small Scale Bridge Deck Model Test Measurements", *Transportation Research Record* 1290, p.179; 1990.

Rytter A. Vibration-based inspection of civil engineering structures. PhD thesis, Department of Building Technology and Structural Engineering, University of Aalborg, Denmark, 1993.

Seo, J., Hu, J., and Lee, J. Summary Review of Structural Health Monitoring Applications for Highway Bridges." *J. Perform. Constr. Faci*, 10.1061/(ASCE)CF.1943-5509.0000824; 2015

Siringoringo D, Fujino Y. System identification of suspension bridge from ambient vibration response. *Eng. Struct.*, pp. 462–477; 2008.

Sohn, H. Effects of environmental and operational variability on structural health monitoring. *Phil. Trans. R. Soc. A* 365, 539–560; 2007

Staszewski W., Tomlinson G., Boller C., and Tomlinson G.. Health monitoring of aerospace structures. Wiley Online Library; 2004.

Wall J. C., Christenson E. R., Anne-Marie H., and McDonnell, P.E. A Non-Intrusive Bridge Weigh-in-Motion System for a Single Span Steel Girder Bridge Using Only Strain Measurements. A Project in Cooperation with the U.S. Department of Transportation Federal Highway Administration; 2009.

WAVE. *Weigh-in-motion of Axles and Vehicles for Europe*. General Report, LCPC; 2001.

Worden K., C.R. Farrar C.R., Manson G., and Park G. The fundamental axioms of structural health monitoring. *Proceedings of the Royal Society A: Mathematical, Physical and Engineering Science*, 463(2082):1639, 2007.

Yannis, G. and C. Antoniou. Integration of Weigh-in-Motion Technologies in Road Infrastructure Management. *Institute of Transportation Engineers Journal*, 75.1, 39-43; 2005.

Znidaric, A., Dempsey, A. , Lavric, I. and Baumgärtner, W., B-WIM Systems without Axle Detectors, *Weigh in Motion of Road Vehicles*, ed. B. Jacob, Hermes Science Publications Paris, pp. 101-110; 1999.

Chapter 2

2. ACQUIRED SHM DATA AND FEATURE EXTRACTION

This chapter presents data obtained from a SHM system installed in an in-service cabled-stayed bridge in Thailand. The SHM system consists of various sensors deployed on the bridge to capture the responses excited by traffic, changing temperature and wind. Multivariate features associated with dynamic characteristics were extracted from the monitored data.

2.1 TARGET BRIDGE AND SHM SYSTEM

The target bridge in this study was the Bhumibol-Bridge-I, which is shown in **Fig.2.1**. This is a cable-stayed bridge crossing the Chaopraya River in Bangkok, Thailand. The bridge was opened on September 2006, and it is a part of the Industrial Ring Road; therefore, not only the passenger cars but also many trucks are crossing per day. The SHM system has been installed for ensuring the structural safety since April 2014 operated by the Department of Rural Road (DRR), Thailand. The acquired data are expected to be appropriately used for the effective operation and maintenance of this important bridge.

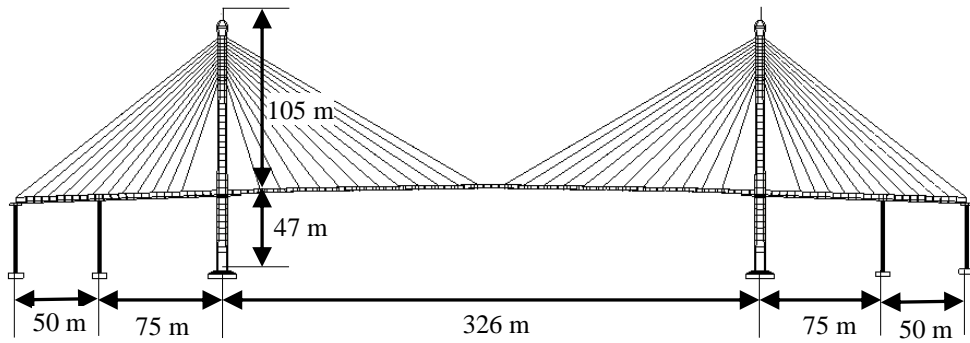


Fig. 2.1 A picture of Bhumibol-Bridge-I

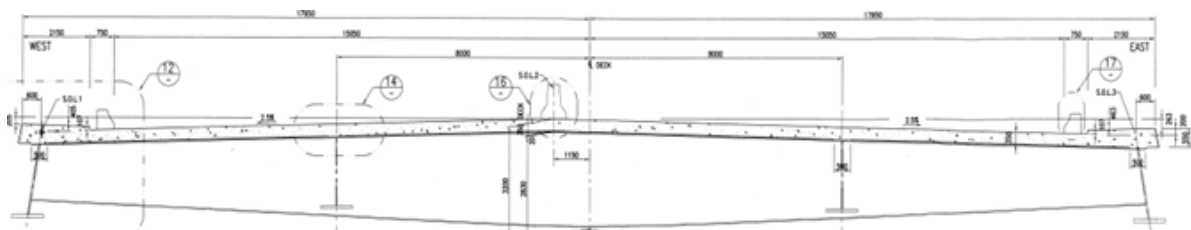
2.1.1 Target Bridge Descriptions

The target cable-stayed bridge consists of the composite deck in the main span with the length of 326 m and the post-tension concrete box decks in each of both side spans, the length of which is 125 m. The deck is supported by the two diamond-shaped towers with the height of 152 m and the four piers in the side span, both of which were constructed from the reinforced concrete as shown in **Fig. 2.2**. The fixed connections between the deck and the towers and piers

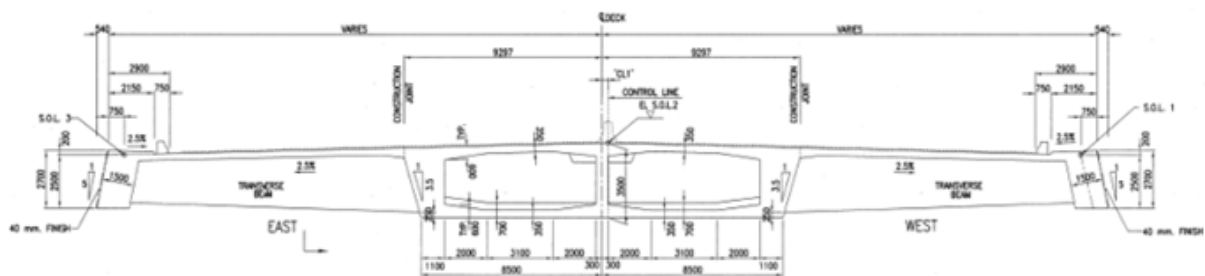
are homogenous stressed concrete, and there are expansion joints at the ends of both sides of the side span deck.



(a) Bridge dimensions



(b) Main span deck



(c) Side span deck

Fig. 2.2 Bridge descriptions

2.1.2 Installed SHM System

The SHM system consists of several kinds of sensors and the data acquisition system. The deployed sensors were six accelerometers (“AC”), five tilt sensors (“TL”), two displacement transducers (“DP”) and five temperature sensors (“TS”), each of which is installed on the main span deck, the top of towers, the stayed-cables, and the expansion joints, as illustrated in **Fig. 2.3**. The accelerometers were the servo-type with the input range of ± 4 g and the sensitivity of 500 ± 15 mV/g, and all of them were the tri-axial (x -, y - and z -directions) ones. The tilt sensors are the bi-axial (x - and y -directions) sensors with the angular range of ± 20 degree and the sensitivity of 100 ± 10 mV/degree, and the temperature sensors were the resistive temperature sensors with the measurement range of -50 to $+400$ °C. The data are acquired continuously with the sampling frequency of 50Hz in all sensors with synchronizations. The acquired data are stored into the database and automatically transferred to a control computer placed on the control office near the bridge every minute.

To acquire the traffic volume information, the traffic counting system using the image processing technique was installed on the bridge. The system is known as a non-intrusive method of traffic-flow measurement using fifteen video cameras mounted on the road sign structures of the bridge. The acquired video data are fed into the processors that count and classify the passing vehicles (Allied Telesis, Inc, AT-MC 130XL model).

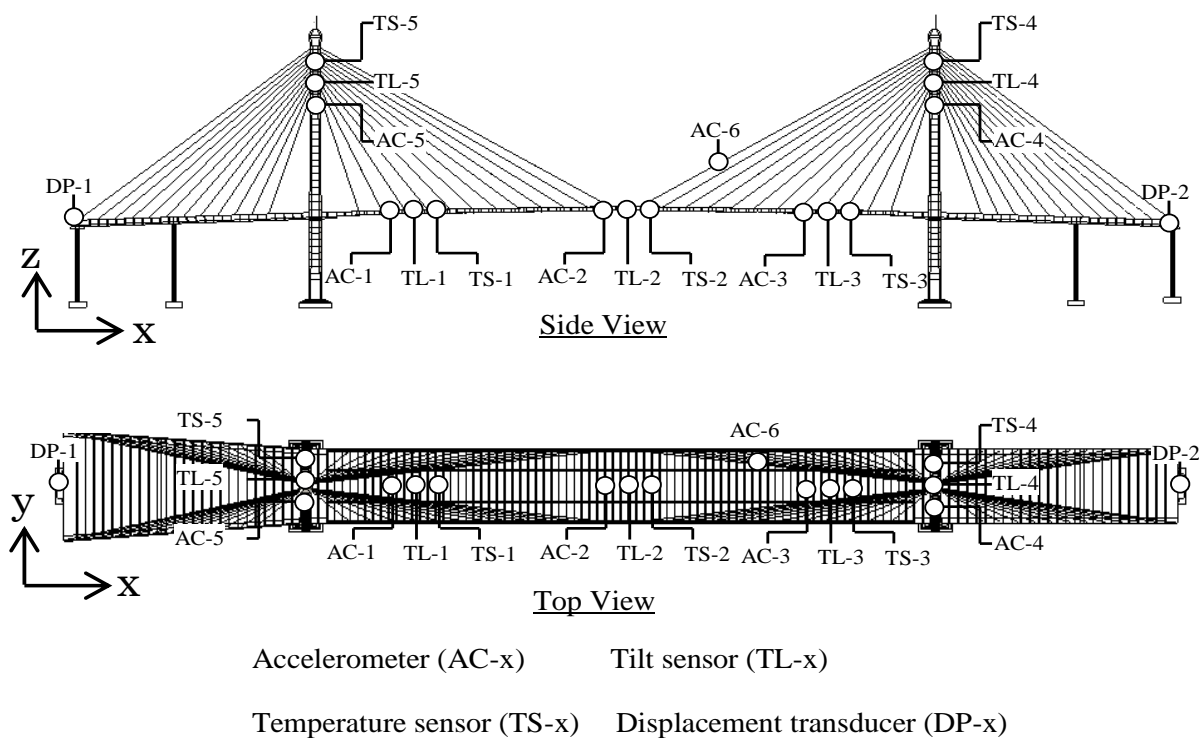


Fig. 2.3 Sensor configuration of the SHM system

2.2 ACQUIRED SHM DATA

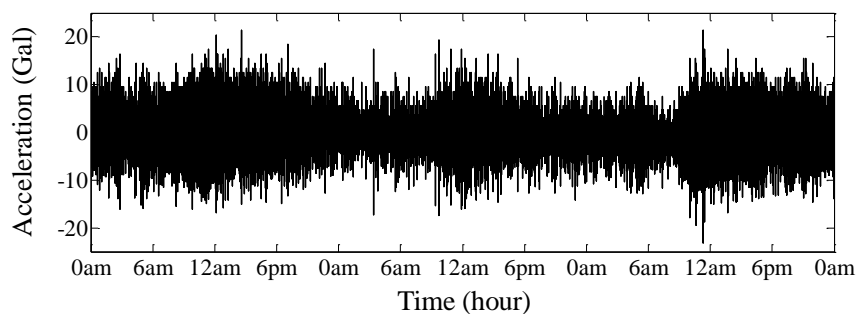
2.2.1 Bridge Responses and Environmental Data

Some data were selected from all SHM data for the verifications in this study; the accelerations (x , y , and z -directions) at the mid-span (AC-2), the tilts (x and y -directions) also at the mid-span (TL-2), the accelerations of the stayed-cable in perpendicular direction (AC-6). The temperature data at the mid-span (TS-2) were also used as the significant environmental effects. Some of selected data; the vertical (z -direction) acceleration from AC-2, the accelerations of the cable AC-6, the longitudinal (x -direction) tilt from TS-2, and the temperature in TS-2 for three days (from May 17th to 19th, 2014), are shown in **Fig.2.4**. It can

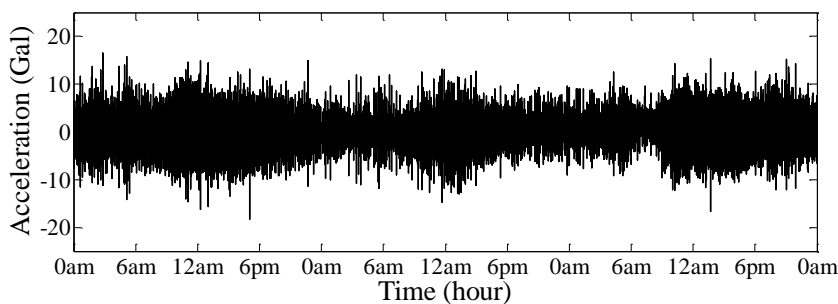
be roughly observed that the amplitudes of all dynamic responses become relatively large during the daytime, and they decrease during the nighttime. In the temperature plot, the daily variance of each day is approximately 2 °C with the range of 29-32 °C. Notice that, in Bangkok, the daily and seasonal temperature variations are small; around 10 °C through a year. Therefore, the use of those three days data was considered to be appropriate for the investigation of the temperature effect in this study.

2.2.2 Traffic Data

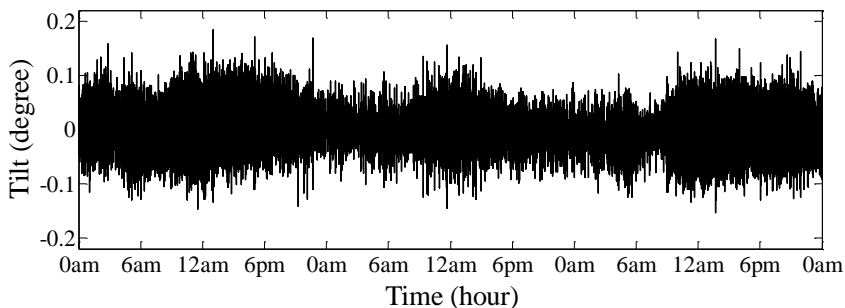
The installed traffic counting system can classify the passing vehicles to several types of vehicles; the passenger car, and the trucks that are categorized to the single truck and the trailer as shown in **Fig. 2.5**. There are restrictions for the axle and gross weights of trucks; 5 tons for the single axle with single-tire, 20 tons for the tandem axles with dual-tires, and 25 and 45 tons for the restrictions of the gross weights of the single truck and the trailer, respectively. The passenger car is the vehicle with definition of the gross weights might vary within the range of 1 to 2 tons; therefore, the weight of 1.5 tons is used as the gross weight in the counting system. In order to represent the total traffic volume, the number of each type of vehicles was converted to the number of equivalent trucks with the gross weight of 25 tons by; multiplying by its gross weight and dividing by 25. **Figure 2.6** shows the acquired traffic data; the plots of the number of equivalent trucks categorized to the passenger cars, the single trucks and the trailers. The figure firstly indicates that the single trucks and the trailers are the dominant vehicles passing on the bridge. The number of the passenger cars shows high volumes only in the evening of three days, and in the morning of Monday. This is considered because the number of passenger cars can effect on the traffic-flow conditions on the bridge. For instance, the high number of passenger cars during the peak-hours can cause the dense traffic or traffic congestion. On the other hand, the number of the single trucks and trailers increases in the daytime and decreases in the nighttime because the trucks avoid the traffic congestion on the road networks during morning and evening peaks. In addition, the large drop in the number of equivalent trucks at around 8:00 am on Monday is due to the traffic congestion that always occurs in weekdays as shown in **Fig. 2.7**. In summary, the traffic volumes have a daily trend and large fluctuations within a day.



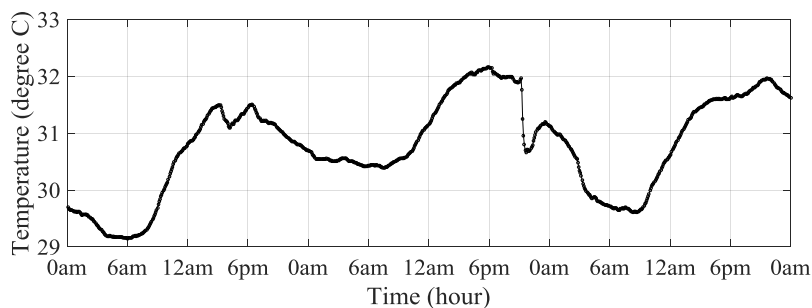
(a) Vertical acceleration of the deck at AC-2



(b) Acceleration of the stayed-cable at AC-6



(c) Longitudinal tilt of the deck TL-2



(d) The averaged temperature at TS-2

Fig. 2.4 Acquired dynamic responses and temperature for three days; Saturday, May 17, 2014, Sunday, May 18, 2014 and Monday, May 19, 2014

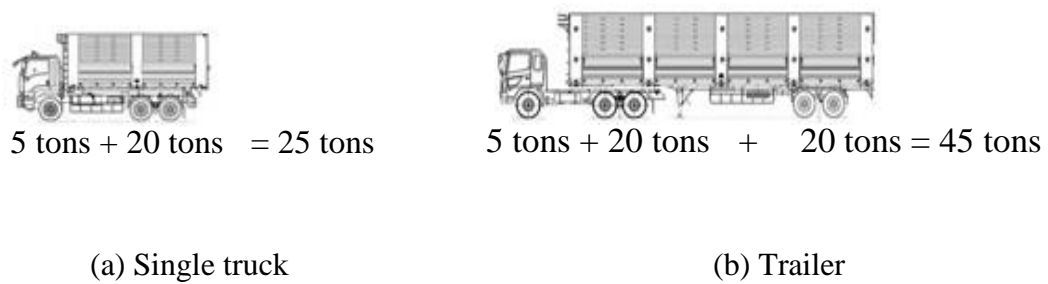


Fig. 2.5 Restricted axle and gross weights of a single truck and trailer

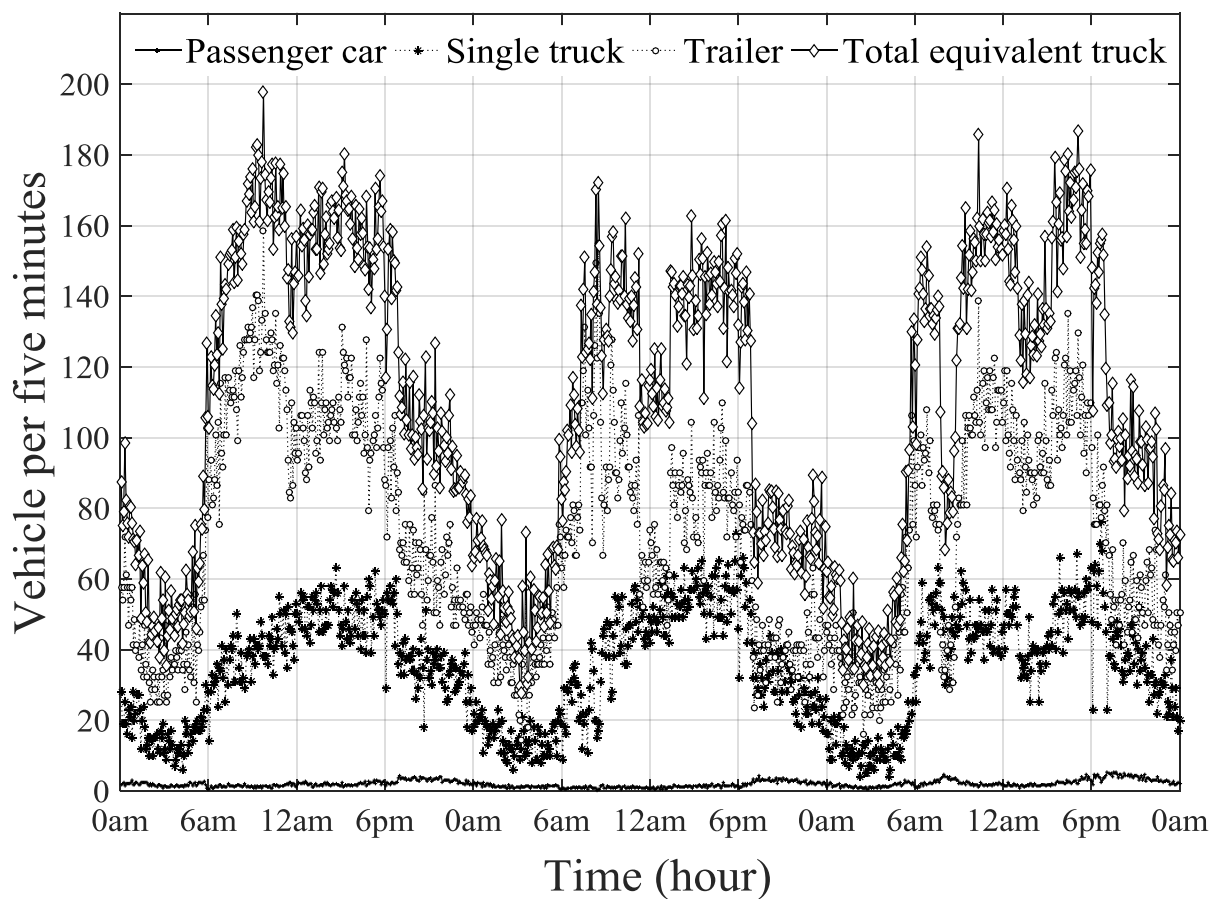


Fig. 2.6. Monitored traffic volume for three days; Saturday, May 17, 2014, Sunday, May 18, 2014 and Monday, May 19, 2014

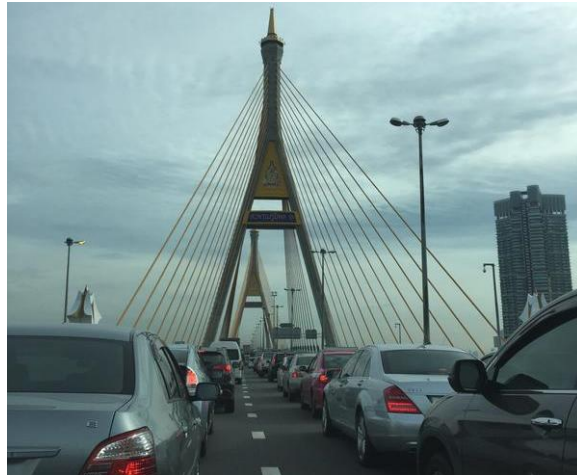


Fig. 2.7. Traffic congestion on the bridge

2.3 MODAL PARAMETERS

2.3.1 Resonant Frequencies

The resonant frequencies were determined from the peak observation on the power spectral density (PSD) of the vertical acceleration of the deck in every five minutes measurement (15,000 data length). **Figure 2.8** shows one of the PSDs and its first ten peaks that indicate the first ten resonant frequencies. It was determined by the Welch method with the FFT length of 15,000, 50% overlap with the hanning window; therefore, the frequency resolution was 0.003 Hz. The plots of the first four peak frequencies through the three days are shown in **Fig. 2.9**. It can be observed that there are slight daily trends in all peak frequencies, in which the frequencies decrease during the daytime and increase during nighttime.

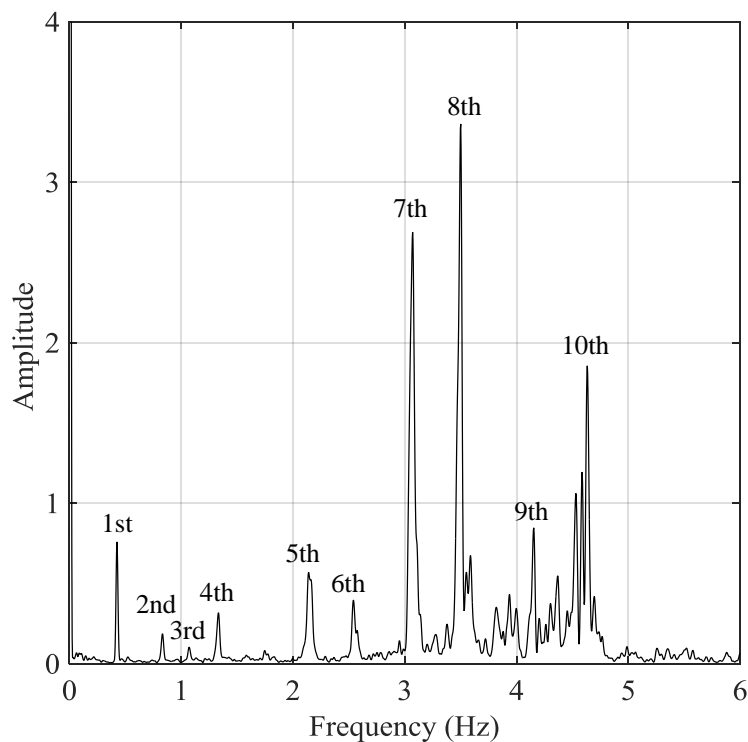
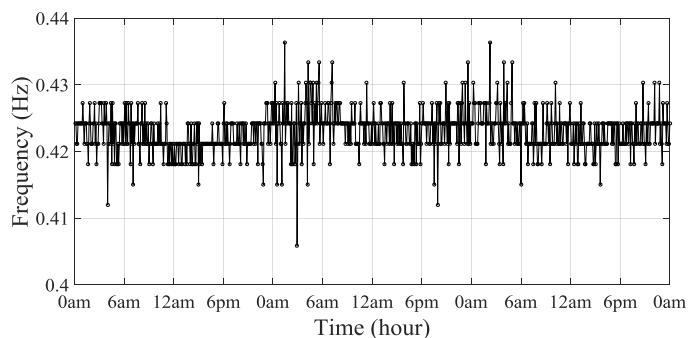
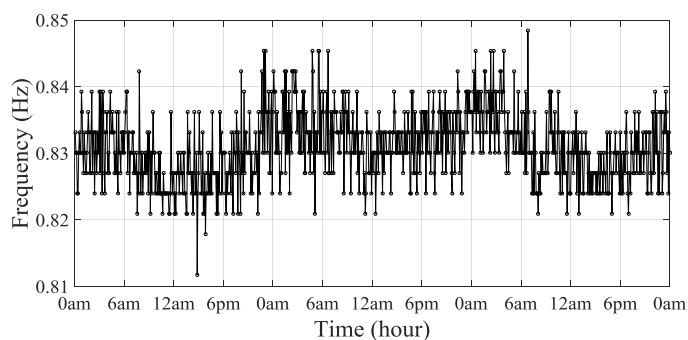


Fig. 2.8 PSD and its first ten peaks of vertical acceleration of the deck

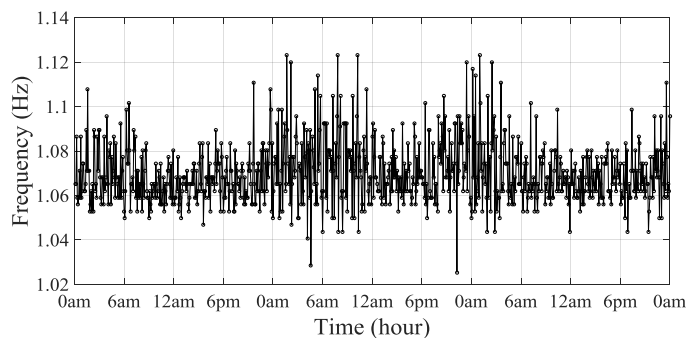
The enlarged spectrum around the first four peak frequencies of the three PSDs derived from the significant time ranges in May 17th, 18th and 19th are shown in **Fig. 2.10**; 3:00 – 3:05am with small traffic (around 40 vehicles per five minutes, 29 °C), 7:00 – 7:05am with medium traffic (around 125 vehicles per five minutes, 29 °C), 11:00 – 11:05am with large traffic (around 165 vehicles per five minutes, 31 °C). It could be considered that both the peak frequencies and their amplitudes had correlations especially with the traffic volume especially in the 1st and 4th peaks. In those figures, when the traffic loads and vibration magnitudes increase, the resonant frequencies tend to decrease, and their amplitudes increase. Therefore, not only the peak frequencies but also the amplitudes were adopted as the features to analyze the traffic and temperature effects.



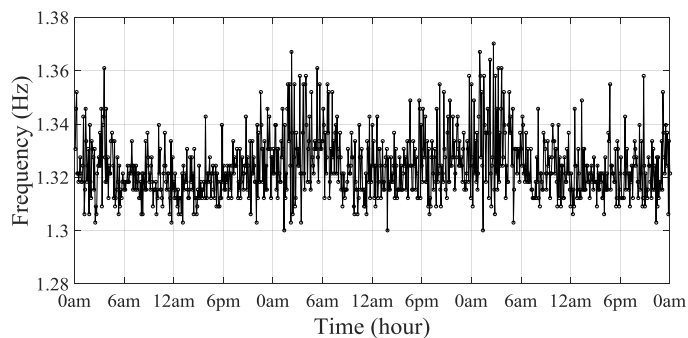
(a) 1st peak frequency



(b) 2nd peak frequency



(c) 3rd peak frequency



(d) 4rd peak frequency

Fig. 2.9 First four peak frequencies

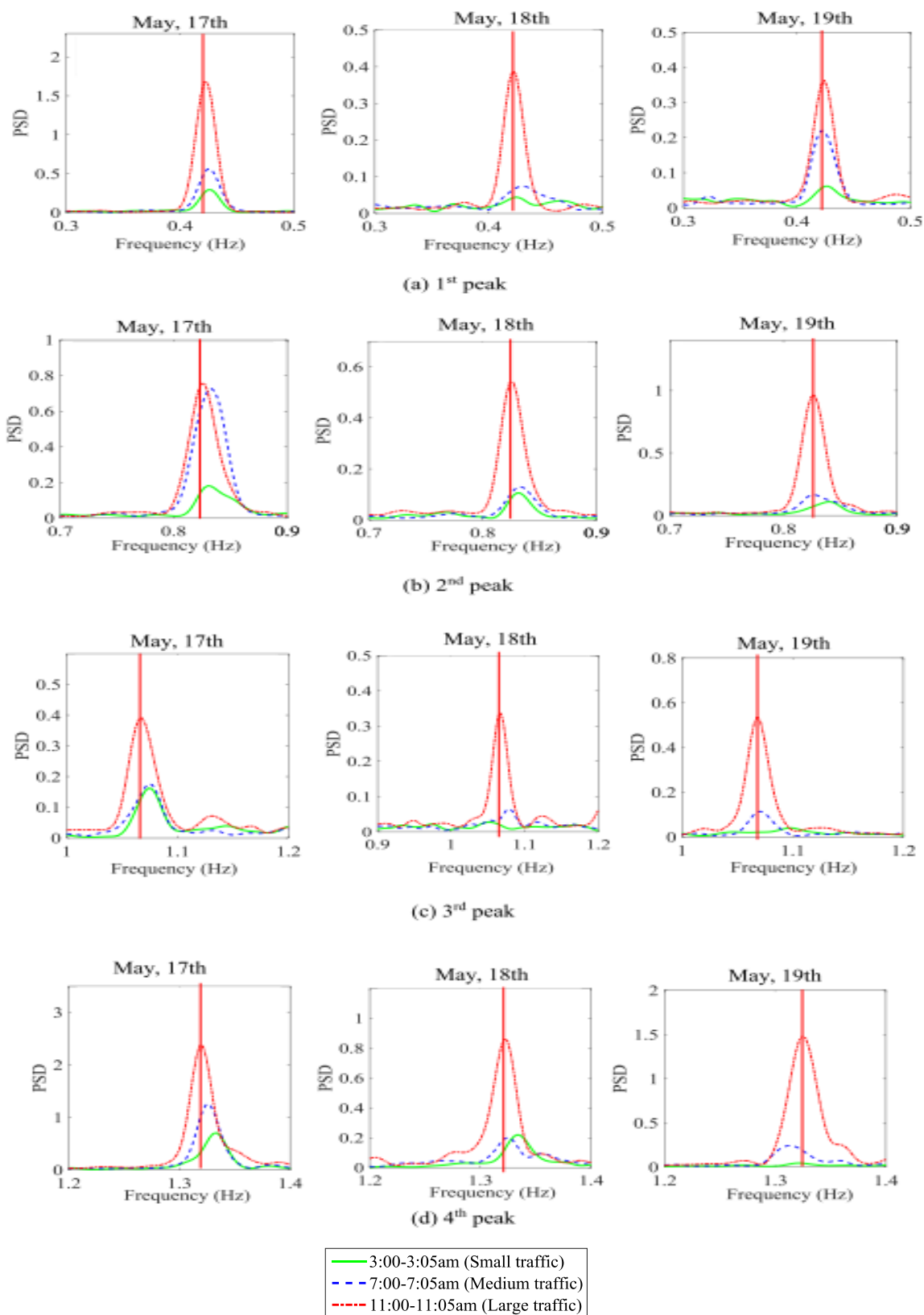


Fig. 2.10 First four peaks of the three PSD determined from the interval of 3:00 – 3:05 am, interval of 7:00 – 7:05 am and interval of 11:00 – 11:05 am ,of May, 17th, 18th and 19th

2.3.2 Mode Shapes

When two or more measured accelerations obtained simultaneously at different locations are acquired, the operational deflection shapes (ODSs) that almost always correspond to the mode shapes can be experimental determined by using ratios of the Fourier amplitudes at resonant frequencies of those locations. In such a way the ODSs are determined by ratios of responses measured at roving locations over a reference location at each modal frequency. The location AC-2 was allocated as a reference station, and the AC-1 and AC-3 were allocated as roving locations. The response ratios of locations AC-1 and AC-3, over the AC-2 were estimated from the ratios of cross power spectral density (CPSD) of AC-1 and AC-2, over PSD of AC-2, respectively. The positive ratios indicate that those locations move in the same direction with the reference location whereas the negative ones mean that they move in the opposite direction. The ODSs were calculated from every 15,000 data points. **Figure 2.11** illustrates the average ODSs of the first four peak frequencies and suggests that the first four modes seem to be the vertical bending modes.

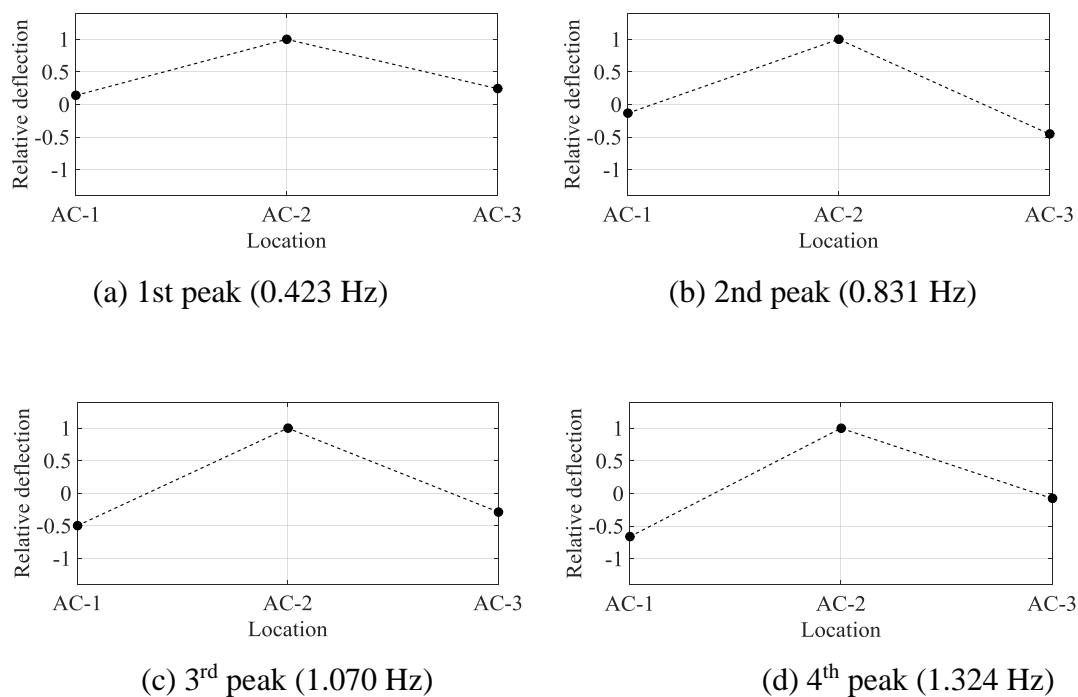
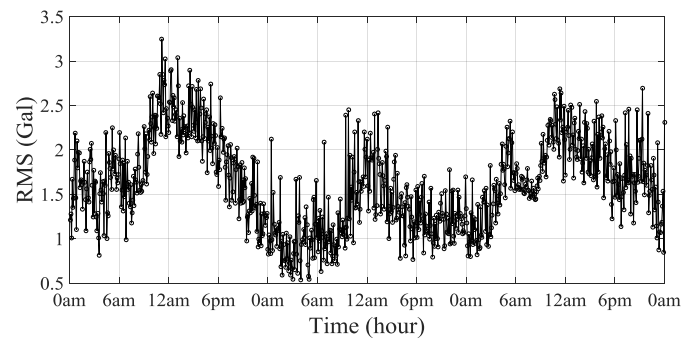


Fig. 2.11 Identified mode shapes

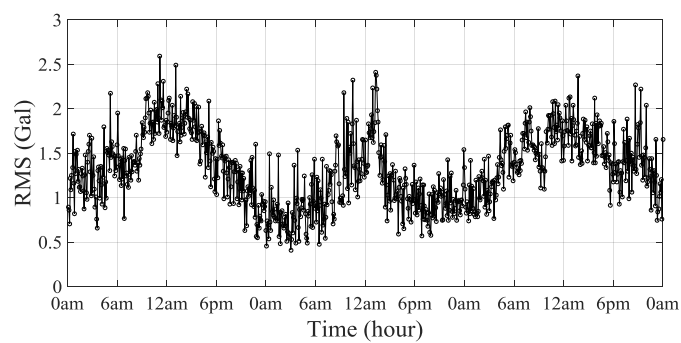
2.4 RMS OF BRIDGE RESPONSES

The feature that we adopted to represent the amplitude of response was the Root-mean-square (RMS) of acquired time-histroy. **Figure 2.12** illustrates the plots of RMS of the vertical accelerations at the mid-span deck (AC-2) and at the stayed-cable (AC-6) and the longitudinal tilt at the mid-span deck (TL-5). They all show the similar trends, in which the RMSs increase during the daytime and decreases during the nighttime. It can be noticed that this trend similars to the trend of the number of equivalent trucks that is shown in **Fig. 2.6**.

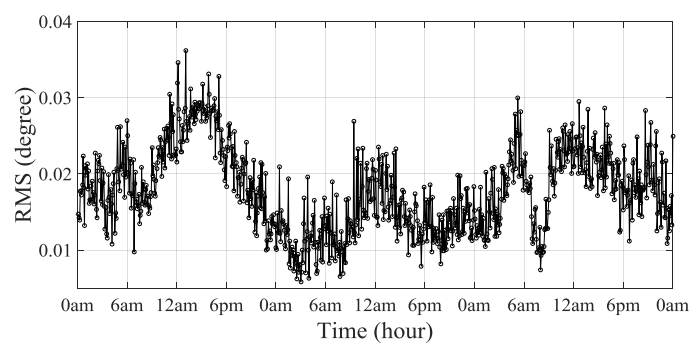
In addition, the raw response signals were filtered by the band-pass filter and examined the amplirude of responses in certain frequency ranges. The frequency ranges of the Butterwise filter here were designed corresponding with the ten peak frequencies as indicated in **Fig. 2.13**; e.g., 0.30-0.50 Hz for the 1st peak, 0.70-0.90 Hz for the 2nd, 0.95-1.15 Hz for the 3rd, and 1.25-1.45 Hz for the 4th peak. **Figure 2.14** (a)-(c) show the plots of extracted RMS of the filtered each of five-minute responses in the first four frequency ranges for the data of AC-2, AC-6, and TL-2, respectively. It can be seen that all plots show the similar trends to the RMS plot of the non-filtered responses in **Fig. 2.15**. However, there are some characteristics in the magnitudes and variations of the filtered RMS plots; for instance, those of the 4th-filtered response are higher than those of the other RMSs with the 1st-3rd filters in all sensors. The RMSs of filtered responses were thus also expected to have the contribution to the traffic volume, and were adopted as the features to analyze the correlations in the next section.



(a) Vertical accelerations of the deck at AC-2

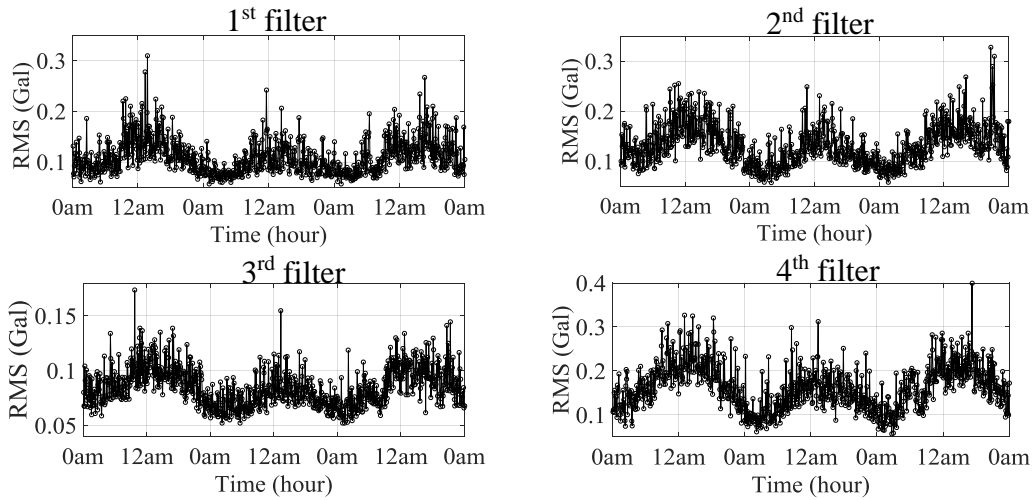


(b) Accelerations of the stayed-cable at AC-6

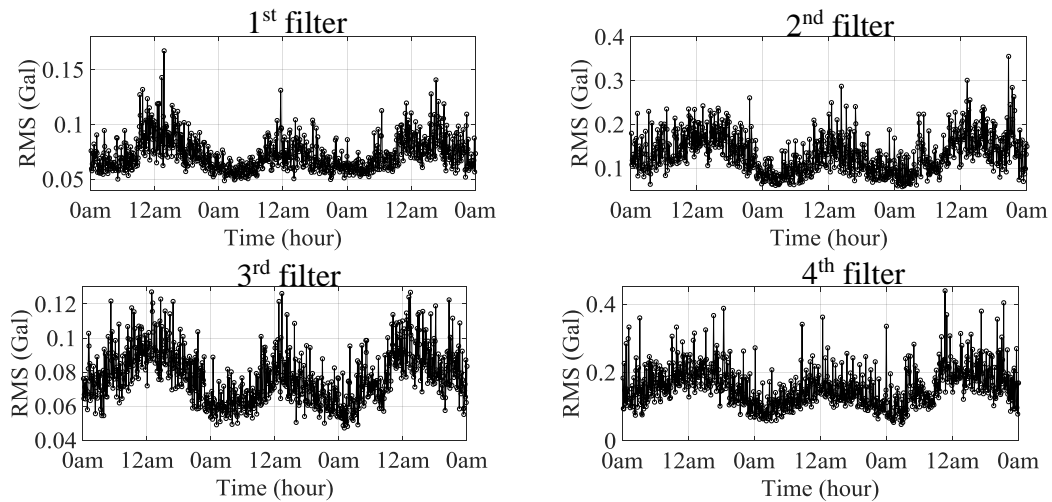


(c) Longitudinal tilts of the deck at TL-2

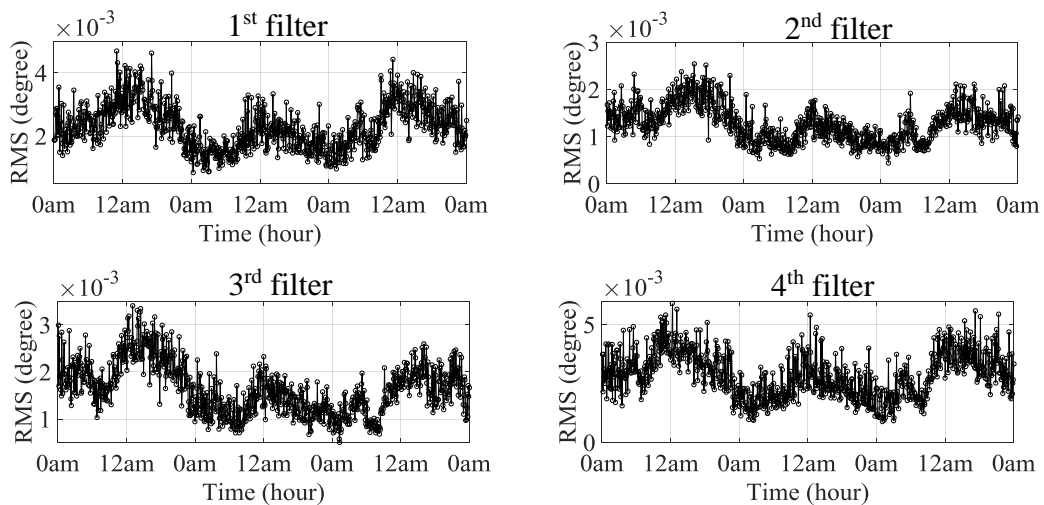
Fig. 2.12 RMS of responses



(a) Vertical accelerations of the deck at AC-2



(b) Accelerations of the stayed-cable at AC-6



(c) Longitudinal tilts of the deck at TL-2

. Fig. 2.13 RMSs of filterd responses

2.5 CONCLUSIONS

The data obtained from a SHM system installed in an in-service cabled-stayed bridge have been presented. The SHM system consisted of various sensors deployed on the bridge to capture the responses excited by traffic, changing temperature and wind. Multivariate features associated with dynamic characteristics were extracted from the monitored data. Based on the acquired data, it could be roughly observed that the amplitudes of all dynamic responses became relatively large during the daytime, and they decreased during the nighttime. For the temperature, the daily variance of each day was approximately 2 °C with the range of 29-32 °C. Notice that, in Bangkok, the daily and seasonal temperature variations were small. Similarly, the number of the single trucks and trailers increased in the daytime and decreased in the nighttime. The traffic volumes had a daily trend and large fluctuations within a day. For the extracted resonant frequencies, it could be considered that both the peak frequencies and their amplitudes had correlations especially with the traffic volume especially in the 1st and 4th peaks. Moreover, not only the peak frequencies but also the amplitudes associated with the traffic volume. Therefore, the RMS of the responses were determined and they all showed the similar trends, in which the RMSs increased during the daytime and decreased during the nighttime. It could be noticed that this trend similar to the trend of the number of equivalent trucks. In addition, the raw response signals were filtered by the band-pass filter and examined the amplitude of responses in certain frequency ranges. The RMSs of filtered responses were thus also expected to have the contribution to the traffic volume, and were adopted as the features to analyze the correlations.

3. BRIDGE RESPONSES IN CHANGING ENVIRONMENTAL AND OPERATIONAL CONDITIONS

This chapter deals with effects due to the changing environmental and operational conditions were investigated by adopting mathematical models. The results of the data analysis show that features extracted from multivariate SHM data demonstrate effectively the operational and environmental effects for this cable-stayed bridge. The mathematical models can capably express the relationships between the environmental and operational variability and the responses of the structure, especially the impacts of traffic loading and temperature on

the fluctuation of the resonant frequencies. Moreover, the model errors can be used as an indicator of structural conditions.

3.1 INTRODUCTION

In assessing conditions of a structure based on monitored structural responses data obtained from a SHM system, changes of measured structural responses can be caused by damage or environmental and operational variability. The effects of varying environmental and operational conditions on measured responses of a structure often have the same magnitude as those of damage (Kullaa, 2011) consequently, structural performance assessment becomes unreliable. It is important to ascertain the normal response of a structure to its changing environmental and operational conditions for developing the reliable SHM (Cross et al., 2013).

For in-service bridges, the time-varying environmental conditions include temperature, humidity and wind, while the operational conditions include traffic loading in term of weight and speed of vehicles. These conditions are undeniable factors affecting on the dynamic responses of the underlying bridges.

The variability of temperature can contribute to the changes in stiffness of structures explained by the asphalt elastic modulus varying due to thermal effect (Peeters et al., 2001). Cornwell et al. (1999) reported that the natural frequencies of Alamasa Canyon Bridge, USA varied up to 6% over a day period due to the temperature differential across the deck. Cross et al. (2013) found that the temperature fluctuation effected on the resonant frequencies of Tamar Bridge, UK and suggested that the seasonal temperature variability had more effect than daily one. Besides temperature, wind speed is an importance environmental factor that plays a role in vibration of long-span bridges. Dionysious and Fujino (2008) studied the ambient vibration response of Hakucho Suspension Bridge, Japan and found that the resonant frequencies were amplitude dependent with respect to the root-mean-squared (RMS) of acceleration which correlated to wind speed. For instance, the resonant frequencies decrease when the RMS of the

deck accelerations increases (consequently, the high wind speed) and this behavior was found in research of Cross et al. (2013) as well.

For the operational conditions, the influences of traffic loading on dynamic characteristics were addressed by Kim et al. (2003) that the measured natural frequencies could change up to 5.4% for short-span bridges but these changes could be hardly detected for middle and long span bridges, because the mass of vehicles was relatively small in comparison to the mass of super-structure. In contrast, Zhang et al. (2002) found that the natural frequencies of global modes varied about 1% due to changing traffic loading within a day and Cross et al. (2013) reported that traffic loading was a dominant factor in daily fluctuation of resonant frequencies for long span bridges.

Data normalization has been used to distinguish the changes of structural responses caused by environmental and operational variations from those caused by structural degradation or damage. Several studies have been proposed some statistical techniques to tackle this issue. Regression analyses can be applied to investigate the relationships of features extracted from structural responses and environmental and operational changing when the measured data of environmental and operational variability is available (Sohn, 2007). The linear regression model was applied to investigate the impact of temperature on natural frequencies in the research of Sohn et al. (1999) and Cross et al. (2013). For Alternative approach, the ARX model was applied to evaluate the thermal dynamics of the bridge (Peeters et al., 2001), Ni et al. (2005) applied the support vector machine (SVM) technique to formulate regression models which quantified the effect of temperature on resonant frequencies.

3.2 RESPONSE DATA

For the study on the dynamic responses variability of the bridge under the changing environmental and operational conditions, 3-days monitored data (2nd - 4th August, 2014) consists of the vertical acceleration of the deck and temperature at the center of the main span, traffic loading on the bridge, and the acceleration of the longest cable. They will be used in the

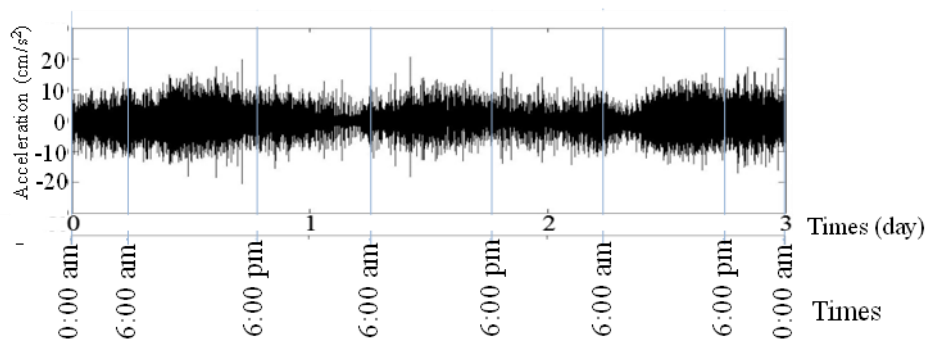
following analysis. **Figure 3.1** illustrates the vertical acceleration of the deck and acceleration of the cable measured with sampling rate 50 Hz. It shows that they vary by the changing environmental and operational conditions.

For the environmental and operational data, **Figure 3.2** shows the half- hourly traffic volume on the bridge, the trucks are the major traffic loading because the bridge is located in the industrial area. The total equivalent single truck volume quite has a similar pattern in each day that shapely increases from around 200 to 1,000 vehicles/half hour in the morning, and has a high volume within the range of 800 – 1200 vehicles/half hour during day time, after that it dramatically decreases in the evening. **Figure 3.3** shows the measured temperature of the deck at the center of the main span varies between 30 – 33 degrees Celsius during three days and there is a fluctuation around 2 degrees Celsius in each day.

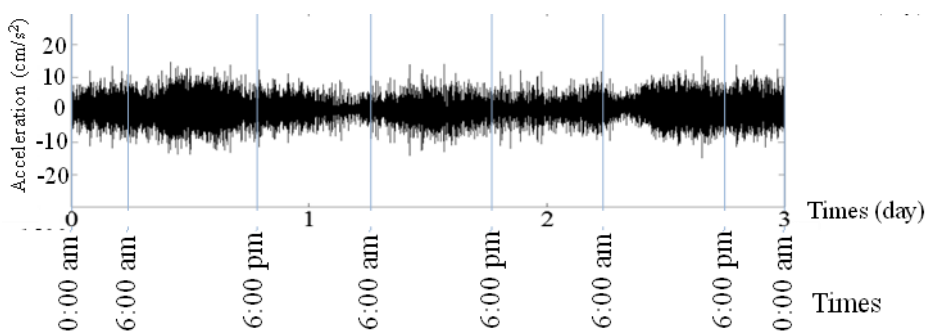
The nine peak frequencies were determined from PSDs (Peak-picking method) in every 30 minute (90,000 data points) as shown in **Fig. 3.4**. **Figure 3.5** shows the extracted resonant frequencies and indicates that there are fluctuations influenced by environmental and operational variability.

Basically, the impact of environmental and operational conditions on the modal frequency fluctuations can be initially investigated by determining the correlation coefficients between them as shown in **Fig. 3.6**. It demonstrates that the correlation coefficients of the resonant frequencies and traffic loading, the RMS of deck acceleration and the RMS of cable acceleration have a similar tendency. They are within the range of 0.3 to 0.6 for the first six modes and around 0.1 to 0.2 for the last three modes.

On the contrary, the correlations of temperature and the resonant frequencies are quite low with coefficients less than 0.3 for the 1st, 3rd, 4th, 5th and 6th modes, and moderate with coefficients between 0.3 to 0.5 for the 2nd, 7th, 8th and 9th modes. It suggests that the resonant frequencies of the lower modes are dominated by traffic loading, the RMS of deck and cable accelerations while that of the higher modes are affected by temperature.



(a) Vertical accelerations of the deck at AC-2



(b) Acceleration of the stayed-cable at AC-6

Fig. 3.1 Acquired dynamic responses for three days; 2nd - 4th August, 2014

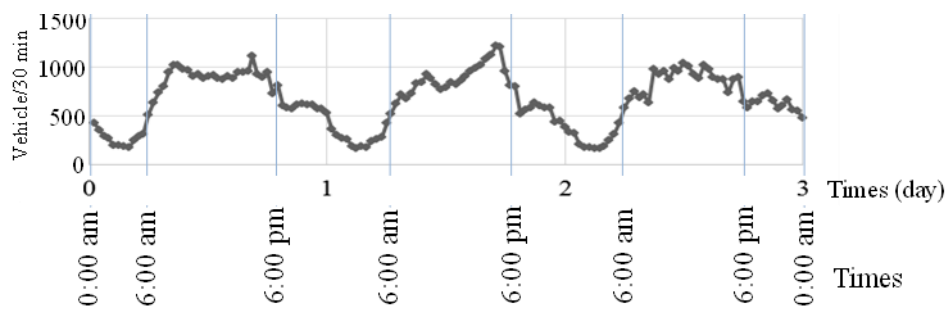


Fig. 3.2 Monitored traffic volume for three days; 2nd - 4th August, 2014

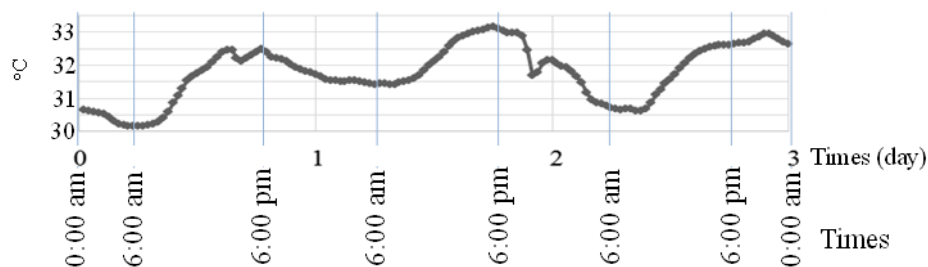


Fig. 3.3 Monitored temperature for three days; 2nd - 4th August, 2014

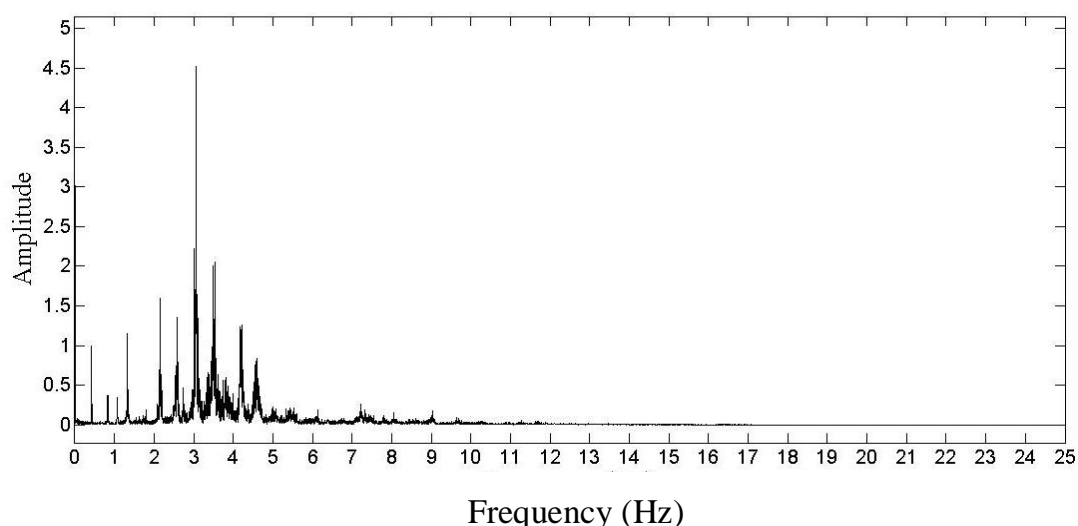


Fig. 3.4 PSD and its first ten peaks of vertical acceleration of the deck

Table 3.1 shows the determined correlation coefficients among traffic loading, temperature and the both extracted RMS of accelerations and indicates that the traffic loading correlates to the RMS of deck and cable accelerations with 0.53 and 0.57 of coefficients, respectively. The RMS of deck acceleration highly correlates to the RMS of cable acceleration with a 0.88 of coefficient, while the temperature has a low correlation to the others.

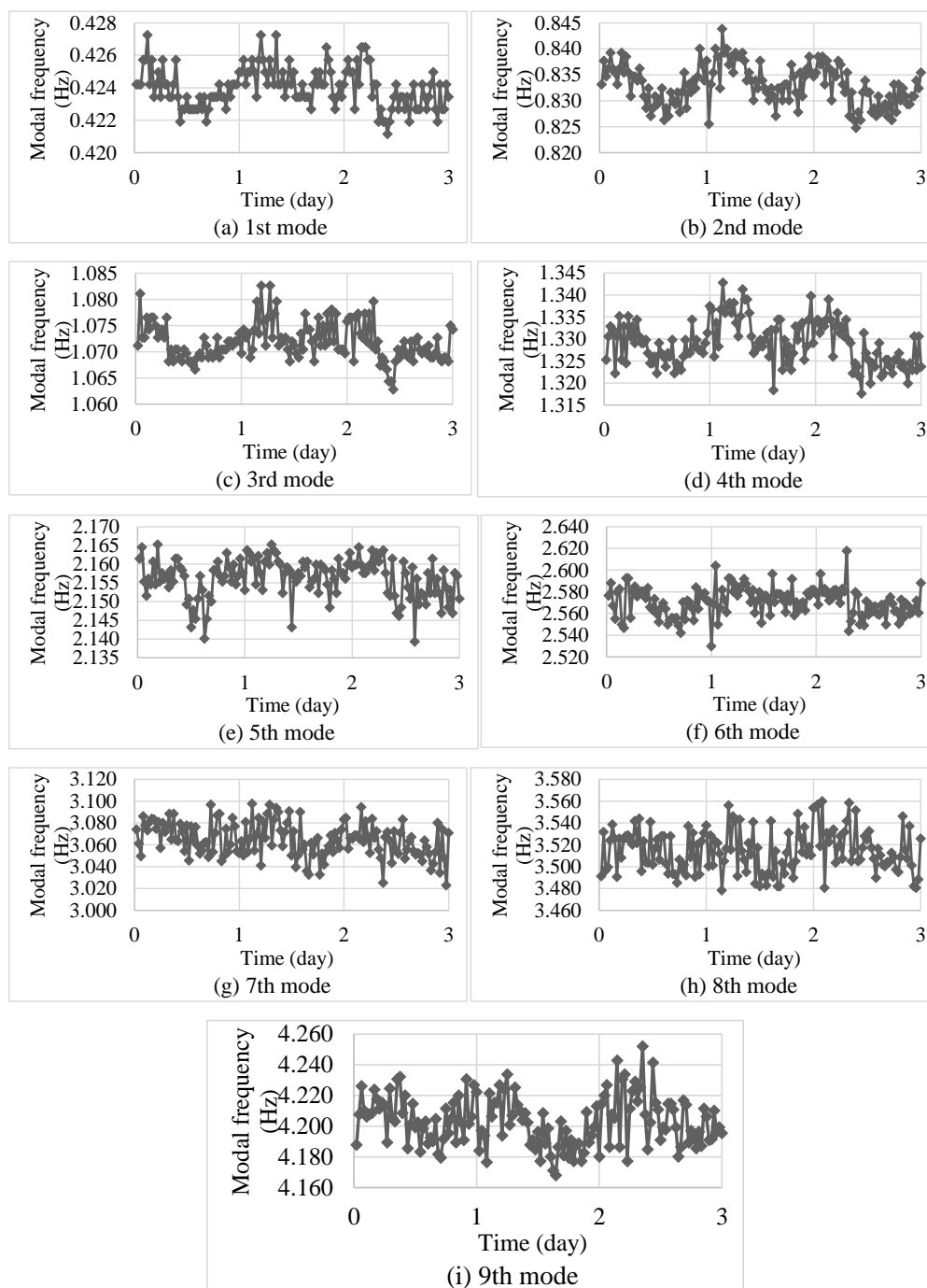


Fig. 3.5 Fluctuations of resonant frequencies (a) 1st mode, (b) 2nd mode, (c) 3rd mode, (d) 4th mode, (e) 5th mode, (f) 6th mode, (g) 7th mode, (h) 8th mode and (i) 9th mode.

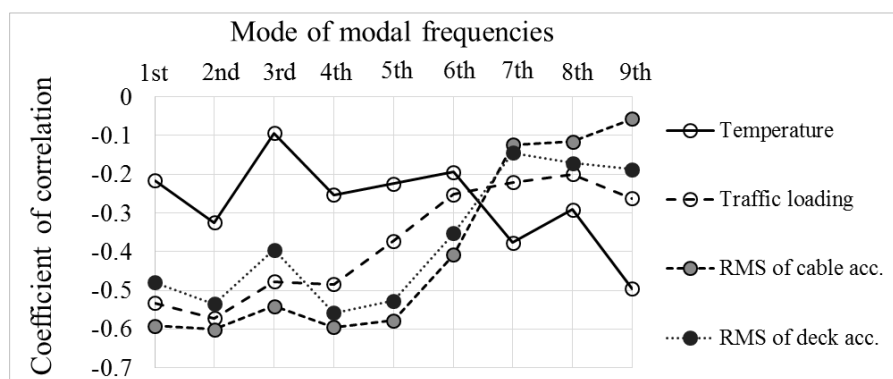


Fig. 3.6 Correlation coefficients between eight resonant frequencies and traffic loading, temperature and RMS of the deck and cable accelerations plotted against mode of resonant frequencies.

Table 3.1 Correlation coefficient matrix of traffic loading, temperature, RMS of the deck accelerations and RMS of cable accelerations.

Variable	Traffic loading	Temperature	RMS of deck acc.	RMS of cable acc.
Traffic loading	1	0.35	0.53	0.57
Temperature		1	0.15	0.02
RMS of deck acc.		Sym.	1	0.88
RMS of cable acc.				1

In summary, traffic loading, the RMS of deck acceleration and RMS of cable acceleration tend to influence on the variability of the first six resonant frequencies whereas temperature has a tendency to effect on the last three resonant frequencies fluctuations.

For better understanding the impacts of traffic loading, temperature, the RMS of deck accelerations and the RMS of cable accelerations on the fluctuations of resonant frequencies, the mathematical model will be applied in this study.

3.3 THEORETICAL DESCRIPTION OF REGRESSION MODELS

The regression analysis is a statistical methodology for describing the stochastic relationship between responses of interest (estimation variable) and associated factors. It often used to understand the contributions of the influential factors to the estimation variables using the observation data. Moreover, it is used to make a stochastic model that describes the relationship between the estimation variables and the factors. The linear regression, which was the simplest regression model and often used in the practical applications extensively (Xin 2009), was adopted in this study. The formula of the linear regression is:

$$y = \beta_o + \sum_{i=1}^k \beta_i X_i + \varepsilon , \quad (3.1)$$

where y is the predicted variable, X_i ($i=1-k$) is the predictor variables, β_i ($i=0, 1-k$) is the unknown constant coefficient, and ε is the random error. The coefficient β_i , which actually indicates the contribution of X_i to variable y , can be obtained by the ordinary least squares (OLS) estimation. To assess the significance of individual parameter, the t -test is used with adopting a null hypothesis of $\beta=0$. This hypothesis states that the predictor variable X with estimated coefficient $\hat{\beta}$ is not important, and it is rejected at the level of significance if the test statistic t becomes higher than the tabulated t -value with $p-k-1$ degrees of freedom, where p is number of observations. The test statistic t can be calculated as:

$$t = \frac{\hat{\beta}}{se(\hat{\beta})} , \quad (3.2)$$

where $se(\hat{\beta})$ is the standard error of $\hat{\beta}$. In the statistical modeling, variable X , which rejects the null hypothesis with the t -test at the significance level of 0.05 (95% confidence), can be adopted in the model.

The accuracy of the model can be measured by the root mean squared error ($RMSE$) that examines the differences between observed values, y_i and predicted values, \hat{y}_i . The $RMSE$ is defined as:

$$RMSE = \sqrt{\frac{\sum_{i=1}^p (\hat{y}_i - \bar{y})^2}{p}}. \quad (3.3)$$

Moreover, it is important to investigate the relationship or collinearity among the predictor variables. If two or more variables in the regression model are highly correlated, there will be multicollinearity leading to instability in the regression coefficients (Chatterjee and Simonoff 2013). In generally, a diagnostic to determine the problem is the variance inflation factor (VIF) for each predicting variable, which is defined as:

$$VIF_j = \frac{1}{1 - R_j^2}, \quad (3.4)$$

where R_j^2 is the R^2 of the regression of the predictor variable X_i on the other predictor variables. There are no formal cutoffs of VIF to identify the multicollinearity problem. The collinearity is generally not an issue when the VIF satisfies

$$VIF < \max\left(10, \frac{1}{1 - R^2}\right). \quad (2.5)$$

3.4 MATHEMATICAL MODELS OF RESONANT FREQUENCIES

From the correlation matrix as shown in **Table 3.1** indicated that the RMS of deck acceleration variable and the RMS of cable acceleration variable are highly correlated. To avoid the multicollinearity issue, the RMS of deck acceleration will not be included as the independent variable for developing the models.

All data was transformed to normalized form by subtracting with its mean and dividing by its standard deviation. The estimated coefficients ($\hat{\beta}$) of normalized data allow to compare the effect of each independent variable on a dependent variable (high value means high effect). As using normalized data, the β_o in the equation (1) will be equal to 0, so the models are formed as:

$$\hat{f}_n = (\beta_{TR,n} * TR) + (\beta_{TA,n} * TE) + (\beta_{CA,n} * CA) \quad (3.6)$$

where \hat{f}_n are the predicted normalized resonant frequencies of the mode n , n is the mode orders ($n=1...9$), TR is the normalized traffic loading, TE is normalized temperature, CA is the normalized RMS of cable acceleration and $\beta_{TR,n}$, $\beta_{TA,n}$ and $\beta_{CA,n}$ are the coefficients of TR , TE and CA of the mode n , respectively.

In this analysis, the independent variables which can reject the null hypothesis of t -test at significance level 0.01 (99% confidence) will be added in the models and the developed models which can reject the null hypothesis of F -test with 99.9% confidence will be considered.

Table 3.2 shows the results of coefficients estimation of regression models for the nine resonant frequencies. The coefficients which equal to 0 imply that their independent variables

are insignificant parameters. The negative coefficients of traffic loading, temperature and the RMS of cable acceleration indicate that the resonant frequencies will decrease when these environmental and operational variables increase. The traffic loading influences on the resonant frequencies of the first three modes while the temperature effects on the resonant frequencies of the last six and the 2nd modes. For the RMS of cable acceleration, it has effects on the resonant frequencies of the first six modes.

Considering the values of the estimated coefficients, it suggests that the RMS of cable acceleration is an important variable for prediction the resonant frequencies of the first six modes whereas in the last three modes, only temperature is a significant variable in the models. In Table. 2, the *R-squared* values represent the prediction capability of the regression models that the prediction models for the first five modes have a moderate performance while the models have a low power in prediction for the last four modes.

For more assessing the prediction performance, the predicted resonant frequencies are plotted together with those obtained from the measurement. **Figure 3.7** illustrates that the predicted resonant frequencies of the 1st and 2nd modes can recreate the general trend but cannot recreate the large spikes of the fluctuations and this characteristic occurs in the remaining modes as well, it might be caused by the short term traffic loading.

Table 3.2 Estimated coefficients of regression models for the nine resonant frequencies.

Mode	Independent variables			<i>R-square</i>
	<i>TR</i>	<i>TE</i>	<i>CA</i>	
1 st	-0.288	0.000	-0.428	0.407
2 nd	-0.221	-0.238	-0.469	0.486
3 rd	-0.249	0.000	-0.398	0.334
4 th	0.000	-0.240	-0.591	0.413
5 th	0.000	-0.211	-0.574	0.379
6 th	0.000	-0.186	-0.404	0.201
7 th	0.000	-0.377	0.000	0.142
8 th	0.000	-0.292	0.000	0.085
9 th	0.000	-0.496	0.000	0.246

Moreover, the errors, ε of the prediction models developed with the measured environmental and operational data, and the responses of the structure under its environmental and operational conditions defined as normal condition can be applied as a tool for detecting anomaly of the structural conditions (Sohn, 2007, Cross et al., 2013). Since the prediction models are conducted by taking account of the environmental and operational variability so their errors are independent from this variability, it means that the errors are consistent even though the environmental and operational conditions vary. If the prediction models produce any large error, it suggests that such error might be caused by the damage or changes in structural conditions. The model prediction errors can be calculated as:

$$\varepsilon = f_n - \hat{f}_n, \quad (3.7)$$

where f_n are the measured normalized resonant frequencies of the mode n . The large error as mentioned earlier can be identified by adopting the confidence limits of the prediction errors (under the assumption of normally distributed error). Any error is considered as a large or anomalous error if it deviates from these limits. The 99.5% confidence limits are used in this study and can be computed as:

$$\bar{\varepsilon} - z_{0.9975}\sigma_{\varepsilon} \leq \varepsilon \leq \bar{\varepsilon} + z_{0.9975}\sigma_{\varepsilon}, \quad (3.8)$$

where $\bar{\varepsilon}$ is the mean of errors (equals to 0), σ_{ε} is standard deviation of the errors, z is the score of standard normal distribution and $z_{0.9975}$ equal to 2.81 (obtained from tabulated standard normal distribution).

Fig. 3.8 shows the prediction errors of the first two resonant frequencies with the limit lines of 9.5% confidence interval. Then the errors were assessed for autocorrelation to achieve the

regression assumptions. **Figure 3.9** shows autocorrelation function of the errors of the second mode frequency and indicates that there is no apparent pattern of the errors or the errors are uncorrelated. Therefore, the prediction errors have no autocorrelation and almost stay within the confidence intervals, indicating that this approach can be applied for detecting the anomalous conditions of the structure.

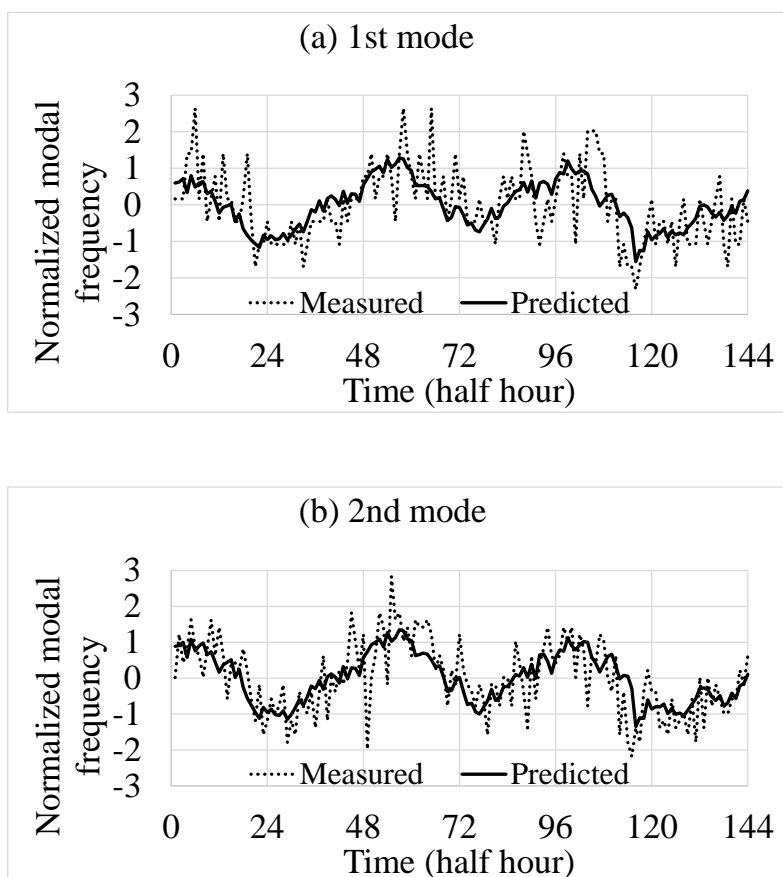


Fig. 3.7 Measured and predicted resonant frequencies of the (a) 1st and (b) 2nd modes

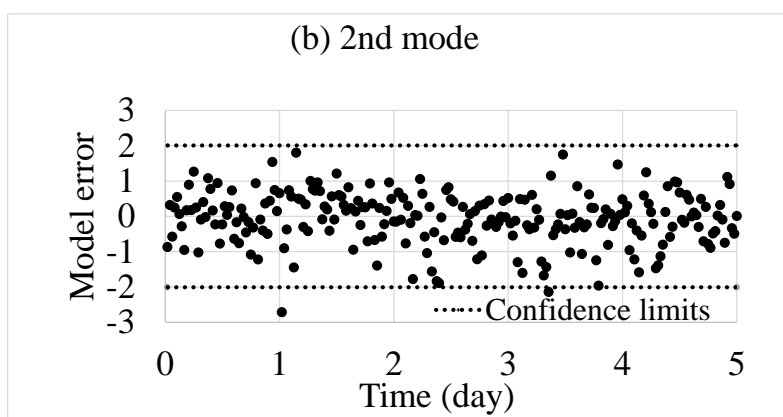
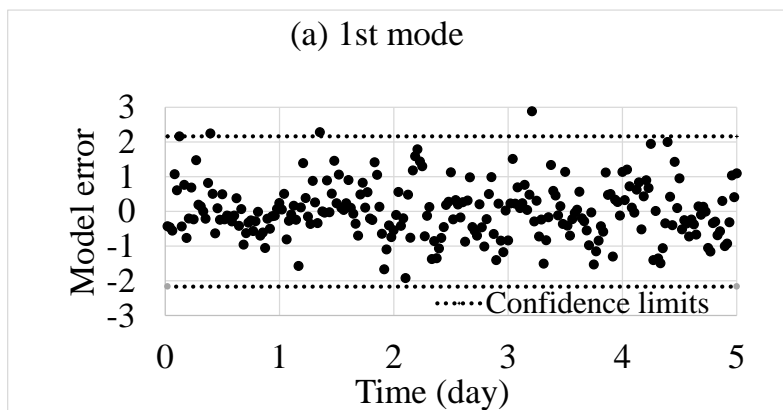


Fig. 3.8 Model prediction errors and theirs 99.5% confidence limits of the (a) 1st and (b) 2nd modes

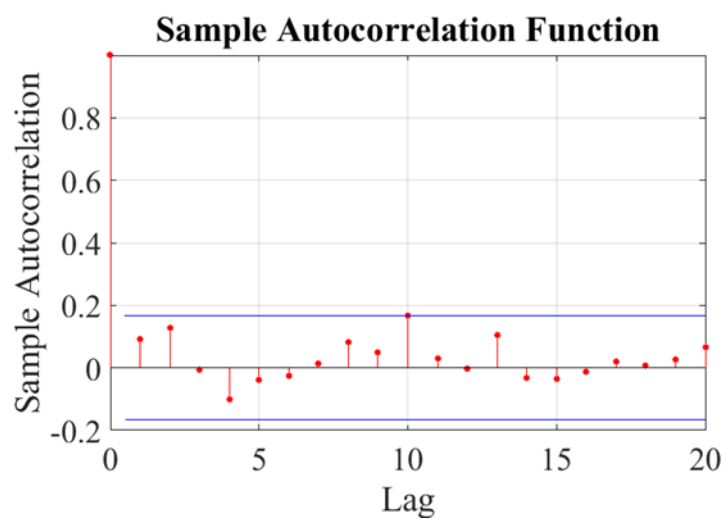


Fig. 3.9 Autocorrelation function of the 2nd modes frequency

3.5 CONCLUSIONS

This chapter has analyzed the effects of environmental and operational conditions on the dynamic response variability such as the changes of resonant frequencies of the Bhumibol-1 Bridge. The temperature and traffic loading were considered as the environmental and operational factors impacting on the fluctuation of nine resonant frequencies extracted from vertical acceleration of the deck. The linear regression models has been adopted to investigate the interaction of those factors and measured resonant frequencies. The developed models revealed that the RMS of cable accelerations played a dominant role in prediction of the resonant frequencies of the first six modes while traffic loading and temperature had a low influence on these resonant frequencies. For the higher modes, only temperature significantly impacted on the changes of resonant frequencies. It should be noted that the trained temperature data collected from a short time period can represent only the daily effect, if a longer time period of measurements that can cover the seasonal effect are considered, the temperature might has a more influence.

The prediction models can reproduce the general trend of the fluctuation of resonant frequencies but cannot recreate some high peaks and large drops. These spikes might be caused by short term traffic loading, in order to improve the prediction performance, a more sophisticated data measurement and a more complex structure of the mathematical model are required to better investigate the resonant frequencies variability. Moreover, the model errors can be adopted as an indicator of structural conditions.

REFERENCES

Chatterjee S. & Simonoff S. J. *Hand book of Regression Analysis*, John Wiley & Sons: New York, 2013.

Cornwell P., Farrar C.R., Doebling S.W. & Sohn H. Environmental variability of modal properties. *Exp. Tech.* 1999; **23(6)**: 45–48.

Cross E. J., Brownjohn J.M.W. & Worden K. Long-term monitoring and data analysis of the Tamar Bridge. *Mechanical Systems and Signal Processing* 2013; **35**: 16-34.

Dancey C., Reidy J. *Statistics Without Maths for Psychology: Using SPSS for Windows*. Prentice Hall: London, 2007.

Kim C., Jung D., Kim N., Kwon S. & Feng M. Effect of vehicle weight on natural frequencies of bridges measured from traffic-induced vibration. *Earthquake Eng. Eng.* 2003; **2(1)**: 109-115.

Newey W. K. & West K. D. A Simple, Positive Semi-Definite Heteroskedasticity and Autocorrelation Consistent Covariance Matrix. *Econometrica*. 1978; **55**: 703–708.

Peeters B. & De Roeck G. Reference based stochastic subspace identification in civil engineering. *Inverse Problems in Engineering* 2001; **8(1)**: 47-74.

Wooldridge J. M. *Introductory Econometrics: A Modern Approach*. South-Western: Tennessee, 2002.

Xin Y. *Linear Regression Analysis: Theory and Computing*. World Scientific: London, 2009.

Zhang Q., Fan L. C. & Yuan W. C. Traffic-induced variability in dynamic properties of cable-stayed bridge. *Earthquake Eng. Struct. Dyn.* 2002; **31**: 2015-2021.

.

Chapter 4

4. FINITE ELEMENT MODELING FOR DYNAMIC RESPONSES

In the chapter 2, the dynamic responses obtained from the SHM system were described based on only the acquired data. However, we can use Finite Element (FE) models to predict the dynamic responses for more understanding the dynamic behaviors of the bridge. This chapter presents FE modeling of the target bridge and analytical dynamic responses, and compares the analytical responses with those from the measurement.

4.1 FINITE ELEMENT MODELING AND MODEL VALIDATION

Using FE models for predicting the dynamic properties of structures is an alternative way to evaluate structural properties. It takes the place of dynamic tests on the structures when working in over-limit situations which are very difficult or impossible to perform by experimental. The FE models require verification for ensuring accuracies of FE model predictions. Therefore, the models must be validated.

In this study, A three-dimensional finite element (FE) model of the Bhumibol I Bridge was developed by using Midas Civil software. The model has a total of 96 cable elements, 1,101 beam elements 385 plate elements and 1,127 nodes. Each node has six degrees of freedom. The connections between the deck and the two towers and the four piers are fixed links. **Figure 4.1** shows the developed FE model. The main span consists of longitudinal and cross steel beams and concrete slabs as shown in **Fig. 4.2**. For the side span decks, they are post tension concrete boxes. The width of the north span varies while the south one is constant. The connections between the side span decks and the main span deck, towers, pillars and cables are assigned as rigid links. **Fig. 4.3** shows FE model of the side span decks and presents the rigid links. The towers supporting the decks are hollow concrete boxes and their supports are assigned as fix supports as shown in **Fig. 4.4**. There are three material assigned in the models, that are concrete, steel and cable. Their moduli of elasticity are 2.10×10^5 , 3.17×10^4 and 1.61×10^5 N/mm² for the concrete, steel and cable, respectively.

For model validation, the results of analytical modal analysis are compared with those obtained from the field measurement. There are three locations of acceleration measurement, therefore, only the lower modes of the peak frequencies and the mode shapes are comparable. The FE calculated mode shapes that correspond to the first four identified ODSs (in chapter 2) are shown in **Fig. 4.5**.

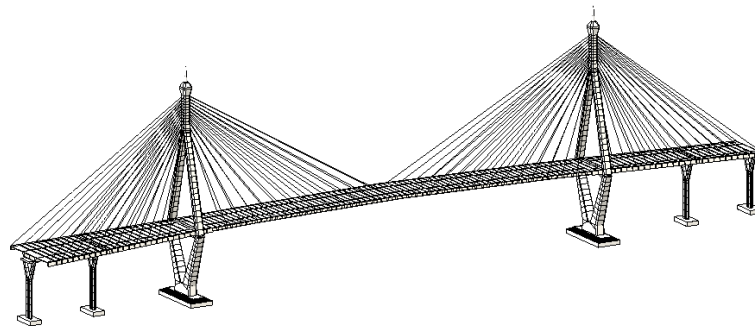
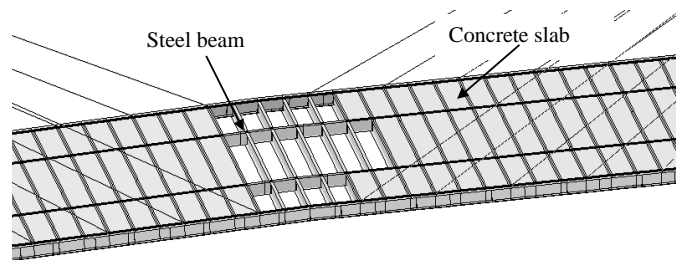
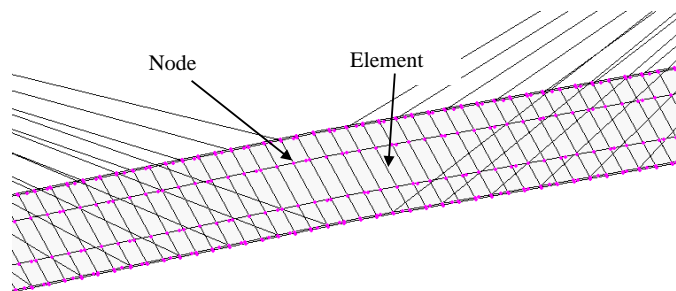


Fig. 4.1 FE model of the Bhumibol I Bridge.

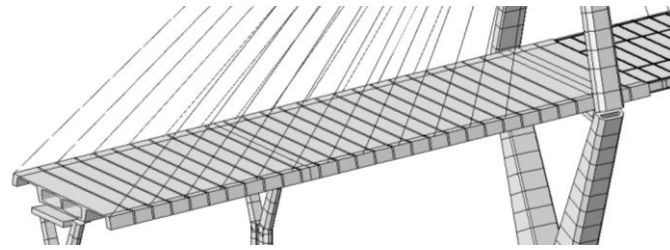


(a) 3D FE model of main span deck

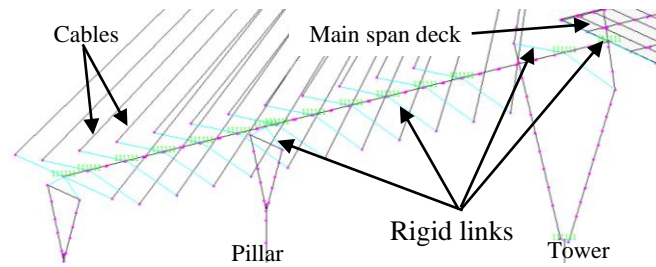


(b) Wire frame model

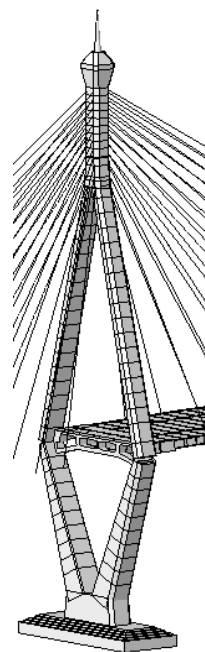
Fig. 4.2 FE model of main span deck (a) 3D model and (b) Wire frame model



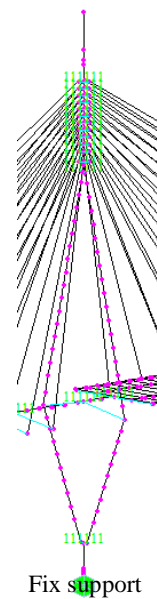
(a) 3D FE model of side span deck



(b) Wire frame model

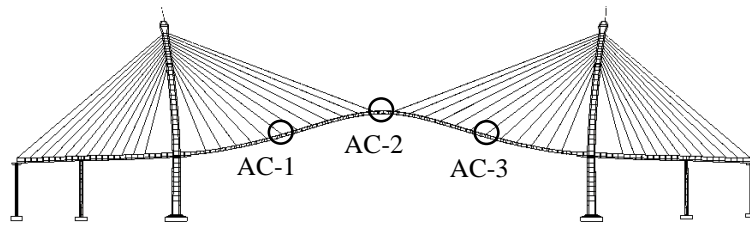
Fig. 4.3 FE model of side span deck (a) 3D model and (b) Wire frame model

(a) 3D FE model of towers

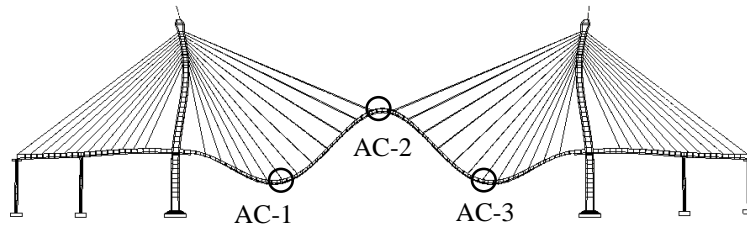


(b) Wire frame of towers

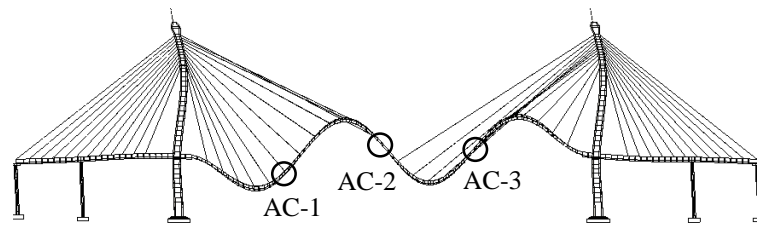
Fig. 4.4 FE model of towers (a) 3D model and (b) Wire frame model



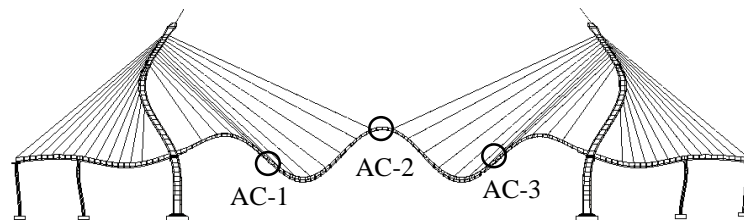
(a) 1st peak (0.428 Hz)



(b) 2nd peak (0.826 Hz)



(c) 3rd peak (1.078 Hz)



(d) 4th peak (1.331 Hz)

Fig. 4.5 Calculated mode shapes

Table 4.1 summarizes the peak frequencies obtained from the field identification and the FE calculation. It indicates that the identified and calculated frequencies achieve a good agreement. Therefore, the FE model is validated and can be use as the base line FE model.

Table 4.1 Calaulated and Identified resonant frequencies.

Mode	FE calculation	Field identification	Difference (%)
1st	0.428	0.423	1.18
2nd	0.826	0.831	0.59
3rd	1.078	1.070	0.76
4th	1.331	1.324	0.54

4.2 TRAFFIC LOAD MODELING AND ASSIGNMENT

In the FE models, the vehicles passing on the bridge were modeled as dynamic loads. The vehicles were defined by; an axle load of 1.5 tons for the passenger cars, a 5 tons axle load and a 20 tons axle load for the single trucks, and a 5 tons axle load and two 20 tons axle loads for the trailers as shown in **Fig. 4.6**. The spacing between the axles is 8 m and the axle width or the spacing of the wheels is 2 m. Based on field observation, the single trucks and trailers usually travel on the left and middle lanes while the passenger cars normally use the right lanes as shown in **Fig. 4.7**. For arrangement of the vehicular loads, the following assumptions have been applied; the left lanes were loaded by the trailers, the middle lanes were loaded by the single trucks and the right lanes were load by the passenger cars as shown in **Fig. 4.8**.

Every vehicle was recorded passing time on the bridge by the traffic counting system. The passing time was used to construct the vehicular load time history in the FE analysis. To model the dynamic vehicular loads, it was assumed that traffic flow speed was 50 km/h in normal condition and during traffic congestion, the speeds were 40 and 30 km/h. Therefore, time lags between the axles with the spacing of 8 m are around 0.6, 0.8 and 1.0 second for the

speeds 50, 40 and 30 km/h, respectively as shown in **Fig. 4.9**. It shows the spacing between the axles of the trailers that the spacing will be longer when the speeds decrease. **Figure 4.10** shows the load time history of the passenger cars, the single trucks and the trailers during 11.00 – 11.01 am with the speed of 50 km/h in the southbound direction on 19th May.

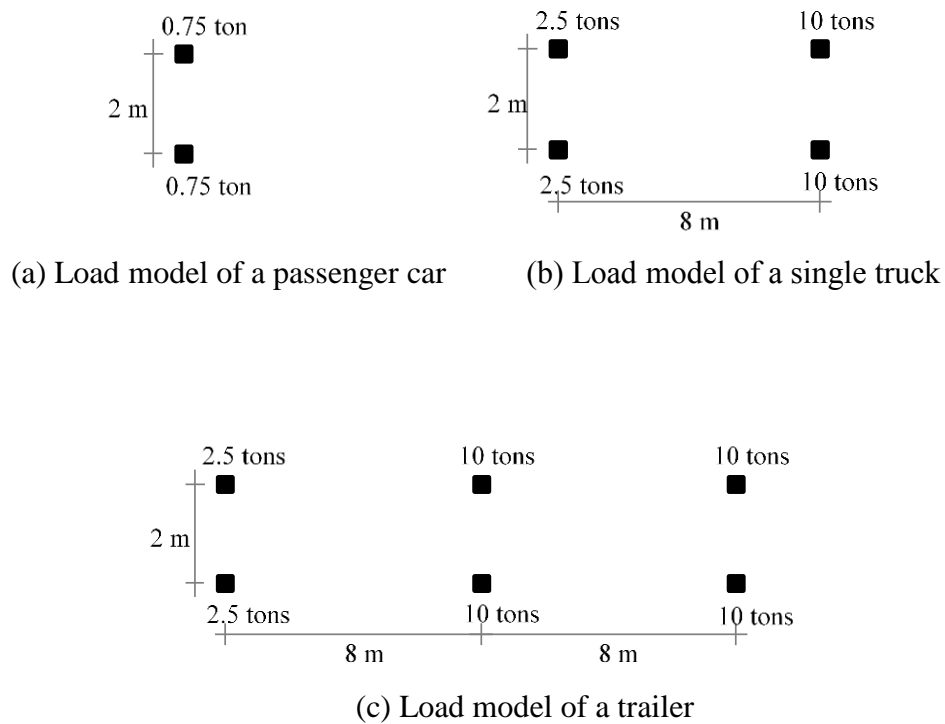


Fig. 4.6 Vehicular load models



Fig. 4.7 Lane occupancies on the Bhumibol I bridge.

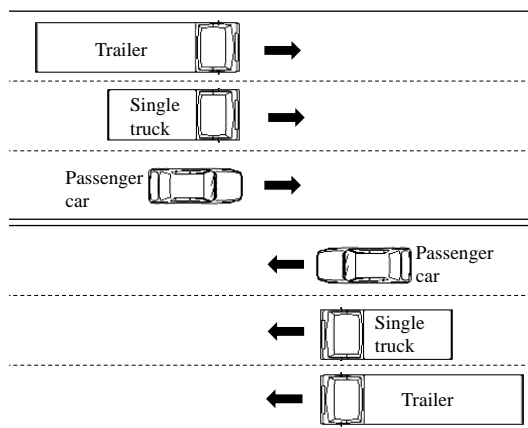


Fig. 4.8 Traffic lane arrangement in the FE model

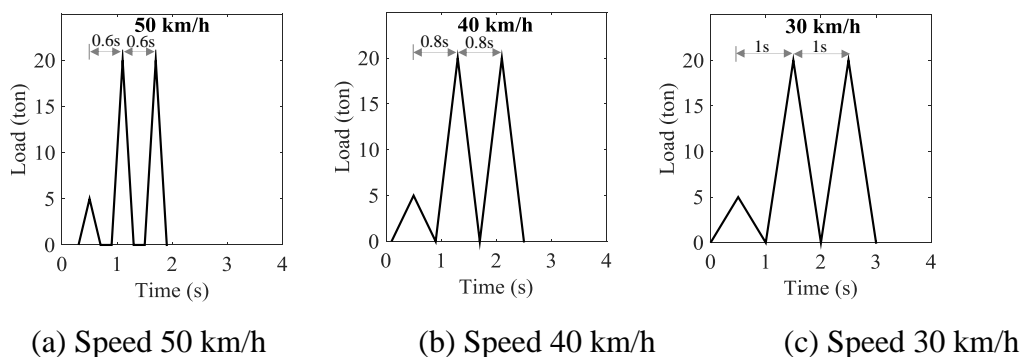


Fig. 4.9 Spacing between the axles of the trailers in load models

Then, each vehicle passing the bridge on Monday, May, 19th was modeled and assigned as dynamic loads in the FE models. The loads (wheel loads) were assigned at the nodes located on the cross-beam of the main-span which were divided into six traffic lanes (three lanes in each direction) as shown in **Fig. 4.11**. Each lane consist of two parallel consecutive nodes with the width of 2 m and the distance between the adjacent lanes is 4 m.

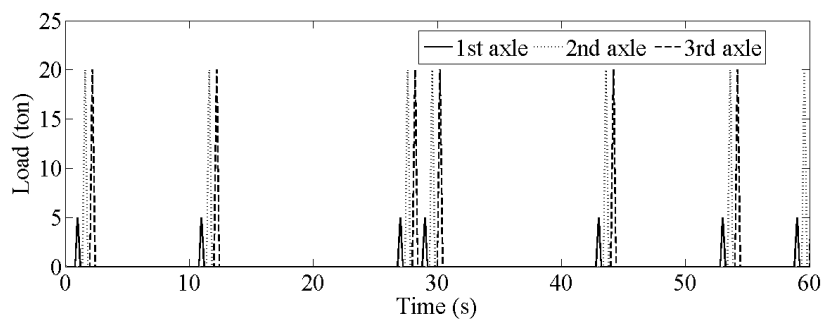
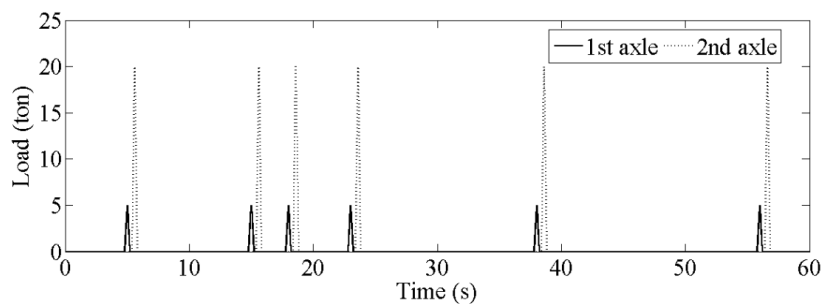
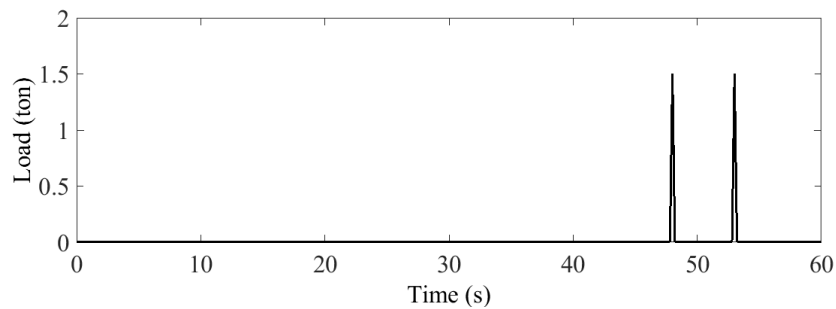


Fig. 4.10 Vehicular load time history during 11.00 – 11.01 am in the southbound direction on 19th May.

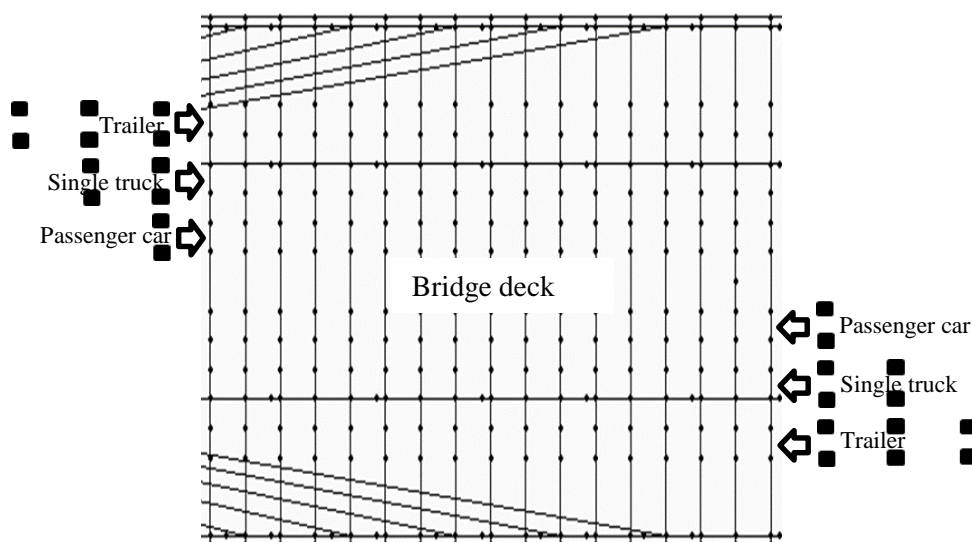


Fig. 4.11 Load assignment on the deck

The actual traffic volume obtained in the traffic counting system on Monday May, 19th as shown in **Fig. 4.12** was used to construct the load time history of the inputs for the FE model. The traffic data have a large fluctuations and include the data during traffic congestion which are the large drop in the number of equivalent trucks at around 8:00 am. Therefore, the selected one-day traffic data can cover all of the traffic conditions for the bridge. The constructed input time history was assigned on each traffic lane node by the different arrival time which depended on the vehicle speeds. **Figure 4.13** shows samples of the input time history of the two consecutive nodes which have spacing of 4 m. The assigned vehicle speed is 50 km/h which is the normal traffic flow speed on the bridge, therefore, the second nodes have input time lag around 0.3 s.

For the FE analysis in this study, effects of the roadway roughness, approach conditions and vehicle suspension on the dynamic responses were not included in the analysis. The one-day time history of the vehicular loads were input in the models in order to obtain one-day time history of the bridge responses. The outputs were calculated in every 0.02 second.

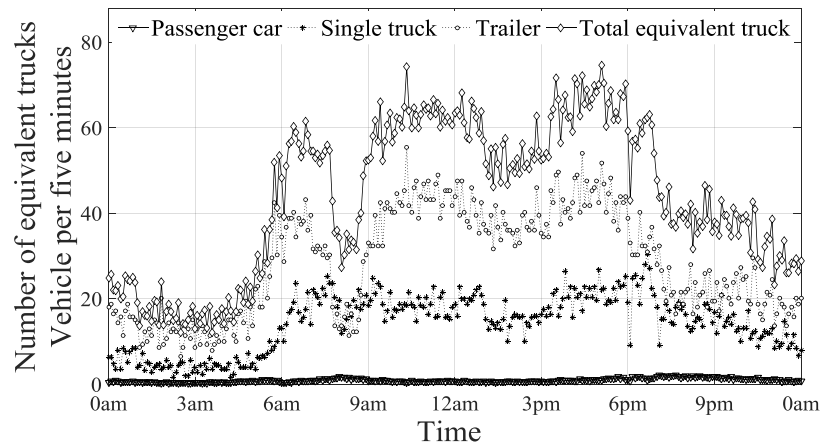
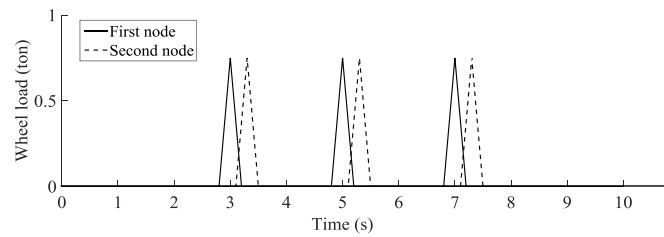
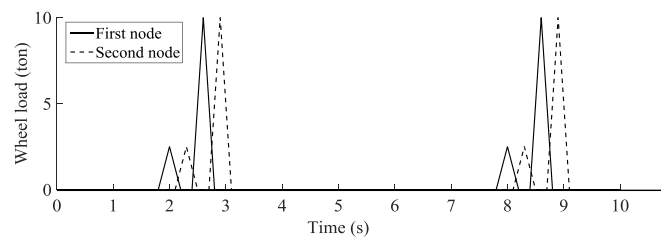


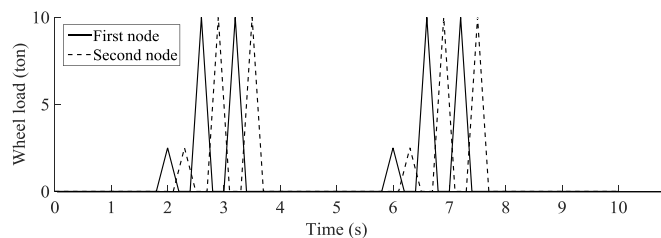
Fig. 4.12. Traffic data on Monday, May 19th for model inputs.



(a) Node for passenger car lanes.



(b) Nodes for single truck lanes.



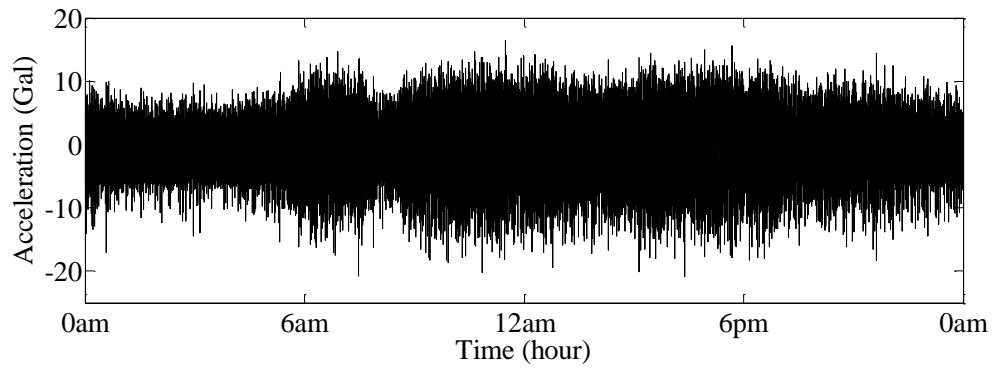
(c) Nodes for trailer lanes.

Fig. 4.13. Samples of input time history for two consecutive nodes.

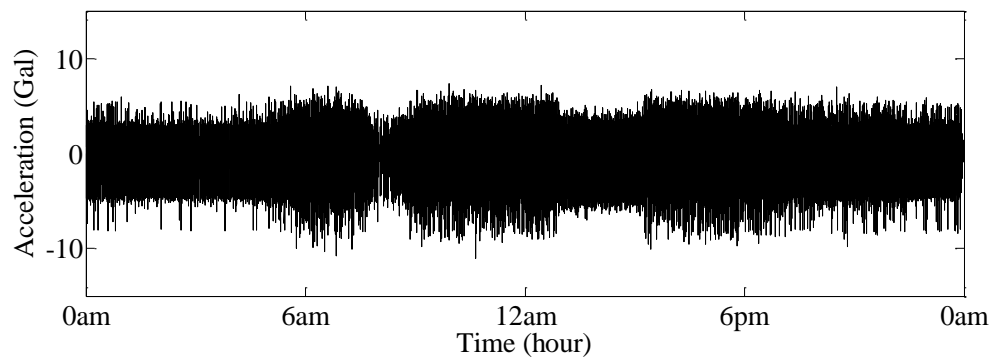
4.3 MODEL OUTPUT VALIDATION

In the FE analysis, dynamic responses excited by the traffic loads were calculated every time increment of 0.02 second. The calculated accelerations of the deck at the location installed the AC-2 sensor and the calculated accelerations of the cable at the location installed the AC-6 sensor, subjected to the traffic loads on 19th May, are shown in **Fig. 4.14**. The calculated acceleration correspond to the measured ones that have the amplitudes during the daytime (6.00 am – 6.00 pm, large traffic volume) larger than those during the nighttime (small traffic volume) and have the drops around 8.00 am (traffic congestion). To more compare the calculated and measured accelerations, their RMSs of every 5 minutes interval were plotted together as shown in **Fig. 4.15**. The RMSs of the calculated deck accelerations are a bit higher than those of the measured accelerations. However, they have the same trend that is large during the daytime and small during the nighttime. Moreover, both RMSs of the calculated and measured accelerations drop around 8.00 am at which the traffic congestion takes place. The drop of the RMSs of the calculated deck accelerations starts at around 7.00 am while the drop of the measured ones starts at around 6.00 am. The discrepancy might be caused by the slow traffic flow on the bridge during this period meanwhile the assigned speed of the vehicles in the FE models is constant. For the RMSs of the cable accelerations, the RMSs of the calculated accelerations have the same trend as those of the deck accelerations and generally have close amplitudes with the RMSs of the measured ones. Except during the traffic congestion, they have the different trend that might be caused by the vehicular speeds as mentioned before. Both RMSs of the calculated accelerations of the deck and cable vary with the assigned traffic volumes in the models and highly associate with the number of the equivalent trucks (**Fig. 2.6**). In order to investigate effects of the vehicular speeds on the accelerations obtained by the FE analysis, the assigned speed of 50 km/h was decreased to 40 km/h during 6.00 am to 7.00 am and to 30 km/h during 7.00 am to 8.00 am. Then the speed was increased to 40 km/h during 8.00 am to 8.30 am and then it was recovered to 50 km/h again. When the speeds of the vehicles decrease, the RMSs of the calculated deck accelerations decrease and they have more agreement with those of the measured ones as shown in **Fig. 4.16**. For the RMSs of the calculated cable accelerations, they decrease as well when the vehicular speeds decrease, and

they are more sensitive to the speeds than those of the deck. However, they cannot recreate fluctuations of the measured ones during the traffic congestion.

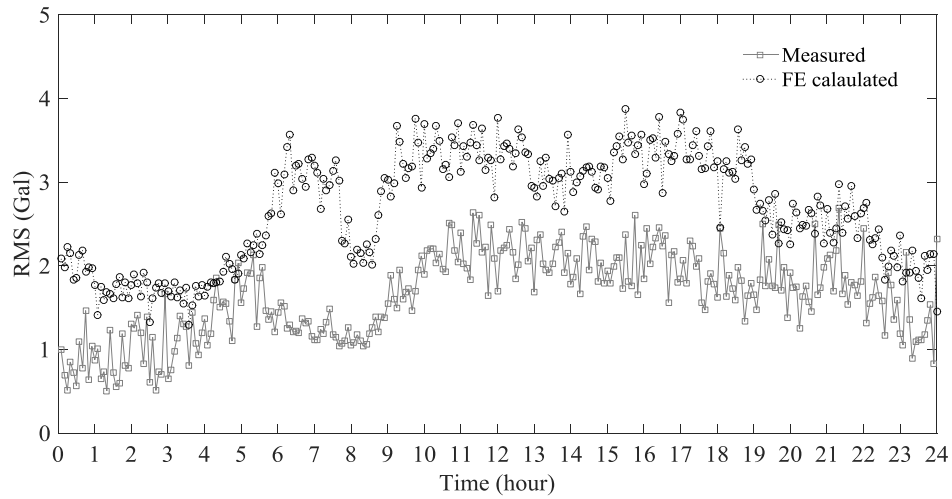


(a) Calculated accelerations of the deck at AC-2

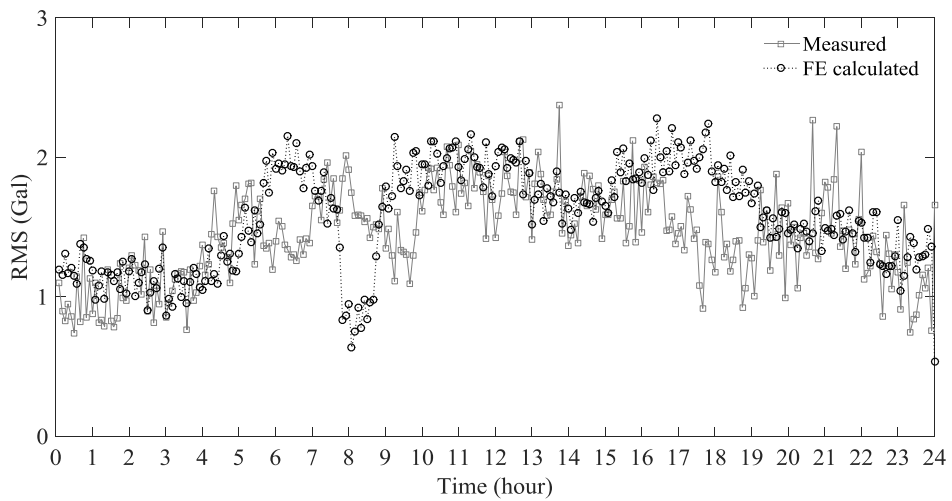


(b) Calculated accelerations of the cable at AC-6

Fig. 4.14 Calculated and measured accelerations on 19th May

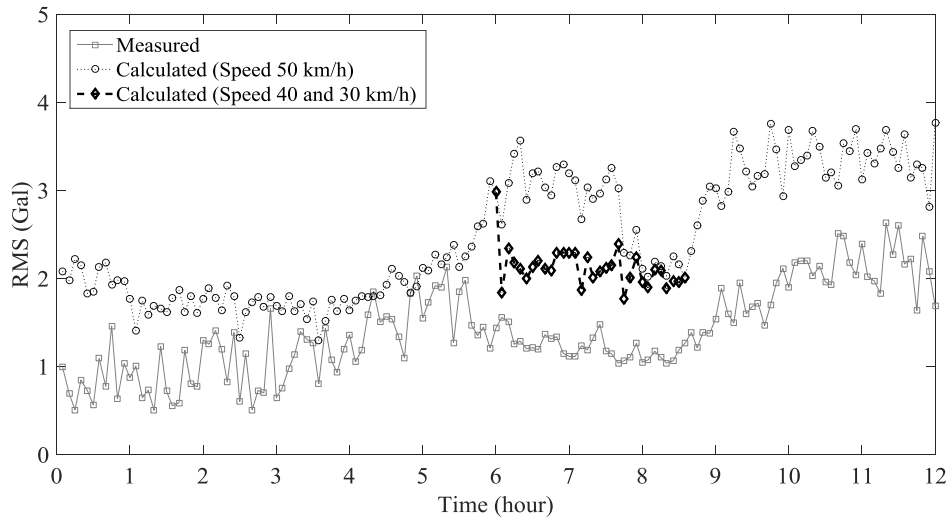


(a) RMSs of deck accelerations at AC-2

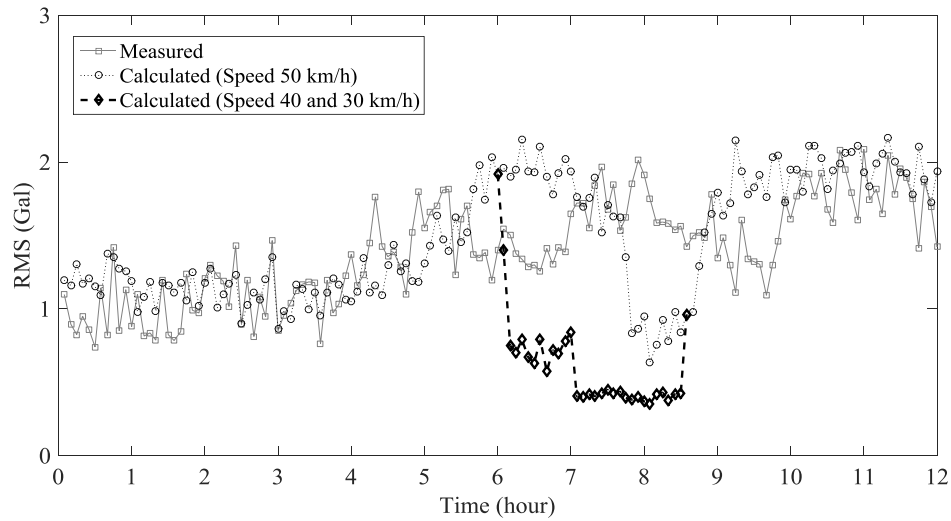


(b) RMSs of cable accelerations at AC-6

Fig. 4.15 RMSs of the calculated and measured accelerations on 19th May



(a) RMSs of deck accelerations at AC-2

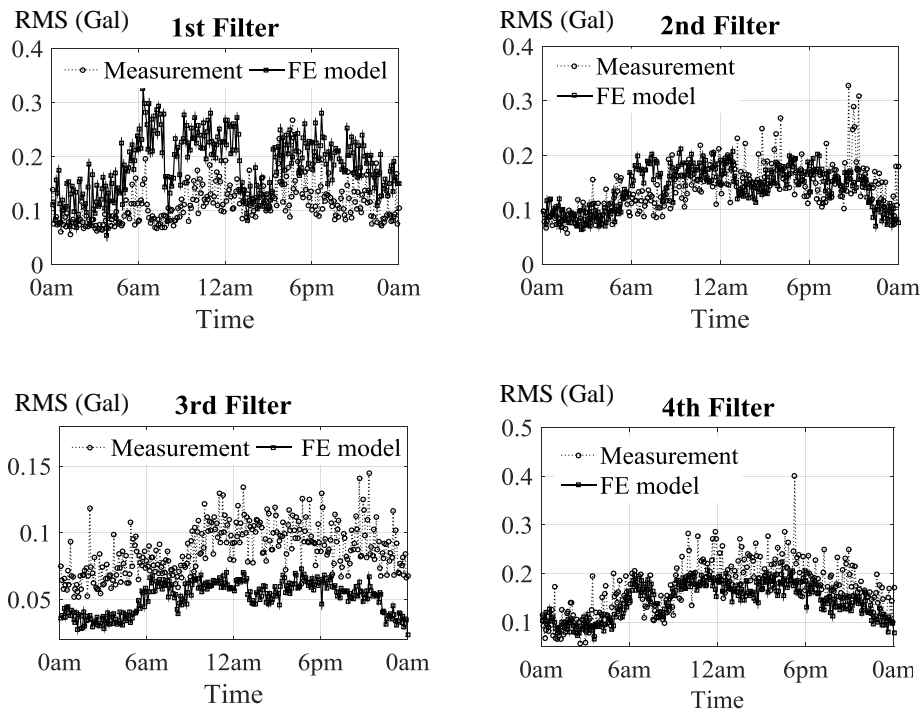


(b) RMSs of cable accelerations at AC-6

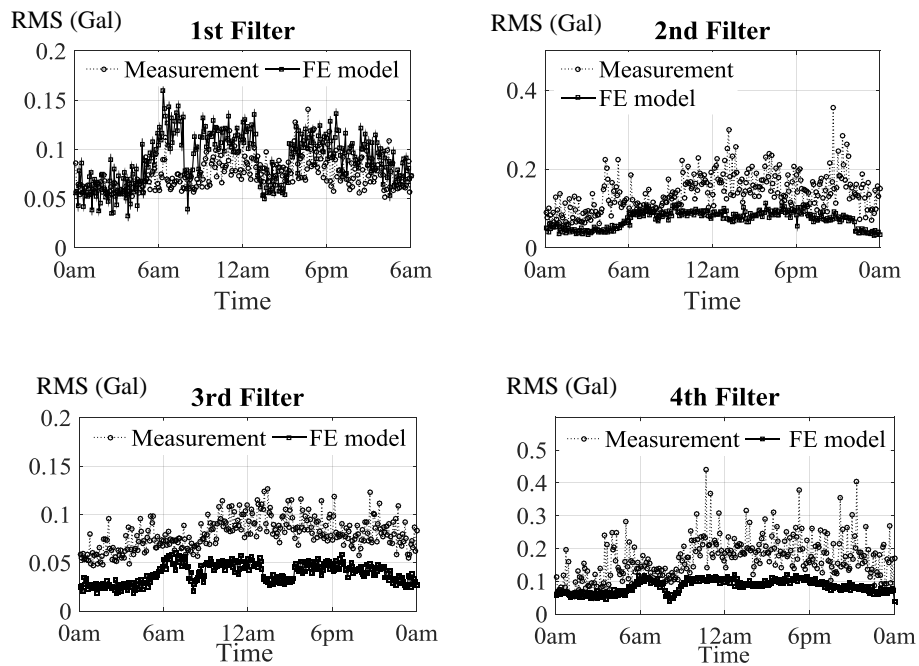
Fig. 4.16 RMSs of the calculated and measured accelerations during traffic congestion on 19th May

For understanding effects of types of the vehicles on the bridge dynamic responses, each vehicular load type was assigned in the FE models with the same volume that is 180 vehicles per hour. It was found that RMSs of the calculated deck accelerations were 0.11, 1.74 and 3.06 Gal for the passenger cars, single trucks, and trailers. RMS ratios of the passenger cars and trailers to the single trucks were 0.06 and 1.76, respectively. For the RMSs of the calculated cable accelerations, they were 0.04, 0.67 and 1.17 Gal for the passenger cars, single trucks, and trailers, respectively. RMS ratios of the passenger cars to the single trucks were 0.06 and 1.75 for the trailers to the single trucks. The RMS ratios corresponded to the ratios of the vehicular weights that are 0.06 and 1.80 for the passenger cars and trailers to the single trucks, respectively. Therefore, the converting each vehicle to the equivalent trucks based on the vehicular weights is reasonable for representing the total traffic volume on the bridge.

In addition, the model outputs were validated not only the raw responses, but also the filtered responses. **Figure 4.17** show the plots of RMSs of the filtered each of five-minute responses in the first four frequency ranges for the measured and calculated accelerations of the deck and cable. In the **Fig. 4.17-a**, it indicates that the RMSs of the 2nd and 4th filtered deck accelerations obtained from the measurement and FE model are more correspondent than the others. **Fig. 4.17-b** shows that the RMS of the 1st filtered cable accelerations has a good agreement between the measurement and FE model. In the previous section, it was found that the RMSs of the deck acceleration filtered with the 2nd and 4th filters, and cable acceleration filtered with the 1st filter were the sensitive features to the traffic volume. Notice that the model output variation was influenced by only the changing traffic volume. As a result, those features obtained from the measurement and Fe model had a good agreement.



(a) Vertical deck accelerations at AC-2



(b) Cable accelerations at AC-6

Fig. 4.17. RMSs of the filtered accelerations of the deck and cable

4.4 EFFECTS OF TRAFFIC VOLUME AND SPEED ON DYNAMIC RESPONSES

In the previous section, it was found that the traffic volume and speed of the traffic flow had correlation with the dynamic responses of the bridge. When the traffic volume or flow speed increase, the amplitudes of vibration also increase. In this section, the effects of traffic volume and speed were more investigated.

4.4.1 Traffic Volume Effects

In order to investigate the effects of traffic volume on the dynamic responses, The PSDs determined from accelerations of the deck that measured at different traffic volumes were compared. The selected traffic volumes consisted of three sets and each set included three different volumes that were small, moderate and large volumes. Three sets of the PSDs in the first four peaks obtained from the measurement are shown in **Fig. 4.18** and those obtained FE models are shown in **Fig. 4.19**. The figures show that when the traffic volume increase, the vibration amplitudes of the first four peaks obtained from both measurement and FE models increase, as well. It could be concluded that the traffic volume directly influenced on the amplitudes of the bridge vibration.

4.4.2 Traffic-flow speed Effects

Actually, the traffic volume its self already includes the speed effects as shown in the **Eq. (4.1)** defined as:

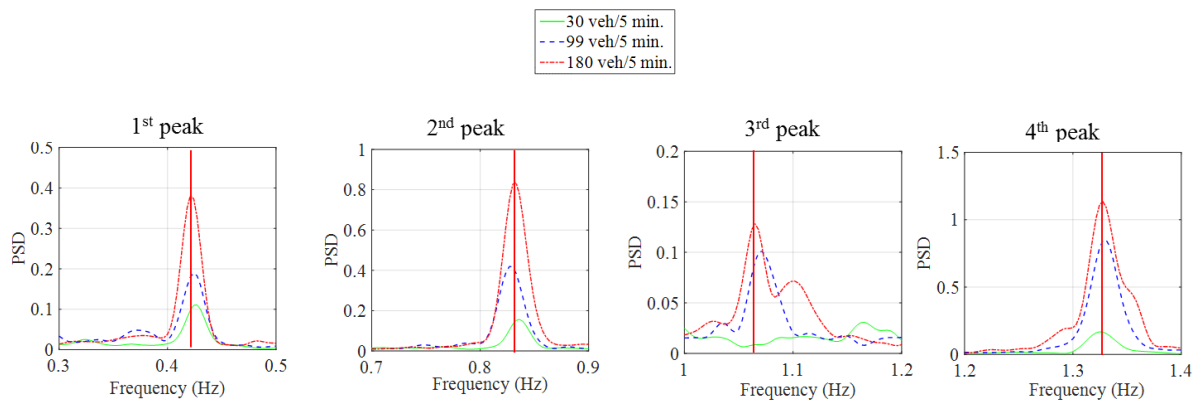
$$N_{TR} = K \times V \quad (4.1)$$

where N_{TR} is traffic volume (A number of vehicles per time), K is traffic density (A number of vehicles per distance) and V is speed of traffic flow (Distance per time). It can be seen that

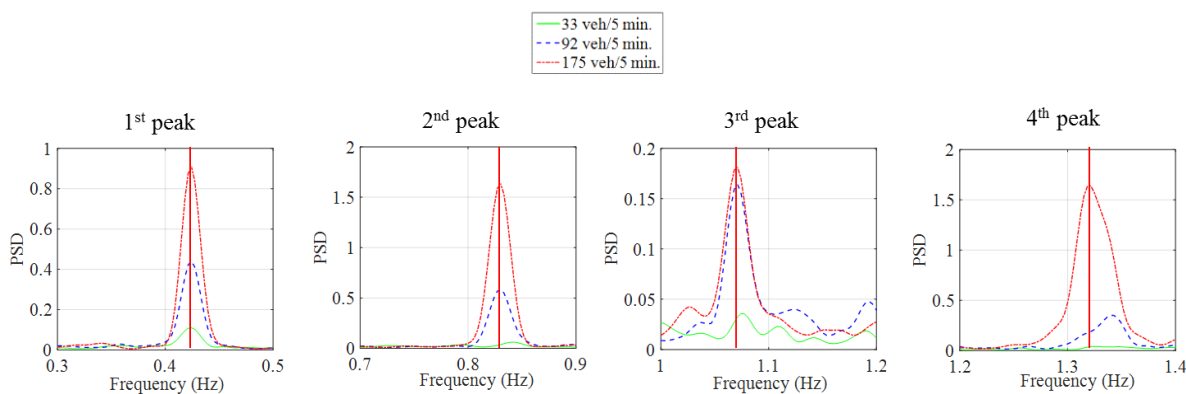
the traffic volume increases when the traffic flow speed increase in the case of same traffic density.

In this section, the traffic flow speed was investigated by using FE models. In the analysis, the traffic volume was kept constant, it means that both traffic density and flow speed were changed. When the traffic flow speed increases, the traffic density will decrease, inversely, when the traffic flow speed decreases, the traffic density will increase, to obtain the constant traffic volume. **Figure 4.20** shows PSDs in the first four peaks obtained from the FE model. The dashed-line PSDs were determined with assigning the traffic flow speed of 50 km/h and the continuous-line ones were determined with assigning the traffic flow speed of 30 km/h. The figure shows that for the lower modes (1st and 2nd peaks), the vibration amplitudes of slow traffic flow are larger than those of the faster traffic flow, and for the higher modes (3rd and 4th peaks), the vibration amplitudes of slow traffic flow are smaller than those of the faster traffic flow. It might be caused by the low-frequency excitation (slow traffic flow) and high-frequency excitation (high traffic flow).

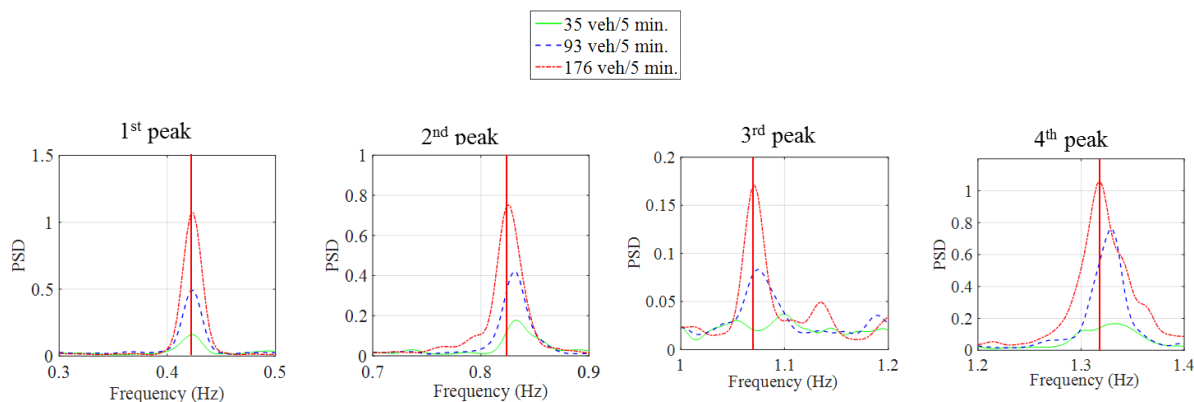
In addition, the effects of the traffic loads were further investigated by changing traffic volumes and vehicle speeds in the model. The trailer load model was assigned in the FE model with the different volumes which were 30, 70 and 100 vehicles per five minutes, and various speeds of 30, 40 and 50 kilometers per hour. **Figure 4.21** shows the plot of the RMSs of accelerations of the deck at AC-2, and the traffic volume in each assigned speed. It can be seen that when the input traffic volumes increase, the accelerations increase for every certain speed, and also when the assigned speeds increase, the accelerations increase for every constant traffic volume. The traffic volume or the number of passing vehicles per time acts as the frequency of the traffic excitation. The large number of passing vehicles that is the high excitation frequency can induce the large responses. For the vehicle speed, it represents the movement of the traffic loads along the bridge. When the loads move faster, the bridge responses are larger as well.



(a) Traffic volumes of 30, 99 and 180 equivalent trucks per five minutes

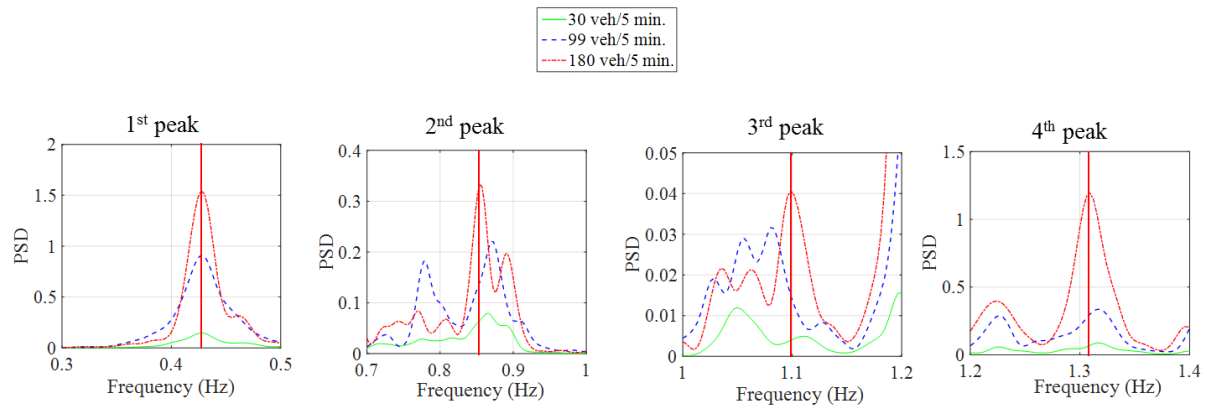


(b) Traffic volumes of 33, 92 and 175 equivalent trucks per five minutes

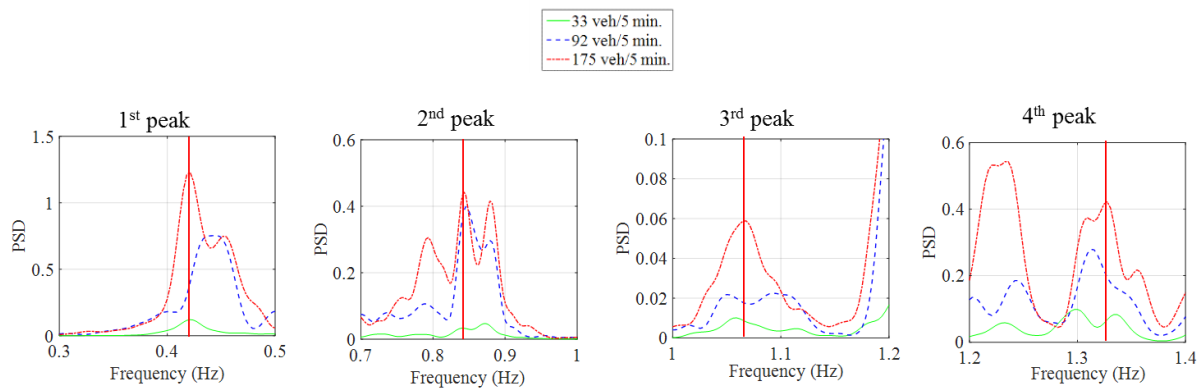


(c) Traffic volumes of 35, 93 and 176 equivalent trucks per five minutes

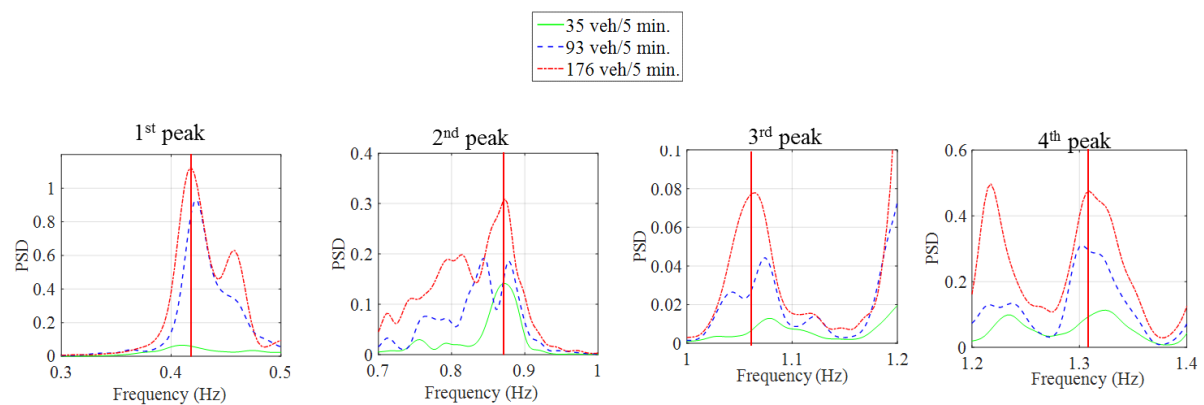
Fig. 4.18 PSDs obtained from the measurement in different traffic volumes



(a) Traffic volumes of 30, 99 and 180 equivalent trucks per five minutes



(b) Traffic volumes of 33, 92 and 175 equivalent trucks per five minutes



(c) Traffic volumes of 35, 93 and 176 equivalent trucks per five minutes

Fig. 4.19 PSDs obtained from FE models assigned different traffic volumes and constant speed of traffic flow.

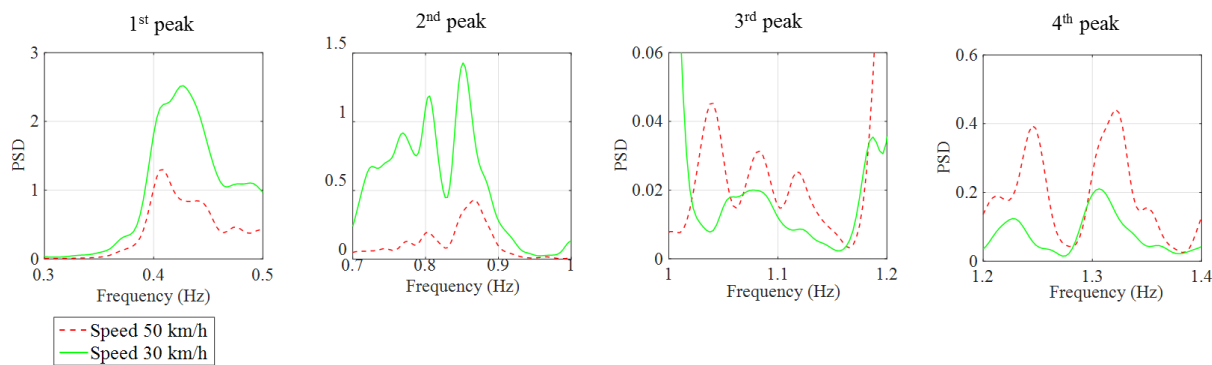


Fig. 4.20 PSDs obtained from FE models assigned constant traffic volume and different speed of traffic flow

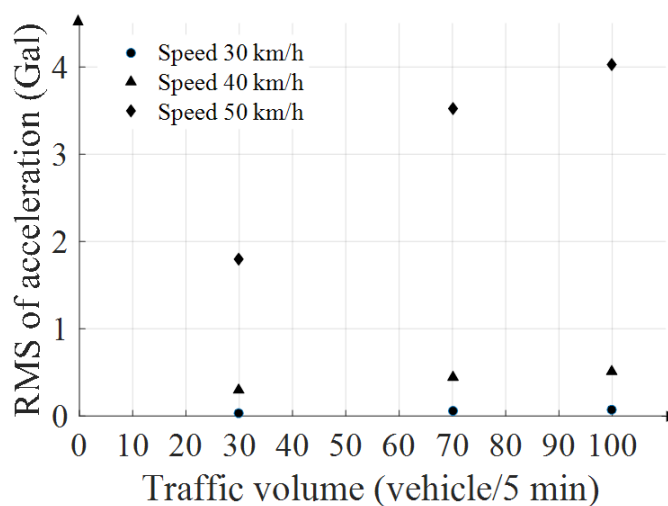


Fig. 4.21. RMSs of deck accelerations

In this section, the constructed FE model was validated and used for investigation of the traffic volume effects on the dynamic responses. It was found that not only the traffic volumes, but also vehicle speeds had effects on the dynamic responses. In the case of the same traffic volumes, the response amplitudes increased when the speeds of vehicles increased. In the next section, the FE model and the traffic volume prediction model will be used in the bridge evaluation.

4.5 CONCLUSIONS

This chapter showed FE modeling for the bridge. The FE models could predict the modal properties that were the resonant frequencies and mode shapes, with a good accuracy. The vehicular loads were modeled for assigning in the FE models, based on the actual vehicles passing on the bridge. Then the vehicular load time history was constructed based on the traffic counting data. The dynamic responses obtained from the FE models showed more that not only the traffic volumes, but also vehicle speeds had effects on the dynamic responses. In the case of the same traffic volumes, the response amplitudes decreased when the speeds of vehicles decreased.

Chapter 5

5. TRAFFIC VOLUME ESTIMATION

Based on the acquired data and analysis results in chapter 2 and 3, it could be concluded that the traffic volumes associated with the extracted features that are the resonant frequencies, RMSs of deck and cable accelerations, and RMSs of deck tilts, while the temperature did not show a significant relation with those features. It was then confirmed by the FE analysis that the RMS of deck and cable accelerations associated with the bridge traffic volumes. In this chapter, some of the response features that showed high correlations were then selected for constructing a linear regression model to estimate the total traffic volume on the bridge.

5.1 CORRELATIONS WITH THE TRAFFIC VOLUME AND TEMPERATURE

The correlation and regression analysis of the dynamic responses at each sensor and the temperature and traffic data to the peak frequencies in the target bridge has been conducted in our previous study (Wattana and Nishio, 2015). Here, it was found that the total traffic volume had high correlations especially with the amplitude of accelerations of the deck and the stayed-cable, and the resonant frequencies of the lower modes. **Figure 5.1** shows the significant results related to this study, in which, it can be seen that all of the 1st to 10th peak frequencies have low correlations with the temperature; on the other hand, the correlations with the total traffic volume show relatively high in the lower modes. This was considered to be because the variation of temperature in the site of the target bridge was low; therefore, the effects of traffic became relatively high. **Figure 5.2** (a) and (b) also show the correlation coefficients between the RMSs of responses (both non-filtered and 1st- to 10th-filtered ones) and the temperature and the total traffic volume, respectively. It was understood that the features of RMS also had low sensitivities to the temperature, and they had high contributions to the traffic volume. In the deck acceleration (AC-2), the correlation coefficients in the RMSs of 1st- to 5th-filtered responses shows relatively high values, especially highest in the 4th-filtered response. Also in the cable acceleration (AC-6) and the tilt of the deck (TL-2), the correlations with the traffic volume also depend on the frequency ranges of the filters. In addition, from the results in **Fig. 5.1** and **Fig. 5.2** (b), it was shown that the correlation coefficients between the traffic volume and the resonant frequencies were basically negative, and those with the RMSs of bridge responses were positive. It was considered that the traffic volume performed as the additional mass on the bridge deck, and that thus caused the decrease of resonant frequencies, and the responses with large amplitudes.

Based on these results, it could be summarized that the peak frequencies and the RMSs of the deck accelerations, the cable acceleration, and the deck tilts associated with the traffic volume. They could be used as candidate input factors for the traffic volume estimation which will be presented in the next section.

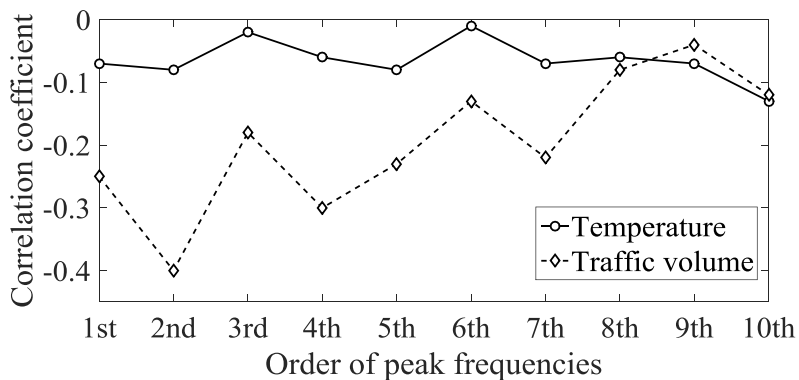
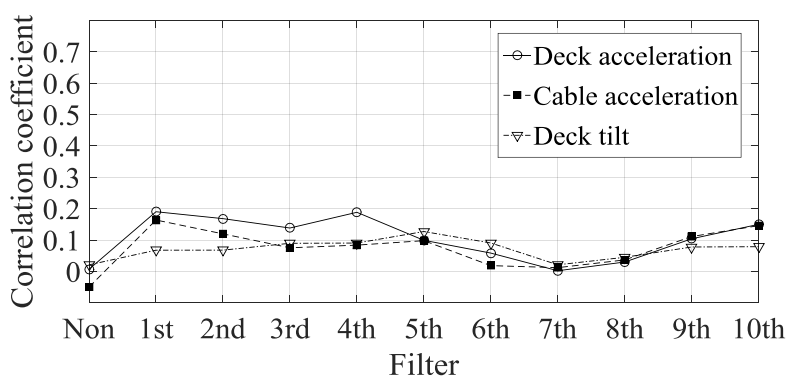
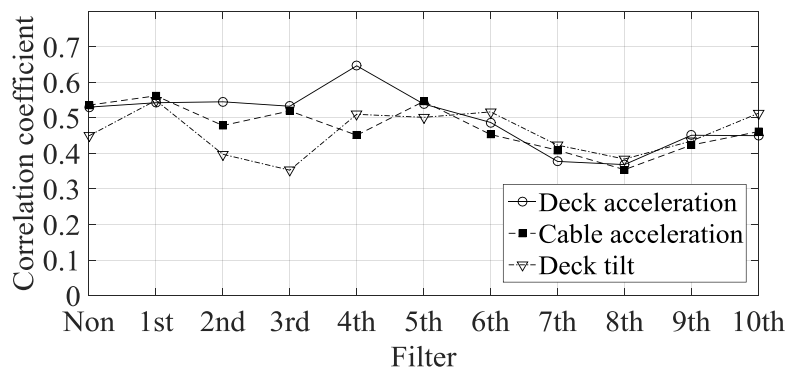


Fig. 5.1 Correlation coefficients between peak frequencies and temperature, and traffic volume plotted against order of peak frequencies



(a) Correlation coefficients between temperature and RMSs of non-filtered and filtered responses



(b) Correlation coefficients between traffic volume and RMSs of non-filtered and filtered responses

Fig. 5.2 Correlation coefficients between the RMSs of responses, and the temperature and the traffic volume data.

Based on these results, it could be summarized that the peak frequencies and the RMSs of the deck accelerations, the cable acceleration, and the deck tilts associated with the traffic volume. They could be used as candidate input factors for the traffic volume estimation which will be presented in the next section.

5.2 SELECTION OF FEATURES FOR ESTIMATION

The linear regression models for estimating the traffic volume were trained on 288 data points of the first day acquired data (the data of May 17th), and the estimated model was examined on the predicted traffic volume of 576 data points of the last two day acquired data (May 18th and 19th). On the basis of the results of the previous verification, the candidate predictor variables were then the ten peak frequencies ($F1$ to $F10$), the RMS of the vertical accelerations of the mid-span deck (RMS_{DE}), the RMS of the accelerations of the cable (RMS_{CA}), the RMS of the longitudinal tilts of the mid-span deck (RMS_{TLX}), the RMS of the transversal tilts of the mid-span deck (RMS_{TLY}), and the RMSs of the 1st- to 10th-filtered responses in each data denoted by RMS_{DEi} , RMS_{CAi} , RMS_{TLXi} and RMS_{TLYi} , where subscript i identifies the applied filters ($i = 1-10$). The total number of the candidate features for the predictor variables became fifty-four; therefore, the procedure for preliminary selection based on the correlation matrix was applied to them. As presented in **Fig.5.3**, the procedure was started from:

(1) the calculation of a correlation matrix, the components of which were the correlation coefficients, of the predicted variable (traffic volume, N_{TR}) and all of candidate response features (peak frequencies and RMSs).

(2) the candidate feature that showed the maximum correlation coefficient with the traffic volume was then selected as the predictor variable.

(3) In the next step, the candidate feature that had the highest correlation coefficient to N_{TR} was selected among the remaining candidates.

(4) examine whether it did not show high correlations with the predictor variables, which were already accepted, or not. If the examination was accepted, the selected candidate feature was included as one of the predictor variables. The procedures (2) to (4) were then repeated for all of fifty-four candidate features. Notice that, the high correlation here indicated the correlation coefficient higher than 0.7 (Dancey and Reidy 2007). This measure is adopted to basically avoid the multicollinearity in the regression analysis.

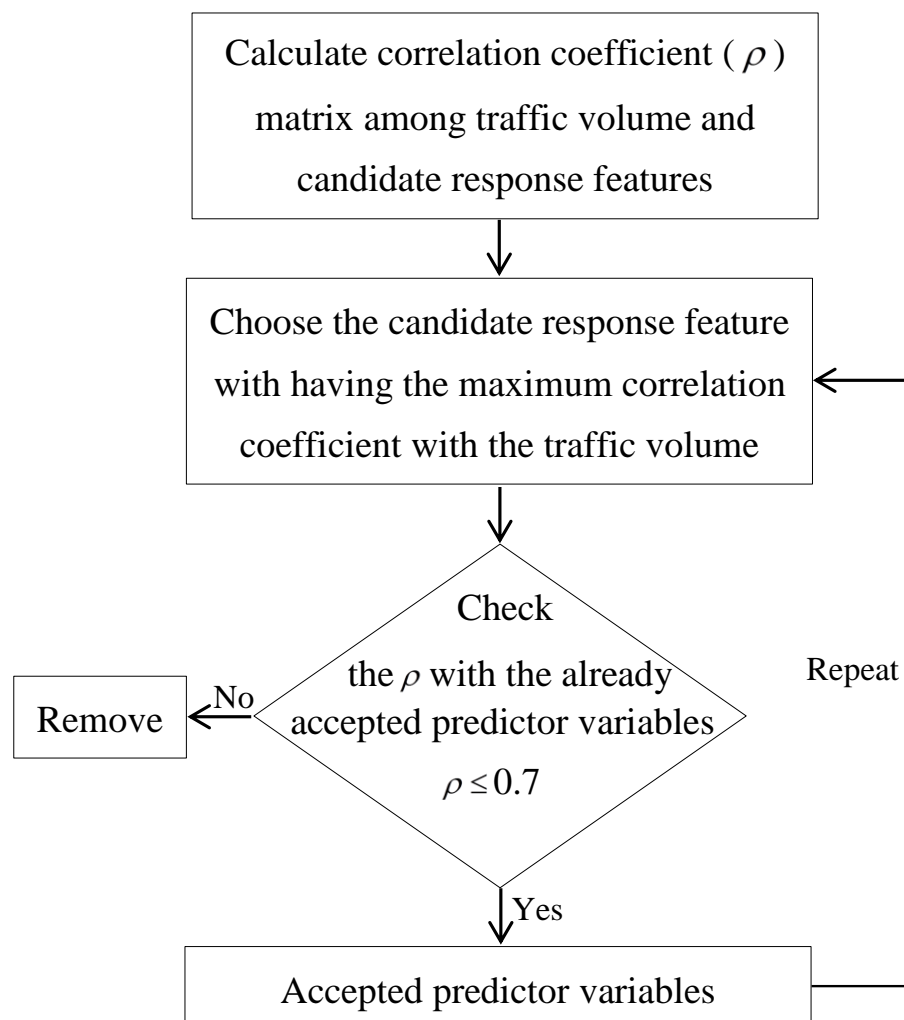


Fig. 5.3 Flow chart for parameter selection

The accepted predictor variables were twenty-one features consisting of the ten peak frequencies and the eleven RMSs of responses. **Table 5.1** presents the correlation coefficients of the accepted ten peak frequencies with the traffic volume calculated for the target one-day data; i.e., May 17th. It actually shows almost the same values as in the plot of **Fig.5.1**, the values in which were calculated from the three-days data. The values indicates that the frequencies of lower modes have higher correlations with the traffic volume, and the 2nd peak frequency shows the highest negative correlation. **Table 5.2** also shows the correlation coefficients of the accepted eleven RMSs with the traffic volume. Here, the RMS of the deck acceleration with the 4th filter shows the highest positive correlation, and the RMSs of the tilt responses in the lateral direction (RMS_{TLX}) are also included as the accepted predictor variables.

Table 5.1 Correlation coefficients between traffic volume variable and peak frequency variables

Variable	Correlation coefficients with traffic volume
<i>F1</i>	-0.26
<i>F2</i>	-0.40
<i>F3</i>	-0.19
<i>F4</i>	-0.29
<i>F5</i>	-0.16
<i>F6</i>	-0.16
<i>F7</i>	-0.16
<i>F8</i>	-0.02
<i>F9</i>	0.00
<i>F10</i>	-0.14

Table 5.2. Correlation coefficients between traffic volume variable and accepted RMS of bridge responses variables

Variables	Correlation coefficients with traffic volume
RMS_{DE4}	0.64
RMS_{DE}	0.58
RMS_{DE2}	0.53
RMS_{CA1}	0.53
RMS_{TLx1}	0.51
RMS_{DE3}	0.49
RMS_{TLy3}	0.43
RMS_{CA2}	0.42
RMS_{CA4}	0.37
RMS_{TLx9}	0.33
RMS_{TLx2}	0.32

5.3 CONSTRUCTED MODEL FOR TRAFFIC VOLUME ESTIMATION

The linear regression requires that the model is linear in regression parameters. It means that the variable can be replaced by the transform variable; generally, the power of two and the logarithm. In order to obtain the best fitting model, three transformed predicted variables; N_{TR} , $(N_{TR})^2$ and $\log(N_{TR})$, and three sets of the accepted predictor variables; X , $(X)^2$ and $\log(X)$, were verified by estimating a linear regression model **Eq.(3.1)** in each of nine cases, which gave nine regression models (Model #1-#9).

In each estimation, all of the transformed predictor variables were firstly ranked by the absolute correlation coefficients with the transformed traffic volume in decreasing order, and the predictor variable with the highest rank was adopted in the model.

Secondly, the predictor variable with the second highest rank was once added in the model, and the static t -value in **Eq. (3.2)** and the VIF factor in **Eq. (3.4)** were calculated. The added variable is adopted when the t -value shows significance and the VIF value satisfies the criterion in Eq. (5); otherwise, it cannot be adopted. These procedures are then repeated until all of the transformed predictor variables are tested.

Finally, the $RMSE$ values in **Eq. (3.3)** are determined to assess the fitting performance of the models. **Table 5.3** summarizes the nine candidate models (Model #1-#9), in which, the adopted transformed predictor variables and the $RMSE$ of each estimated model are indicated; here, the Model#3 shows the best fitting performance with the lowest $RMSE$ of 29.72. The model provides the estimated traffic volume \hat{N}_{TR} with three transformed predictor variables; $\log(RMS_{DE4})$, $\log(RMS_{CA1})$, and $\log(RMS_{DE2})$.

In **Table 5.4**, the estimated parameter coefficients β , their significant levels at the t -test and the VIF values in the estimated Model#3 are presented. All of three predictor variables are significant without the multicollinearity issue because those VIF values become less than 10. The positive coefficients β in all predictor variables indicate that they have positive correlations with the traffic volume. The highest positive coefficient in $\log(RMS_{DE4})$ was understandable because the feature RMS_{DE4} had the highest correlation coefficient in **Table 5.2**.

Table 5.3 Candidate models for traffic volume estimation and the root mean squared error

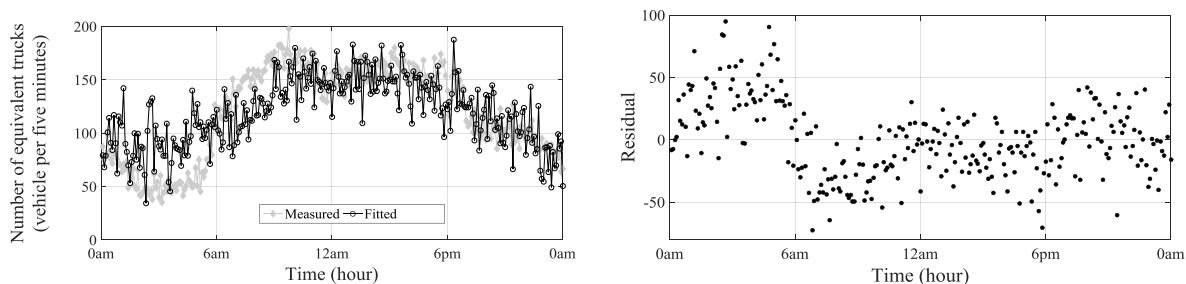
Model#	Transformed		RMSE
	predicted variable	Adopted transformed predictor variable	
1	N_{TR}	$RMS_{DE4}, RMS_{CA1}, RMS_{DE2}, F8$	30.21
2	N_{TR}	$(RMS_{DE4})^2, (RMS_{CA1})^2, (RMS_{DE2})^2, (RMS_{TLx1})^2, (F2)^2$	30.99
3	N_{TR}	$\log(RMS_{DE4}), \log(RMS_{CA1}), \log(RMS_{DE2})$	29.72
4	$(N_{TR})^2$	$RMS_{DE4}, RMS_{CA1}, RMS_{DE2}, F2$	29.97
5	$(N_{TR})^2$	$(RMS_{DE4})^2, (RMS_{CA1})^2, (RMS_{DE2})^2, (RMS_{TLX1})^2, (F2)^2$	30.06
6	$(N_{TR})^2$	$\log(RMS_{DE4}), \log(RMS_{CA1}), \log(RMS_{DE2})$	32.53
7	$\log(N_{TR})$	$RMS_{DE4}, RMS_{CA1}, RMS_{DE2}, F8$	32.88
8	$\log(N_{TR})$	$(RMS_{DE4})^2, (RMS_{CA1})^2, (RMS_{DE2})^2, (F2)^2, (F8)^2$	34.66
9	$\log(N_{TR})$	$\log(RMS_{DE4}), \log(RMS_{CA1}), \log(RMS_{DE2}), \log(F8)$	31.31

Table 5.4 Estimated parameter coefficients, significant levels in OLS, variance inflation factors, coefficient standard errors (SE) obtained by OLS and HAC estimates, and adjusted significant levels in HAC

Coefficient	Variable	Estimated coefficient	Significant level in OLS	VIF	OLS SE	HAC SE	Adjusted significant level in HAC
β_0	Constant	420.55	0.00	-	22.93	27.56	0.00
β_1	$\log(RMS_{DE4})$	150.61	0.00	1.74	19.22	21.23	0.00
β_2	$\log(RMS_{CA1})$	112.77	0.00	1.46	24.25	28.37	0.00
β_3	$\log(RMS_{DE2})$	68.67	0.00	1.62	19.27	21.87	0.00

Figure 5.4 (a) is then the overlay of the fitted traffic volumes in May 17th on the actual traffic volume data. It shows that the estimated model can recreate the fluctuations of the traffic volume. However, the model could not recreate the traffic volumes with high accuracies in the time of small traffic, which was the nighttime, and the time with high traffic volumes in the daytime. These points can be understood also by **Fig. 5.4** (b) that is the plot of the residual errors; i.e., the differences between the model outputs and the measured data. There is a slight daily trend, in which relatively large positive residuals are distributed in the nighttime (small traffic volume) and large negative residuals are distributed in the daytime (large traffic volume). This trend implies that the residuals contain autocorrelation. It is then ascertained by the autocorrelation function of the residuals in **Fig. 5.5** that shows the evidence of the autocorrelation in the residuals. In the presence of autocorrelation, the standard errors of the estimated coefficients obtained by the OLS estimate are invalid (Wooldridge 2002). Therefore, the t -tests in the **Eq. (2)** are no longer valid for testing the significances of the estimated coefficients. The heteroscedasticity and autocorrelation consistent (HAC) estimate (Newey and West 1987) was adopted to obtain the robust standard errors of the coefficients as shown in **Table 5.4**. The estimated standard errors of the coefficients obtained by the HAC estimate are a bit larger than those obtained by the OLS estimate. However, the adjusted significant levels of each coefficient indicate that all of coefficients are still significant after correction the autocorrelation problem.

The constructed model for estimating the traffic volume showed the accurate fitting performance to the one day trained data (May, 17th), and it was also capable of predicting the traffic volume on the bridge for three-days data (May, 18th, 19th and 21st). Furthermore, it was considered that on the workdays (May, 19th and 21st), the traffic volumes have a same tendency and there is traffic congestion during the morning peak-hour (around 8.00 am) as shown in **Fig. 5.6**. Moreover, the actual and predicted average traffic volume per day (Average Daily Traffic, ADT) generally used in bridge evaluation and planning are shown in Table 2. It shows that the predicted ADT on the workdays (19th and 21st) have a more accuracy (differences of 2% and 6%) than those on Sunday, 18th (10% difference). It might be caused by the speed of vehicles on Sunday that is relatively higher than those on workdays or the accuracy of the predicted traffic volume involves with the speed of the vehicles.



(a) Estimated and predicted traffic volumes (b) Estimated and predicted residuals

Fig. 5.4 Estimated and predicted traffic volumes from the constructed model and their residuals

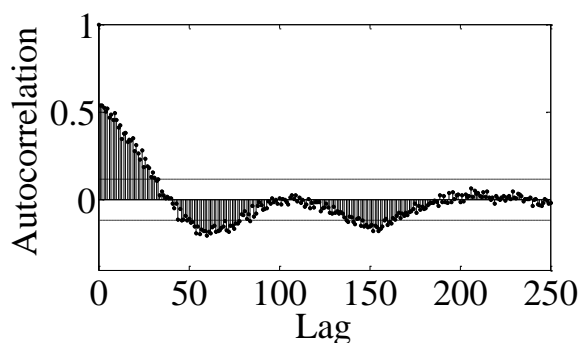
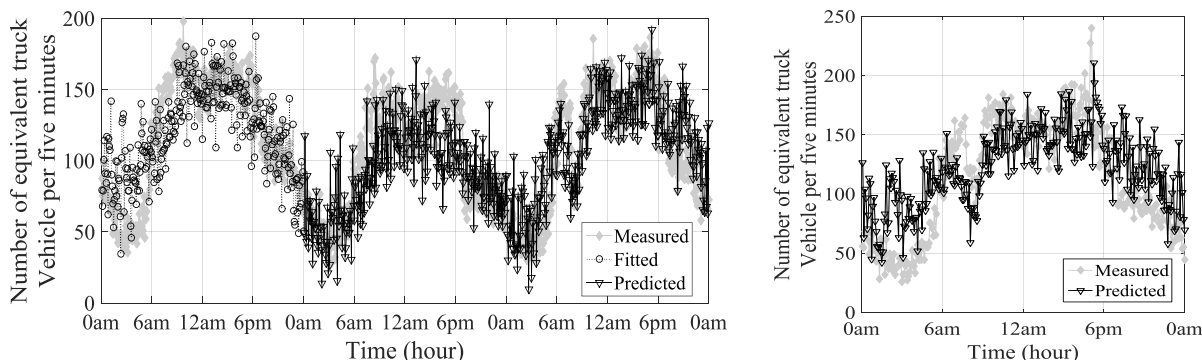


Fig. 5.5 Autocorrelation function of the residuals of estimated traffic volumes



(a) Measured, fitted and predicted traffic volumes on Saturday, May 17th, 2014, Sunday, May 18th, 2014 and Monday, May 19th, 2014.

(b) Measured and predicted traffic volumes on Wednesday, May 21st, 2014.

Fig. 5.6 Measured, fitted and predicted traffic volumes

Table 5.5. Actual and predicted average traffic volume per day
(Number of equivalent trucks per day).

Date	Actual	Predicted	Difference (%)
Sunday, 18th	28,844	25,895	10
Monday, 19th	31,613	32,173	2
Wednesday, 21st	32,964	34,949	6

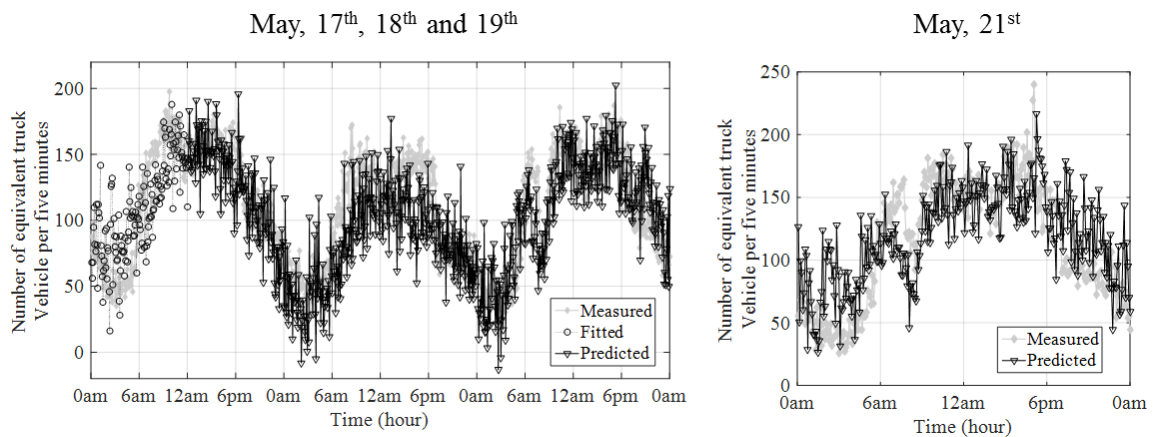
In order to investigate the effects of the length of trained data on the model performance, the performance of the model constructed from three different lengths of trained data that are a half-day, a day and two-day trained data are compared as shown in the **Table 5.6** and **Fig. 5.7** shows then the overlay of the fitted and predicted traffic volumes on the actual traffic volume data of the model constructed from a half-day and two-day trained data. It shows that the accuracy of the model constructed from a half-day trained data is less than those of the models constructed from a day and two-day trained data. The performance of the models constructed from a day and two-day trained data are very close, it could be said that a day trained data are enough for constructing prediction model.

Table 5.6. Estimated parameters and the root mean square error of the models constructed from a half-day, a day and two-day trained data

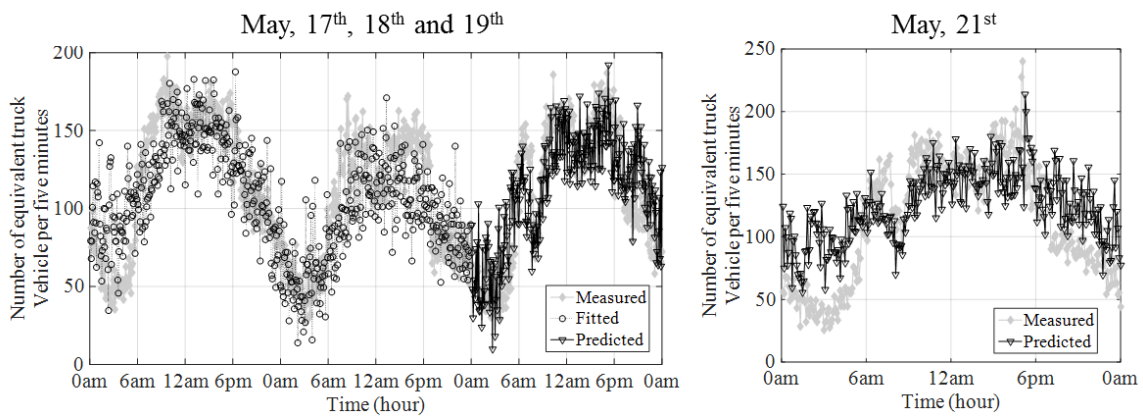
Model #	Trained data	Estimated coefficients			RMSE	
		Constant	$\log(RMS_{DE4})$	$\log(RMS_{DE2})$		$\log(RMS_{CA1})$
1	0.5 day	458.04	184.26	76.49	120.19	33.01
2	1 day	420.55	150.61	68.67	112.77	31.43
3	2 day	402.10	106.65	73.60	119.63	31.58

It was then concluded that the constructed regression model for estimating the traffic volume only from the structural dynamic responses was applicable. In addition, the estimation model can recreate the daily fluctuations of the traffic volume especially during the time of the traffic congestion. In other words, it can accurately predict traffic volume on the bridge in both normal and congested traffic conditions. In the congested traffic condition, the vehicle speeds

are slow. As a result, the traffic volume decreases and al-so the dynamic responses of the bridge drop during this condition, as verified by the FE analysis in the previous section. Therefore, the predicted traffic volume based on the dynamic responses is small and has a good agreement with the measured traffic volume.



(a) Half-day trained data



(b) Two-day trained data

Fig. 5.7 Measured, fitted and predicted traffic volumes on May, 17th, 18th, 19th and 21st, 2014

5.4 CONCLUSIONS

In this chapter, the statistical modeling for estimating the traffic volume on the target cable-bridge bridge from the dynamic responses was presented. The significant conclusions are summarized in below:

- The correlations of the response features extracted from the SHM data; peak frequencies and amplitudes of responses, and the temperature and the traffic volume were investigated. The results revealed that the traffic volume was a dominant factor that influenced on variances of the peak frequencies and the RMSs of the deck accelerations, the cable acceleration, and the deck tilts while the temperature showed low effects on them in the target bridge.
- The response features used for constructing the traffic volume estimation model, were selected by the procedure based on the correlation coefficients among those features and the traffic volume. The procedure could provide the appropriate features that were adopted as the predictor variables of the regression model for estimating the traffic volume.
- The constructed model for estimating the traffic volume showed the accurate fitting performance to the data, and it was also capable of predicting the traffic volume on the bridge.

The predicted traffic volumes from the SHM data are then expected to be applied for the bridge evaluation and the effective bridge planning; e.g. enhancing the bridge inspection scheduling by taking account of the traffic volume, the capacity and congestion analysis, forecasting the future traffic demand, estimating the economic benefits. The considerations for appropriate applications will be worked in our future study. However, it could be clearly shown that the dynamic response data acquired in the SHM system could be also used to construct a statistical model for estimating the traffic volume on the bridge, with the proposed methodology of modeling based on the correlation coefficients in this study.

REFERENCES

Dancey C., Reidy J. *Statistics Without Maths for Psychology: Using SPSS for Windows*. Prentice Hall: London, 2007.

Newey W. K. & West K. D. A Simple, Positive Semi-Definite Heteroscedasticity and Autocorrelation Consistent Covariance Matrix. *Econometrica*. 1978; **55**: 703–708.

Wattana K., Nishio M. A Analysis of multivariate SHM data of a cable-stayed bridge considering operational and environmental effects. *Proc. 7th international conference on Structural Health Monitoring of Intelligent Infrastructure*, Italy, July 2015.

Wooldridge J. M. *Introductory Econometrics: A Modern Approach*. South-Western: Tennessee, 2002.

Chapter 6

6. SAFE LOAD CAPACITY AND RELIABLY EVALUATION

In the last chapter, the traffic volumes were estimated by using the SHM data. The estimated traffic volumes can be used to estimated vehicular live loads used in evaluating safe load capacity of the bridge. In this chapter, the bridge will be evaluated safety based on the the *Load and Resistance Factor Rating (LRFR)* method provided in *The Manual for Bridge Evaluation* (AASHTO, 2013) and reliability analysis.

6.1 LOAD AND RESISTANCE FACTOR RATING

In this research, bridge load rating was performed for determining the safe load capacity of the bridge by following the AASHTO LRFR methods developed to provide uniform

reliability in the load rating. The AASHTO load rating is based on existing structural conditions, material properties, loads and traffic conditions.

6.1.1 Load Rating Procedure

The LRFR method is comprised of three distinct procedures; design load rating, legal load rating, and permit load rating, by using different live load models and evaluation criteria. For evaluating the Bhumibol I bridge, the permit load rating was not performed because only legal vehicles are allowed to pass the bridge. A flow chart of the LRFR for the bridge is shown in **Fig. 6.1**. The design load rating is a first-level for the evaluation. It is based on the *AASHTO LRFD Bridge Design and Specifications* (AASHTO, 2012) by using HL-93 loads as shown in **Fig. 6.2** and uses dimensions and properties of the bridge in its present as inspected condition. There are two checking levels for the design load rating; first, an inventory level reliability, the bridge is screened for the strength limit state at LRFD design level of reliability, and second, an operating level screens the bridge for the lower level of reliability of the LRFD design. The design load rating can identify the bridge that should be load rated for legal loads. If the bridge passes the design load check (Rating factor, $RF \geq 1$) at the inventory level, no further evaluation is necessary. If the bridge passes HL-93 screening only at the operating level, It will have adequate capacity for AASHTO legal loads as shown in **Fig. 6.3** but may not pass for state legal loads (**Fig. 6.4**) that are significantly heavier than the AASHTO legal loads. The legal load rating is a second level rating evaluation providing a single safe load capacity for a given truck configuration applicable to the AASHTO and state loads. The results of the legal load rating could be used as a basis for load posting or bridge strengthening.

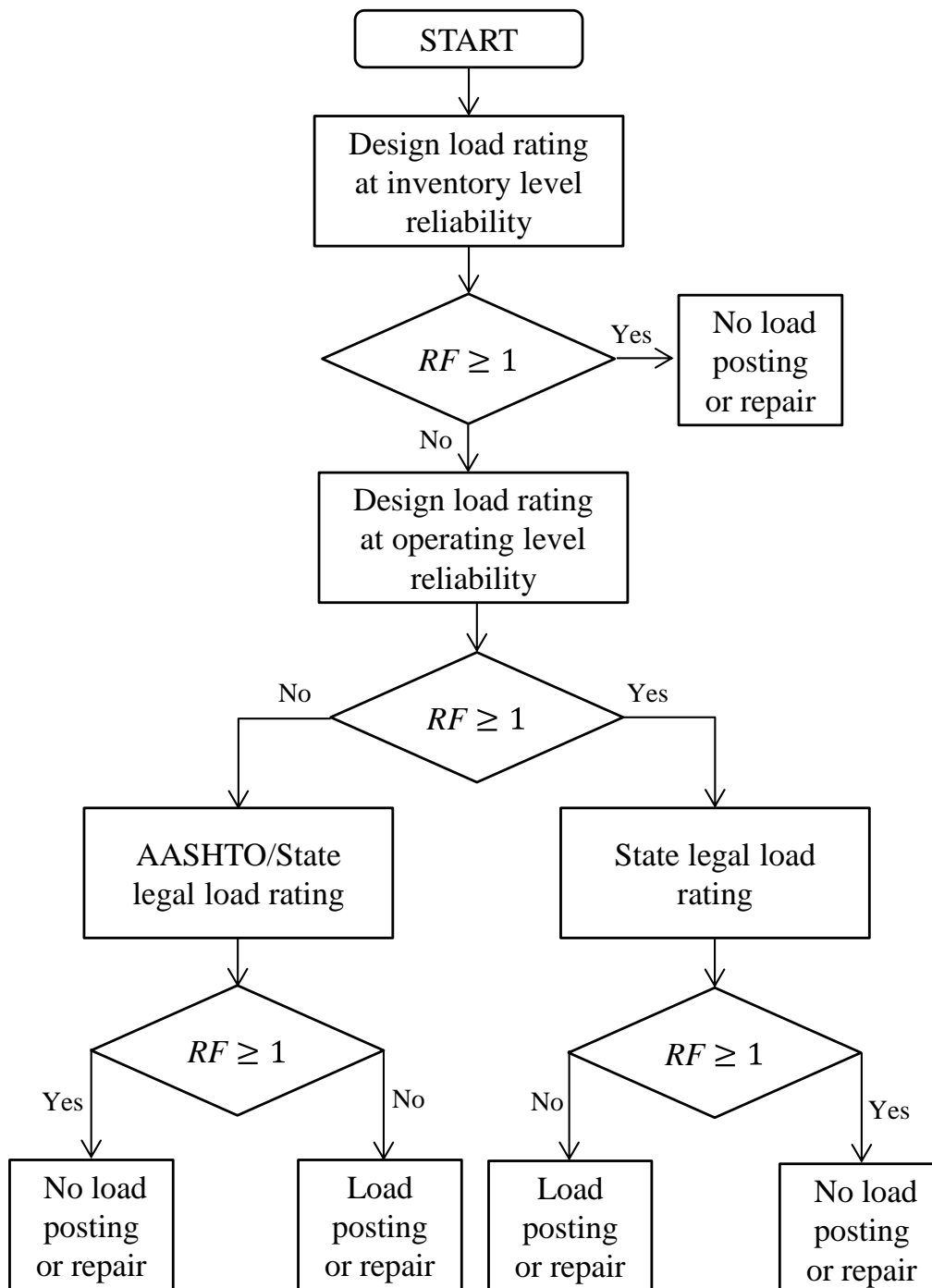


Fig. 6.1 AASHTO LRFD flow chart (AASHTO, 2013) for the Bhumibol I Bridge

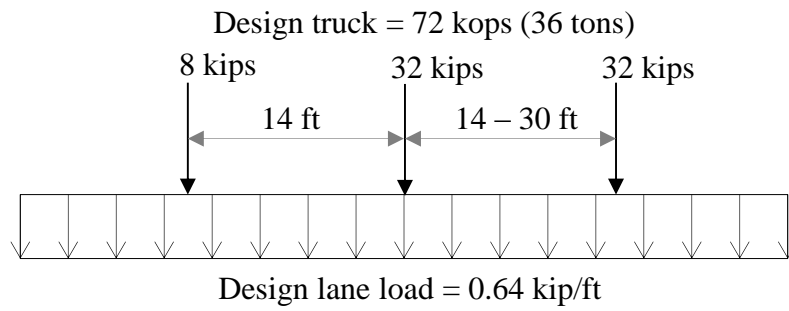


Fig. 6.2 HL-93 design live load (AASHTO, 2013) for the Bhumibol I Bridge

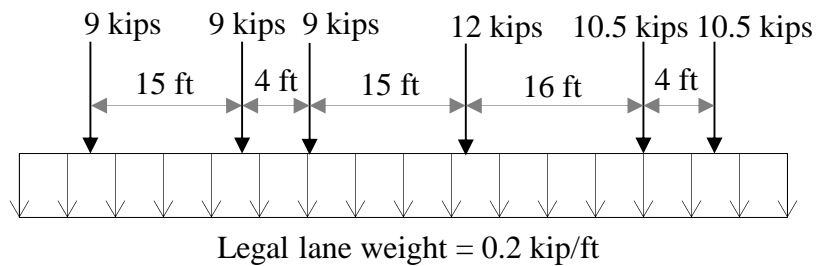


Fig. 6.3 AASHTO legal load (AASHTO, 2013) for the Bhumibol I Bridge

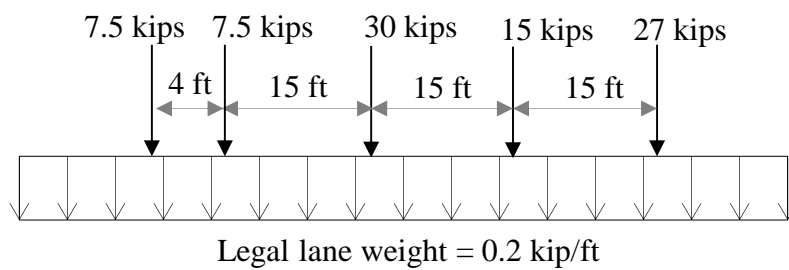


Fig. 6.4 State legal load and AASHTO lane load for the Bhumibol I Bridge

In determining the load rating of each component subjected to a single force effect (i.e., axial force, flexure, or shear), the AASHTO LRFR provides the following general equation for calculating a rating factor:

$$RF = \frac{C - (\gamma_{DC})(DC) - (\gamma_{DW})(DW) \pm (\gamma_P)(P)}{(\gamma_{LL})(LL + IM)}, \quad (6.1)$$

where $C = \phi_C \phi_S \phi R_n$, (6.2)

$$\phi_C \phi_S \geq 0.85, \quad (6.3)$$

RF = Rating factor,

C = Capacity,

R_n = Nominal member resistance,

DC = Dead load effect due to structural components and attachments,

DW = Dead load effect due to wearing surface and utilities,

P = Permanent loads other than dead loads,

LL = Live load effect,

IM = Dynamic load allowance,

γ_{DC} = LRFD load factor for structural components and attachments,

γ_{DW} = LRFD load factor for wearing surface and utilities,

γ_P = LRFD load factor for permanent loads other than dead loads (= 1),

γ_{LL} = Evaluation live load factor,

ϕ_C = Condition factor,

ϕ_S = System factor, and

ϕ = LRFD resistance factor.

6.1.2 Determination of force effect

For cable-stayed bridges, dead load and live load are transferred through cables to the towers. Therefore, the bridge tower was chosen to be a load rated component. In the load rating, the compression stress at the critical section of the tower was defined as the force effect and member resistance. When all spans are not loaded evenly, the compression stress due to the bending moment varies with live load combinations. To obtain the maximum load effect, five live load combination (LL1 to LL5) have been considered as shown in **Fig. 6.5**. The AASHTO HL-93 lane load and the bridge dead load were used in calculating compression stress on the tower by using the FE models. The analysis results showed that the tower section just under the deck of the Tower2 was the critical section and only the main span loaded (LL5 combination) gave the maximum load effect as shown in **Fig. 6.6**. Therefore, the live load combination, LL5 was used to determine the force effect for the bridge load rating. **Table 6.1** shows the calculated compression stress at the critical section due to three load cases that are the AASHTO HL-93 load, AASHTO legal load and the state legal load. The AASHTO HL-93

load creates the maximum stress on the tower, followed by the state legal load and the AASHTO legal load, respectively. For the effect of the dead load, the calculated compression stress is 28.8 N/mm^2 at the tower critical section.

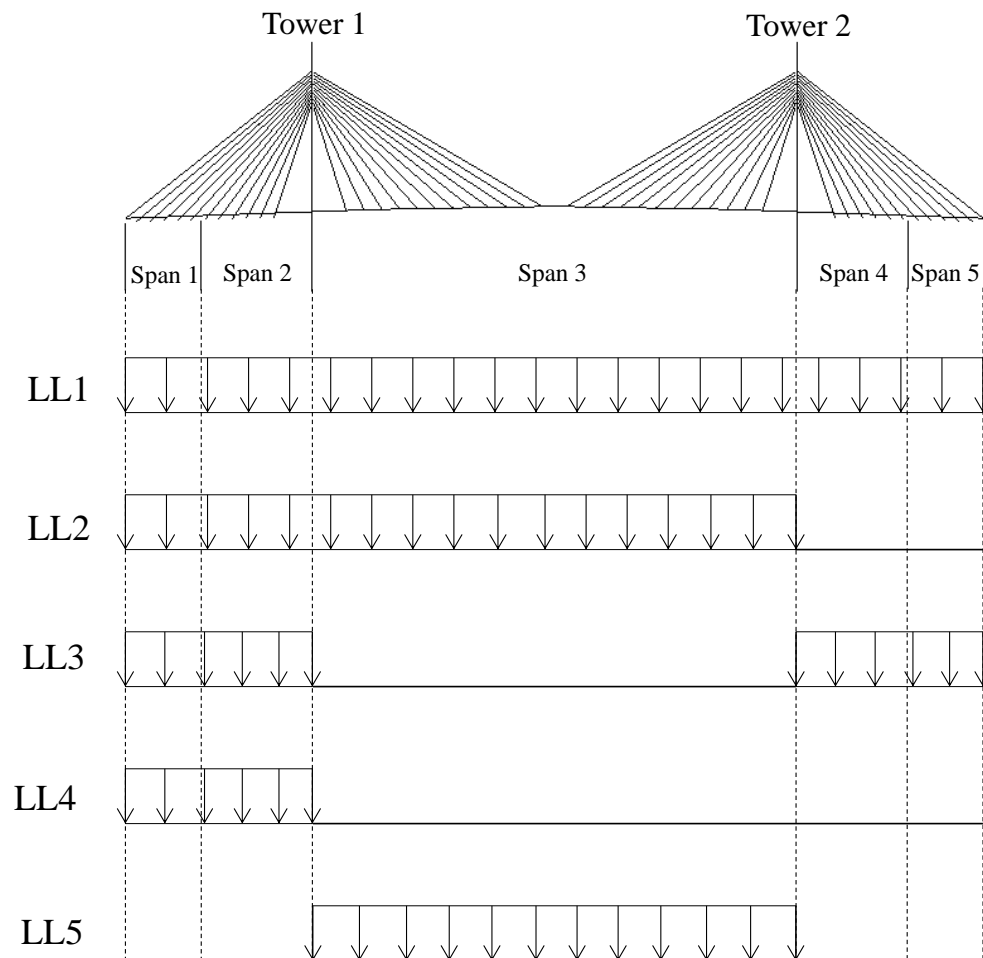


Fig. 6.5 Live load combinations

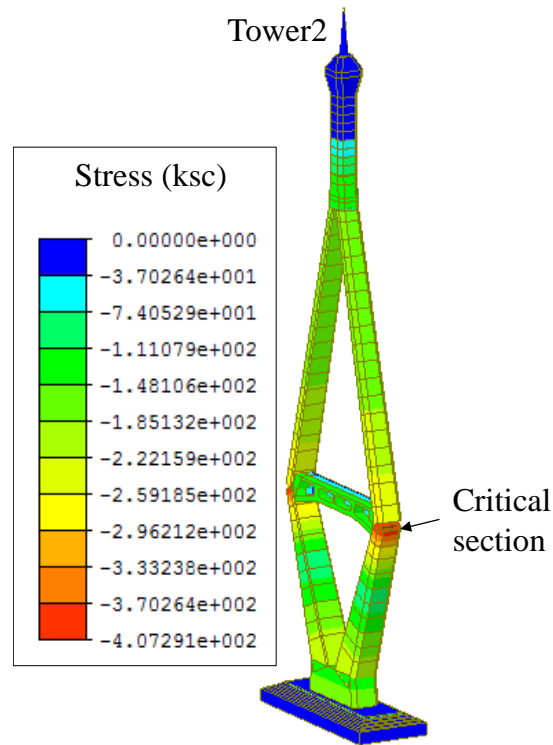


Fig. 6.6 Stress contour of the bridge tower due to dead load and AASHTO HL-93 lane load applied only on the main span

Table 6.1 Calculated tower compression stress at the critical section

Load case	Compression stress (N/mm ²)			Parameters in Eq. (6.1)			
	Lane load	Truck load	Dead load	<i>DC</i>	<i>DW</i>	<i>P</i>	<i>LL+IM</i>
	(1)	(2)	(3)	=(3)	none	none	=(1)+1.33*(2)
AASHTO HL-93	11.90	2.21	14.11	14.11	0.00	0.00	20.98
AASHTO legal	3.71	1.82	5.53	5.53	0.00	0.00	9.17
State legal	3.71	2.68	6.39	6.39	0.00	0.00	11.18

6.1.3 Load Rating Factor and Rating Factor Determination

The factors in the **Eq. (6.1)** and **(6.2)** for the Bhumibol I Bridge were determined based on material properties and traffic conditions of the bridge. The material properties were obtained from the bridge inspections and the traffic conditions were obtained from the traffic volume estimation. The following factors were used in the bridge load rating:

- Condition factor, ϕ_C provides a reduction to account for the member deterioration due to natural causes which increases uncertainty in the bridge resistance. The condition information can be obtained by structural inspections. The bridge was inspected in 2011, and found that the tower was in the good condition. According to *The Manual for Bridge Evaluation*, the ϕ_C equals to 1.

- System factor, ϕ_S reflects the level of redundancy of the complete superstructure system. The bridge redundancy is the capability of a system to carry loads after the failure of one or more of its members. For the Bhumibol I Bridge, the ϕ_S was assigned as 1.

- Resistance factor, ϕ according to the *AASHTO LRFD Bridge Design and Specifications*, the ϕ was taken as 0.90 for tension-controlled reinforced concrete sections.

- Nominal member resistance, R_n for compression stress of the bridge tower was obtained by the Schmidt Hammer testing. The testing compressive strength was higher than those in the design. Therefore, the design compressive strength (500 ksc) was used as the nominal resistance.

- Dynamic load allowance, IM is an increment to be applied to the truck loads to account for wheel load impact from moving vehiculars. For the bridge tower, the IM was taken as 33%.

- LRFD dead load factors (γ_{DC} and γ_{DW}) specified in the manual are equal to 1.25 for the strength limit state.

- Evaluation live load factors, γ_{LL} vary with the evaluation levels and traffic conditions. In the design load rating, the factors were taken as 1.75 and 1.35 for the inventory and operating level, respectively. Whereas for the AASHTO and state legal load rating, the maximum generalized factor provided in the manual is 1.45 for the bridges that have the average daily truck traffic (ADTT) greater than 5,000 in one direction. The factor is warranted to increase due to conditions not accounted in the manual. From the traffic data, the maximum number of the equivalent single trucks was 198 vehicles per five minutes. Based on the FE analysis, if the traffic flow speed is 50 km/h or 4.17 km/five minutes, the vehicular load will equal to 1.19 tons/m. For the AASHTO and state legal lane load (0.2 kip/ft), the total lane loads are 1.38 tons/m in the case of the Bhumibol I Bridge carrying seven traffic lanes. It can be seen that the AASHTO and state legal lane load govern the actual traffic load. Therefore, based on current traffic condition, the evaluation live load factor provided in the manual does not need to be increased.

The factors used in determining rating factors in each level of evaluation are summarized in **Table 6.2**.

Table 6.2 factors used in determining rating factors in each level of evaluation

Factors in Eq. (6.1)	Level of evaluation		
	Inventory design	Operating design	AASHTO/State legal
φ_C	1	1	1
φ_S	1	1	1
φ	0.9	0.9	0.9
γ_{LL}	1.75	1.35	1.45
γ_{DC}	1.25	1.25	1.25

According to **Eq. (6.1)**, the determined RF for the design load rating at the inventory and operating levels were 0.35 and 0.45, respectively. It could be concluded that the bridge did not have adequate capacity for the strength limit at the LRFD design standards and should be load rated for the state and AASHTO legal loads. Then the RF for the state and AASHTO legal load rating were determined. It was found that the bridge did not pass the state legal load screening ($RF = 0.85$) but it passed the AASHTO legal load screening with the RF of 1.01. It suggested that the bridge had a safe load capacity for the AASHTO legal load having the equivalent truck weight of 40 tons, but did not have adequate capacity for the state legal truck having weight greater than 40 tons. Based on the AASHTO bridge evaluation manual, the restricted truck weight should be 40 tons for the Bhumibol I Bridge.

6.2 RELIABILITY ANALYSIS

Structures should have a desirable level of reliability, which is used for ensuring safety of the structures subjected to all action loads. For evaluation of the reliability, it is based on a probabilistic theory. The reliability evaluation was performed for the bridge by using the estimated traffic loads and statistical data based on previous studies.

6.2.1 Background Theory

Reliability procedure usually begins with a limit state function. All load effects incorporated into a variable, Q and the resistance incorporated into a variable, R . In the general case, the limit function of a system is related to any possible failure scenario and defined as:

$$g(R, Q) = R - Q, \quad (6.3)$$

both R and Q are random variables, so the quantity $R - Q$ is a random variable, as well. The limit function can be expressed as a function of resistance and load variables (X_1, X_2, \dots, X_n):

$$g(X) = g(X_1, X_2, \dots, X_n), \quad (6.4)$$

where X_i are input parameters. From the definition of the limit function, it can be presented that when $g(X) < 0$, it indicates failure and if $g(X) \geq 0$, it indicates non-failure or acceptable performance. The function as $g(X) = 0$ is the failure surface. The probability of the failure can be determined by integrating the joint density function of the variables over the domain of $g(X) < 0$ (Thoft-Christensen and Baker, 1982) defined as:

$$P_f = \int_{g(X) < 0} \dots \int f_{X_1, X_2, \dots, X_n}(x_1, x_2, \dots, x_n) dx_1 \dots dx_n, \quad (6.5)$$

where P_f is the probability of failure and f_X is the joint probability density function of X_1, X_2, \dots, X_n .

The **Eq. (6.5)** is difficult to evaluate because there is usually not sufficient data to define the joint probability density function for all variables. In practice, indirect procedures such as the reliability index are adopted to estimate the probability of failure. The reliability of structures can be calculated by using the first-order second-moment methods (FOSM) (Cornell, 1967). Based on the FOSM approach, Hasofer and Lind (1974) proposed the function for calculating the reliability index as:

$$\beta = \frac{\mu_R - \mu_Q}{\sqrt{\sigma_R^2 + \sigma_Q^2}}, \quad (6.6)$$

where β is the reliability index, μ_R is mean value of the resistance, σ_R^2 is variance of the resistance, μ_Q is mean value of the load and σ_Q^2 is variance of the load. Then the probability of failure can be obtained through the **Eq. 6.7** as:

$$P_f = \Phi(-\beta), \quad (6.7)$$

where Φ is the standard normal distribution function.

6.2.2 Reliability Index Determination

The reliability index for the selected section of the tower was calculated. The resistance variable, R was defined as the design compressive strength of 50 N/mm² as aforementioned. The statistical parameters for the compressive strength recommended in the "Reliability-Based Calibration for Structural Concrete" (Nowak and Szerszen, 2001) are: a bias factor, λ (ratio of mean to nominal) equals to 1.12 and a coefficient of variation, V (ratio of variance to mean) is 0.11. For the load variable, Q consists of: the compressive stress due to the dead load, Q_{DL} that is 28.8 N/mm², and the compressive stress due to the live load, Q_{LL} . Dead load variation can be caused by variation of the material weights and dimensions. The statistical parameters for the dead load used in this research are based on the available data in a literature by Nowak (1999). They are 1.05 for a bias factor and 0.10 for a coefficient of variation. For the live load, the vehicular load is considered as a uniformly distributed load with value 1.19 tons/m (normal condition, flow speed 50 km/h) which induces compressive stress of 3.21 N/mm². The statistical parameters of the uniformly distributed live load for long span bridges proposed by

Lutomirska (2009) are: a bias factor of 1.20 and a coefficient of variation of 0.08 for bridge spans greater than 300 m. Then the mean values and variances of the resistance and load were determined. They are μ_R of 56.00 N/mm², σ_R^2 of 6.16 N/mm², μ_Q of 34.09 N/mm² and σ_Q^2 of 3.33 N/mm². According to **Eq. (6.6)** and **Eq. (6.7)**, the determined reliability index, β is 7.11 and the probability of failure, P_f is almost zero or the bridge is always safe for this condition.

Furthermore, the reliability analysis was performed for the congested traffic condition in the northbound direction. Based on the traffic data obtained in the traffic counting system, it was found that during this condition combination of the vehicles consisted of the passenger cars of 76%, the single trucks of 14% and the trailers of 10%. The vehicles have been placed on the bridge with the lengths and clearance distances obtained by observation. They are the length of 5 m and the clearance of 2 m for the passenger cars, the length of 12 m and the clearance of 2 m for the single trucks, and the length of 18 m and the clearance of 2 m for the trailers. The vehicles were added on the bridge until the total length reached the bridge length in every lane. Then, the total load of all vehicles was calculated and divided by the bridge length to obtain the uniformly distributed load which is 2.20 tons/m. For the southbound direction, there is no traffic congestion and the uniformly distributed load is 0.58 ton/m (97 equivalent single trucks per five minutes). Therefore, the total uniformly distributed load during the traffic congestion is 3.00 tons/m and it induces compressive of 8.09 N/mm². The determined reliability index, β is 5.08 and the probability of failure, P_f is almost zero or the bridge is always safe for this condition, as well. In addition, the reliability analysis was performed for the standard code load that are AASHTO HL-93, AASHTO legal load, State legal load and British Standard, BS 5400 (2006). Then the reliability indices were calculated and found that the β was 2.72 for the AASHTO HL-93 design load or the bridge had the probability of failure of 0.003. Regarding to the target reliability index ($\beta \geq 3.5$), it can be concluded that the bridge is not reliable at the AASHTO HL-93 design load. For the AASHTO legal load, State legal load and British Standard, BS 5400 (2006), the β were 6.13, 5.78 and 4.52, respectively. It can be said that the bridge is reliable at those standard codes. The nominal values and the statistical parameters of the variables used in the reliability analysis, and the reliability indices (β) are summarized in **Table 6.3**. Based on the reliability results, the bridge

should be performed maintenance if the reliability analysis considers only the standard loads. In contrary, when the reliability analysis considers the actual operating loads that can be obtained by the traffic volume prediction model, the bridge does not need repairing corresponding with the results from the bridge inspection. It could be said that the predicted traffic volume was applicable for bridge safety evaluation.

Table 6.3 Nominal values and the statistical parameters of the variables

Level of evaluation	Nominal value (N/mm ²)	Bias factor	Coefficient of variation	Reliability index
Operating level (normal condition)	3.21	1.20	0.08	7.11
Operating level (traffic jam)	8.09	1.20	0.08	5.08
AASHTO Standard (AASHTO HL-93)	14.11	1.20	0.08	2.72
AASHTO Standard (AASHTO legal)	5.53	1.20	0.08	6.13
AASHTO Standard (State legal)	6.39	1.20	0.08	5.78
British Standard (BS 5400)	9.48	1.20	0.08	4.52

6.3 CONCLUSIONS

This chapter showed safety evaluation of the bridge considering the actual operating loads that can be obtained by the traffic volume prediction model. The bridge has been evaluated the safety, based on the the *Load and Resistance Factor Rating (LRFR)* method provided in *The Manual for Bridge Evaluation* and the reliability analysis. It was found that the bridge did not have adequate capacity for the strength limit at the LRFD design standards and should be load rated for the state and AASHTO legal loads. Then the *RF* for the state and AASHTO legal load rating were determined. The results showed that the bridge did not pass

the state legal load screening ($RF = 0.85$) but it passed the AASHTO legal load screening with the RF of 1.01. It suggested that the bridge had a safe load capacity for the AASHTO legal load having the equivalent truck weight of 40 tons, but did not have adequate capacity for the state legal truck having weight greater than 40 tons. Based on the AASHTO bridge evaluation manual, the restricted truck weight should be 40 tons for the bridge. The reliability analysis of the bridge was performed as well. The analysis results showed that the bridge was safe for the current operating traffic conditions that were the maximum traffic volume and traffic congestion situations. It was shown that the predicted traffic volume was applicable for bridge safety evaluation.

REFERENCES

American Association of State Highway and Transportation Officials (AASHTO). *The Manual for Bridge Evaluation second edition*. Washington, DC: American Association of State Highway and Transportation Officials; 2013.

American Association of State Highway and Transportation Officials (AASHTO). *AASHTO LRFD Bridge Design Specifications sixth edition*. Washington, DC: American Association of State Highway and Transportation Officials; 2012.

Cornell C. A. Bounds on the Reliability of Structural Systems. *Journal of the Structural Division*, ASCE, 93 (ST1), 171-200; 1967.

Hasofer A.M., Lind N.C. "An Exact and Invariant First Order Reliability Format. *Journal of Structural Mechanics Division*, ASCE, Vol. 100, No. 1; 1974.

Lutomirska M. Live load model for long span bridge, Doctoral Dissertation; 2009.

Nowak A.S. *Calibration of LRFD Bridge Design Code*. NCHRP Report 368, Transportation Research Board, Washington, D.C., USA.; 1999.

Nowak, A.S. & Szerszen, M. M. *Reliability-Based Calibration for Structural Concrete*. Report UMCEE 01-04, Department of Civil and Environmental Engineering, University of Michigan, Ann Arbor, Mich., Nov.; 2001.

7. CONCLUSIONS

This study aims to estimate the traffic live loads by using available dynamic response data obtained from the SHM system installed on an in-service cable-stayed bridge, and to evaluate the safe load capacity and reliability of the bridge based on the estimated traffic loads. The target cable-stayed bridge consists of the composite deck in the main span with the length of 326 m and the post-tension concrete box decks in each of both side spans, the length of which is 125 m. The deck is supported by the two diamond-shaped towers with the height of 152 m and the four piers in the side span, both of which were constructed from the reinforced concrete. The fixed connections between the deck and the towers and piers are homogenous stressed concrete, and there are expansion joints at the ends of both sides of the side span deck. The SHM system consists of several kinds of sensors and the data acquisition system. The deployed sensors were six accelerometers, five tilt sensors, two displacement transducers and five temperature sensors, each of which is installed on the main span deck, the top of towers, the stayed-cables, and the expansion joints. The data are acquired continuously with the sampling frequency of 50Hz in all sensors with synchronizations. The acquired data are stored

into the database and automatically transferred to a control computer placed on the control office near the bridge every minute.

The data obtained from a SHM system installed in an in-service cabled-stayed bridge have been presented. The SHM system consisted of various sensors deployed on the bridge to capture the responses excited by traffic, changing temperature and wind. Multivariate features associated with dynamic characteristics were extracted from the monitored data. Based on the acquired data, it could be roughly observed that the amplitudes of all dynamic responses became relatively large during the daytime, and they decreased during the nighttime. For the temperature, the daily variance of each day was approximately 2 °C with the range of 29-32 °C. Notice that, in Bangkok, the daily and seasonal temperature variations were small. Similarly, the number of the single trucks and trailers increased in the daytime and decreased in the nighttime. The traffic volumes had a daily trend and large fluctuations within a day. For the extracted resonant frequencies, it could be considered that both the peak frequencies and their amplitudes had correlations especially with the traffic volume especially in the 1st and 4th peaks. Moreover, not only the peak frequencies but also the amplitudes associated with the traffic volume. Therefore, the RMS of the responses were determined and they all showed the similar trends, in which the RMSs increased during the daytime and decreased during the nighttime. It could be noticed that this trend similar to the trend of the number of equivalent trucks. In addition, the raw response signals were filtered by the band-pass filter and examined the amplitude of responses in certain frequency ranges. The RMSs of filtered responses were thus also expected to have the contribution to the traffic volume, and were adopted as the features to analyze the correlations.

The first task was to investigate effects of varying environment and operation on the measured responses of the bridge especially, the effects of traffic loads. The effects of environmental and operational conditions on the dynamic response variability such as the changes of resonant frequencies of the Bhumibol-1 Bridge were analyzed. The temperature and traffic loading were considered as the environmental and operational factors impacting on the fluctuation of nine resonant frequencies extracted from vertical acceleration of the deck. The linear regression models has been adopted to investigate the interaction of those factors and measured resonant frequencies. The regression analysis is a statistical methodology for

describing the stochastic relationship between responses of interest (estimation variable) and associated factors. It often used to understand the contributions of the influential factors to the estimation variables using the observation data. Moreover, it is used to make a stochastic model that describes the relationship between the estimation variables and the factors. The developed models revealed that the RMS of cable accelerations played a dominant role in prediction of the resonant frequencies of the first six modes while traffic loading and temperature had a low influence on these resonant frequencies. For the higher modes, only temperature significantly impacted on the changes of resonant frequencies. It should be noted that the trained temperature data collected from a short time period can represent only the daily effect, if a longer time period of measurements that can cover the seasonal effect are considered, the temperature might has a more influence. The prediction models can reproduce the general trend of the fluctuation of resonant frequencies but cannot recreate some high peaks and large drops. These spikes might be caused by short term traffic loading, in order to improve the prediction performance, a more sophisticated data measurement and a more complex structure of the mathematical model are required to better investigate the resonant frequencies variability. Moreover, the model errors can be adopted as an indicator of structural conditions.

As the dynamic responses obtained from the SHM system were described based on only the acquired data. Therefore, FE models were used to predict the dynamic responses for more understanding the dynamic behaviors of the bridge. This chapter presents FE modeling of the target bridge and analytical dynamic responses, and compares the analytical responses with those from the measurement. The three-dimensional FE models were developed by using Midas Civil software. The model has a total of 96 cable elements, 1,101 beam elements 385 plate elements and 1,127 nodes. The connections between the deck and the two towers and the four piers are fixed links. The main span consists of longitudinal and cross steel beams and concrete slabs. For the side span decks, they are post tension concrete boxes. The width of the north span varies while the south one is constant. The connections between the side span decks and the main span deck, towers, pillars and cables are assigned as rigid links. The towers supporting the decks are hollow concrete boxes and their supports are assigned as fix supports. The analysis results showed that the FE models could predict the modal properties that were the resonant frequencies and mode shapes, with a good accuracy. The vehicular loads were modeled for assigning in the FE models, based on the actual vehicles passing on the bridge.

Then the vehicular load time history was constructed based on the traffic counting data. The dynamic responses obtained from the FE models showed more that not only the traffic volumes, but also vehicle speeds had effects on the dynamic responses. In the case of the same traffic volumes, the response amplitudes decreased when the speeds of vehicles decreased.

Based on the correlation analysis results, it could be concluded that the traffic volumes associated with the extracted features that are the resonant frequencies, RMSs of deck and cable accelerations, and RMSs of deck tilts, while the temperature did not show a significant relation with those features. It was then confirmed by the FE analysis that the RMS of deck and cable accelerations associated with the bridge traffic volumes. Then, some of the response features that showed high correlations were then selected for constructing a linear regression model to estimate the total traffic volume on the bridge. Based on correlation analysis results, it was found that the peak frequencies and the RMSs of the deck accelerations, the cable acceleration, and the deck tilts associated with the traffic volume. And then they were used as candidate input factors for the traffic volume estimation. The statistical modeling for estimating the traffic volume on the target cable-bridge bridge from the dynamic responses was constructed and the significant conclusions were summarized that: (1) the correlations of the response features extracted from the SHM data; peak frequencies and amplitudes of responses, and the temperature and the traffic volume were investigated. The results revealed that the traffic volume was a dominant factor that influenced on variances of the peak frequencies and the RMSs of the deck accelerations, the cable acceleration, and the deck tilts while the temperature showed low effects on them in the target bridge, (3) the response features used for constructing the traffic volume estimation model, were selected by the procedure based on the correlation coefficients among those features and the traffic volume. The procedure could provide the appropriate features that were adopted as the predictor variables of the regression model for estimating the traffic volume, and (4) the constructed model for estimating the traffic volume showed the accurate fitting performance to the data, and it was also capable of predicting the traffic volume on the bridge.

The predicted traffic volumes from the SHM data were then applied for the bridge evaluation. The estimated traffic volumes were used to estimated vehicular live loads used in evaluating safe load capacity of the bridge. The bridge was evaluated safety based on the the

Load and Resistance Factor Rating (LRFR) method and reliability analysis. The safety evaluation of the bridge was performed by considering the actual operating loads that can be obtained by the traffic volume prediction model. It was found that the bridge did not have adequate capacity for the strength limit at the LRFD design standards and should be load rated for the state and AASHTO legal loads. Then the *RF* for the state and AASHTO legal load rating were determined. The results showed that the bridge did not pass the state legal load screening ($RF = 0.85$) but it passed the AASHTO legal load screening with the *RF* of 1.01. It suggested that the bridge had a safe load capacity for the AASHTO legal load having the equivalent truck weight of 40 tons, but did not have adequate capacity for the state legal truck having weight greater than 40 tons. Based on the AASHTO bridge evaluation manual, the restricted truck weight should be 40 tons for the bridge. The reliability analysis of the bridge was performed as well. The analysis results showed that the bridge was safe for the current operating traffic conditions that were the maximum traffic volume and traffic congestion situations. It was shown that the predicted traffic volume was applicable for bridge safety evaluation. Moreover, based on the reliability results, the bridge should be perform maintenance if the reliability analysis considers only the standard loads. In contrary, when the reliability analysis considers the actual operating loads that can be obtained by the traffic volume prediction model, the bridge does not need repairing corresponding with the results from the bridge inspection. It could be said that the predicted traffic volume was applicable for bridge safety evaluation.

Finally, the predicted traffic volumes are then expected to be applied for the bridge evaluation and the effective bridge planning and the effective bridge planning; e.g. enhancing the bridge inspection scheduling by taking account of the traffic volume, the capacity and congestion analysis, forecasting the future traffic demand, estimating the economic benefits. The considerations for appropriate applications will be worked in our future study. However, it could be clearly shown that the dynamic response data acquired in the SHM system could be also used to construct a statistical model for estimating the traffic volume on the bridge, with the proposed methodology of modeling based on the correlation coefficients in this study.